UAB
Universitat Autònoma de Barcelona

UNVEILING THE EPIGENETIC DRIVERS OF METASTATIC NEUROBLASTOMA USING MOUSE MODELS

Adrià Molero Valenzuela

PhD thesis

UNVEILING THE EPIGENETIC DRIVERS OF METASTATIC NEUROBLASTOMA USING MOUSE MODELS

Adrià Molero Valenzuela

Degree of Doctor of Philosophy (PhD) in

Biochemistry, Molecular Biology and Biomedicine

Performed at the Neural Tumors Laboratory of the Childhood Cancer and Blood Disorders Group at Vall d'Hebron Research Institute

Supervisor: Miguel F. Segura Ginard

Tutor: Jose Ramón Bayascas Ramírez

Thesis affiliated to the PhD program in Biochemistry, Molecular Biology and Biomedicine from the Department of Biochemistry and Molecular Biology of the Universitat Autònoma de Barcelona

2026

ACKNOWLEDGEMENTS

Agradecimientos

ABSTRACT

Resumen

ABSTRACT

Approximately half of neuroblastoma (NB) patients present with metastatic disease at diagnosis, most commonly affecting bone, bone marrow, liver, lymph nodes, and lungs. Increasing evidence indicates that epigenetic deregulation plays a major role in NB initiation, progression, and metastasis. Based on this, we hypothesized that systematic characterization of chromatin alterations in metastatic lesions—and the identification of metastasis-associated transcriptomic features—would improve our understanding of metastatic NB biology and support the discovery of new therapeutic strategies.

Metastatic NB models were generated by tail-vein injection of ten NB cell lines engineered to express dual luciferase/mCherry reporters in immunodeficient SCID beige mice. Metastatic growth was monitored weekly using *in vivo* bioluminescence imaging, and tumors and organs with potential micrometastatic lesions were collected for histological evaluation. Next, four selected models (SK-N-BE(2), SK-N-AS, CHLA-90, NBL-S), chosen for their clinically relevant dissemination patterns, were evaluated both intravenously (to generate metastases) and subcutaneously (to generate primary-like reference tumors). Human tumor cells were isolated from primary tumors and liver and bone lesions, processed and profiled by ATAC-seq and RNA-seq to compare metastatic versus primary states.

Most cell lines formed macroscopic metastases, with seven (SK-N-BE(2), SHSY-5Y, SK-N-AS, CHLA-90, NBL-S, IMR-32, KELLY) showing dissemination to clinically relevant sites including bone marrow, liver, adrenal glands, lung, and kidneys. Notably, SK-N-BE(2), SK-N-AS, and CHLA-90 displayed liver and bone marrow involvement in more than 80% of animals. Additional metastatic sites such as ovary and lymph nodes were also observed in specific models.

ATAC-seq analyses revealed widespread chromatin accessibility remodeling in metastatic lesions, indicating recurrent epigenetic reprogramming during dissemination and colonization. However, these accessibility changes were not consistently mirrored by matched transcriptomic alterations, highlighting a frequent discordance between chromatin state and gene expression. Despite this, cross-model comparisons identified shared epigenetic programs across cell lines with distinct genetic backgrounds, supporting a set of metastasis-associated regulatory patterns and nominating candidate therapeutic targets.

Overall, this work establishes metastatic NB cell line models that recapitulate major human metastatic sites and provides a framework to investigate site-specific chromatin remodeling in metastatic disease. By integrating epigenomic and transcriptomic profiling, we identify reproducible metastasis-associated regulatory patterns and generate a focused list of candidate therapeutic targets supported by epigenetic evidence.

Resumen

Aproximadamente la mitad de los pacientes con neuroblastoma (NB) presentan enfermedad metastásica al diagnóstico, afectando con mayor frecuencia a hueso, médula ósea, hígado, ganglios linfáticos y pulmones. La evidencia creciente indica que la desregulación epigenética desempeña un papel clave en la iniciación, progresión y metástasis del NB. En base a ello, planteamos la hipótesis de que la caracterización sistemática de las alteraciones de la cromatina en las lesiones metastásicas, junto con la identificación de rasgos transcriptómicos asociados a la metástasis, mejoraría la comprensión de la biología del NB metastásico y favorecería el desarrollo de nuevas estrategias terapéuticas.

Se generaron modelos metastásicos de NB mediante inyección intravenosa de diez líneas celulares modificadas para expresar reporteros duales luciferasa/mCherry en ratones inmunodeprimidos SCID beige. El crecimiento metastásico se monitorizó semanalmente mediante imagen de bioluminiscencia in vivo, y se recogieron tumores y órganos con sospecha de afectación micrometastásica para su evaluación histológica. Posteriormente, cuatro modelos seleccionados (SK-N-BE(2), SK-N-AS, CHLA-90 y NBL-S), elegidos por reproducir patrones de diseminación clínicamente relevantes, fueron evaluados tanto por vía intravenosa como subcutánea para generar, respectivamente, metástasis y tumores primarios de referencia. Se aislaron células tumorales humanas de tumores primarios y lesiones hepáticas y óseas, que posteriormente fueron procesadas y analizadas mediante ATAC-seq y RNA-seq para comparar estados metastásicos y primarios.

La mayoría de las líneas celulares formaron metástasis macroscópicas, siete de ellas (SK-N-BE(2), SHSY-5Y, SK-N-AS, CHLA-90, NBL-S, IMR-32 y KELLY) mostrando diseminación a localizaciones clínicamente relevantes como médula ósea, hígado, glándulas suprarrenales, pulmones y riñones. De forma destacada, SK-N-BE(2), SK-N-AS y CHLA-90 presentaron afectación hepática y de médula ósea en más del 80% de los animales. En algunos modelos también se observaron metástasis ováricas y en ganglios linfáticos.

Los análisis de ATAC-seq revelaron un amplio remodelado de la accesibilidad de la cromatina en las lesiones metastásicas, indicando una reprogramación epigenética durante la diseminación y colonización. Sin embargo, estos cambios no siempre se reflejaron de manera consistente en alteraciones transcriptómicas, poniendo de manifiesto una frecuente discordancia entre accesibilidad cromatínica y expresión génica. A pesar de ello, la comparación entre modelos permitió identificar programas epigenéticos compartidos entre líneas celulares con distintas características genéticas, apoyando la existencia de patrones regulatorios asociados a la metástasis y permitiendo nominar potenciales dianas terapéuticas.

En conjunto, este trabajo establece modelos metastásicos de líneas celulares de NB que reproducen el patrón de diseminación observado en pacientes y proporciona un marco experimental para investigar la remodelación de la cromatina específica de cada localización metastásica. Mediante la integración de perfiles epigenómicos y transcriptómicos, identificamos patrones reguladores asociados a la metástasis y generamos una lista priorizada de posibles dianas terapéuticas respaldadas por evidencia epigenética.

INDEX

LIST OF FIGURES

LIST OF TABLES

ABBREVIATIONS

#	3′-UTR	3′-Unstranslated Region
A	ADAMTS1	A disintegrin and Metalloproteinase with thrombospondin motifs 1
	ADRN	Adrenergic
	ATAC-seq	Assay for transposase-accessible chromatin using sequencing
	Aurora CS	Aurora cell sorter
B	BMP	Bone morphogenic protein
C	CAR-T	Chimeric antigen receptor T-cell therapy
	Cas9	CRISPR-associated protein 9
	CgA	Chromogranin A
	CNS	Central nervous system
	CRC	Core regulatory circuitry
	CRISPR	Clustered regularly interspaced short palindromic repeats
	CTCs	Circulating tumor cells
D	DFMO	Difluoromethylornithine
	DLL3	Delta-like ligand 3
	DMSO	Dimethyl sulfoxide
	DTCs	Disseminated tumor cells
E	EMT	Epithelial-mesenchymal transition

F	FBS	Fetal bovine serum
	FLUC	Firefly luciferase
G	GD2	Ganglioside 2
	GEMM	Genetically engineered mouse models
	GFRA2	Glial cell line-derived neurotrophic factor receptor alpha 2
	GN	Ganglioneuroblastoma
	GNBn	Ganglioneuroblastoma nodular
	GNBi	Ganglioneuroblastoma intermixed
	GO	Gene ontology
	GRK5	G protein-coupled receptor kinase 5
H	H&E	Hematoxylin and eosin
	HIF	Hypoxia-inducible factor
	HS6ST3	Heparan sulfate 6-0-sulfotransferase 3
	hNCCs	Human neural crest cell progenitors
	HVA	Homovanilic acid
I	IHC	Immunohistochemistry
	IMDM	Iscove's modified bulbecco's medium
	INRGSS	International neuroblastoma risk group staging System
	INSS	International neuroblastoma staging system
	IVIS	In vivo imaging system
K	KCNIP1	Potassium voltage-gated channel-interacting protein
	KCNMB4	Potassium calcium-activated channel subfamily M regulatory beta subunit 4

	LDH	Lactate dehydrogenase
L	LMNB1	Lamin B1 protein
	LN	Lymph node
	MAPK	Mitogen-activated protein kinase
	MES	Mesenchymal
	miRNA	micro-RNA
M	MRI	Magnetic resonance imaging
	mRNA	Messenger RNA
	MTD	Maximum tolerated dose
	MYCN	Neuroblastoma MYC
	NB	Neuroblastoma
	NC	Neural crest
N	ncRNA	non-coding RNA
	NDD	Neuroblastoma drug development
	NK	Natural killer
	OBD	Optimal biological dose
O	OMS	Opsoclonus myoclonus syndrome
	OSBPL3	Oxysterol-binding protein-like 3
	PBS	Phosphate buffered saline
	PCA	Principal component analysis
P	PDX	Patient derived xenograft
	PET	Positron emission tomography

R	RET	Rearranged during transfection
	RMS	Rhabdomyosarcoma
	RNA-seq	RNA sequencing
	RNAi	RNA interference
S	SCID	Severe combined immunodeficiency
	scRNA-seq	Single-cell RNA sequencing
	SE	Super-enhancer
	SIOPEN	International Society of Pediatric Oncology European Neuroblastoma
	STC	Stem cell transplantation
T	TERT	Telomerase reverse transcriptase
	TF	Transcription factor
	TSS	Transcription start site
V	VSNL1	Visinin-Like 1
	VST	Variance stabilizing transformation
W	WES	Whole exome sequencing

1.INTRODUCTION

1.1 Childhood cancer

Childhood cancer comprises malignancies diagnosed in children aged 0–14 years and represents a rare group of diseases[1]. Over the last four decades, outcomes in childhood cancer have improved substantially in developed countries, with overall cure rates now approaching 80%, largely due to advances in disease characterization, risk-adapted treatment, and supportive care[2–4]. However, cancer remains the leading cause of death by disease among children and adolescents, with 280.000 new diagnosis per year worldwide in children between 0 and 19 years old[5]. Many children who survive cancer suffer from long-term sequelae of surgery, cytotoxic chemotherapy and radiotherapy, such as mental disabilities, organ toxicities and secondary cancers, decreasing the quality of life for survivors[6–8].

1.1.1 Cancer origin: Childhood cancer vs adult cancer

Cancer is a group of diseases that are the result of an accumulation of mutations over time which eventually leads to the formation of a tumor[9]. These mutations occur in a single cell that accumulates them until it starts presenting cancerous features[10]. The accumulation of these mutations results from intrinsic stochastic events over time and other external factors such as alcohol, smoking, and diet. In fact, 66% of adult cancers are environment-related, and 38% of all cases could be actually preventable[11].

In contrast, since most pediatric cancers arise during early childhood or even during fetal development, the accumulation of mutations over time does not fully explain this tumor formation (Figure 1)[12]. Indeed, in around 10% of all pediatric tumors, no driving mutations can be identified. Moreover, the limited contribution of known environmental risk factors to childhood cancer is consistent with its distinct biological basis and partly explains why its tumor spectrum differs markedly from that observed in adults[13]. Furthermore, the variety of mutations that occur in

pediatric cancers is remarkably different than what is seen in adult cancers, even in tumors with similar histology[14].

In this context, childhood cancer could be viewed as arising predominantly through stochastic events, analogous to adult cancers without an established environmental basis. However, the distribution of tumor types and tissue origin differs markedly between children and adults, indicating that pediatric cancers cannot be explained solely by the absence of environmental exposure[15]. Indeed, leukemias are almost one third of all pediatric malignancies and the most common cancers in children, but it is only the 12th most common cancer when looking at all age groups [16]. Moreover, neuroblastoma (NB) is the most common extracranial tumor in childhood[17], but extremely rare in adults[18] and, in contrast, glioblastoma is rarely seen in pediatric patients but is the most common brain tumor in adults[19]. These differences in tissue of origin suggests that other mechanisms such as epigenetic reprogramming, chromosomal rearrangements and germline mutations must be involved in pediatric cancer development and new insights on these alterations would lead to a better understanding of the origin and progression of the disease[20–22].

Due to their low mutational burden and the presence of genomic alterations that are rare in adult cancers, the identification of actionable alterations and the implementation of targeted therapies in childhood cancer remain more challenging [12]. Furthermore, the anatomical distribution of pediatric tumors often necessitates age-specific surgical approaches, as resection must be performed in smaller and still-developing organs, with potential long-term sequelae[9].

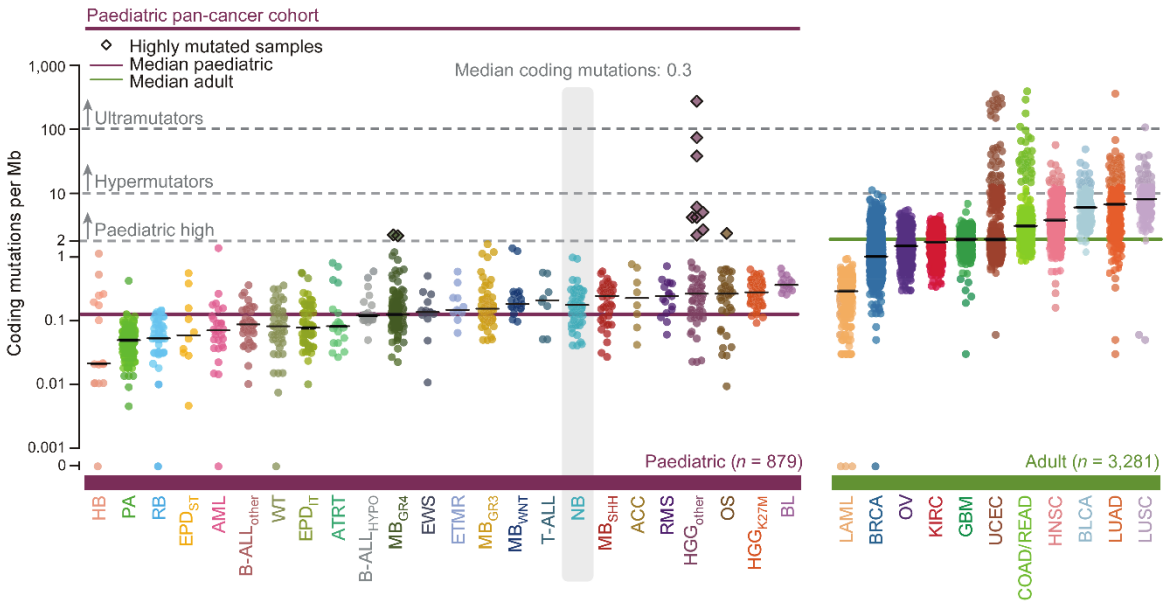

Figure 1. Mutational burden of pediatric and adult cancers. HB: Hepatoblastoma. PA: Pilocytic astrocytoma. RB: Retinoblastoma. EPDst: Ependymoma supratentorial. AML: Acute myeloid leukaemia. B-ALLother: B-cell acute lymphoblastic leukaemia non-hypodiploid. WT: Wilms tumor. EPDit: Ependymoma infratentorial. ATRT: Atypical Teratoid/Rhabdoid Tumor. B-ALLhypo: B-cell acute lymphoblastic leukaemia hypodiploid. MB: Medulloblastoma. EWS: Ewing's sarcoma. T-ALL: T-cell acute lymphoblastic leukaemia. NB: Neuroblastoma. ACC: Adrenocortical carcinoma. RMS: Rhabdomyosarcoma. HGG: High grade glioma. OS: Osteosarcoma. BL: Burkitt's lymphoma. LAML: Acute myeloid leukaemia. BRCA: Breast adenocarcinoma. OV: Ovarian serous carcinoma. KIRC: Kidney renal clear cell carcinoma. GBM: Glioblastoma. COAD/READ: Colon/rectal carcinoma. HNSC: Head and neck squamous carcinoma. BLDA: Bladder urothelial carcinoma. LUAD: Lung adenocarcinoma. LUSC: Lung squamous cell carcinoma. Adapted from Gröbner et al., 2020[12].

1.2 Epigenetics

During development, differences are generated in the embryo between identical cells that will lead to spatial re-organization and generation of different cell types. In this process, signal transduction and control of gene expression regulated by a network of molecular mechanisms result in changes of cell state, movement and growth, that consequently lead to cell lineage determination generating functional organs hierarchically organized that constitute a complex living organism[23–25]. Currently, it is widely accepted that the activation and silencing of concrete genes, resulting in a specific gene expression program, is required for the development of specialized cell roles[26].

Epigenetics is the term used to describe all the heritable changes in gene expression patterns that occur independently of alterations to the primary DNA sequence

(Figure 2). In this sense, DNA contains information to guide every cellular function, and epigenetics modulates the packaging of DNA to control gene expression[27]. Epigenetic heritability is due to the intrinsic capacity of epigenetic traits to remain through meiosis, resulting in intergenerational epigenetic heritability, as well as through mitosis, resulting in the maintenance of epigenetic traits in cell lineages within an individual organism. These epigenetic traits are the response to certain external or internal stimuli and consist of different chemical modifications of the chromosomes, known as epigenetic signals, which modify the condensation states of the chromatin, the nuclear substance formed by the complex of DNA and its associated structural and regulatory proteins[28]. These chromatin states have been classified into the opened and transcriptionally active euchromatin, and the closed and transcriptionally repressed heterochromatin, and they both are accomplished by the four epigenetic regulators: Writers, Erasers, Readers and Remodelers[29,30]. Epigenetic writers and erasers are proteins endowed with enzymatic activities that respectively deposit or remove epigenetic modifications from DNA and histones. These modifications do not directly alter chromatin architecture; instead, they serve as molecular marks that are recognized by a distinct class of proteins: epigenetic readers. Upon binding to these marks, readers recruit additional factors that actively drive chromatin remodeling and regulate gene expression. The proteins responsible for establishing and preserving these chromatin configurations are often referred to as chromatin remodelers or epigenetic maintainers, as they play a central role in sustaining specific chromatin states over time[31]. Gene expression, then, is facilitated when transcription start sites are in a nucleosome-free state and is repressed with compacted nucleosome occupancy. The chromatin modifications that trigger these processes can be summarized in three main levels: DNA methylation, histone modifications, and non-coding RNA regulation.

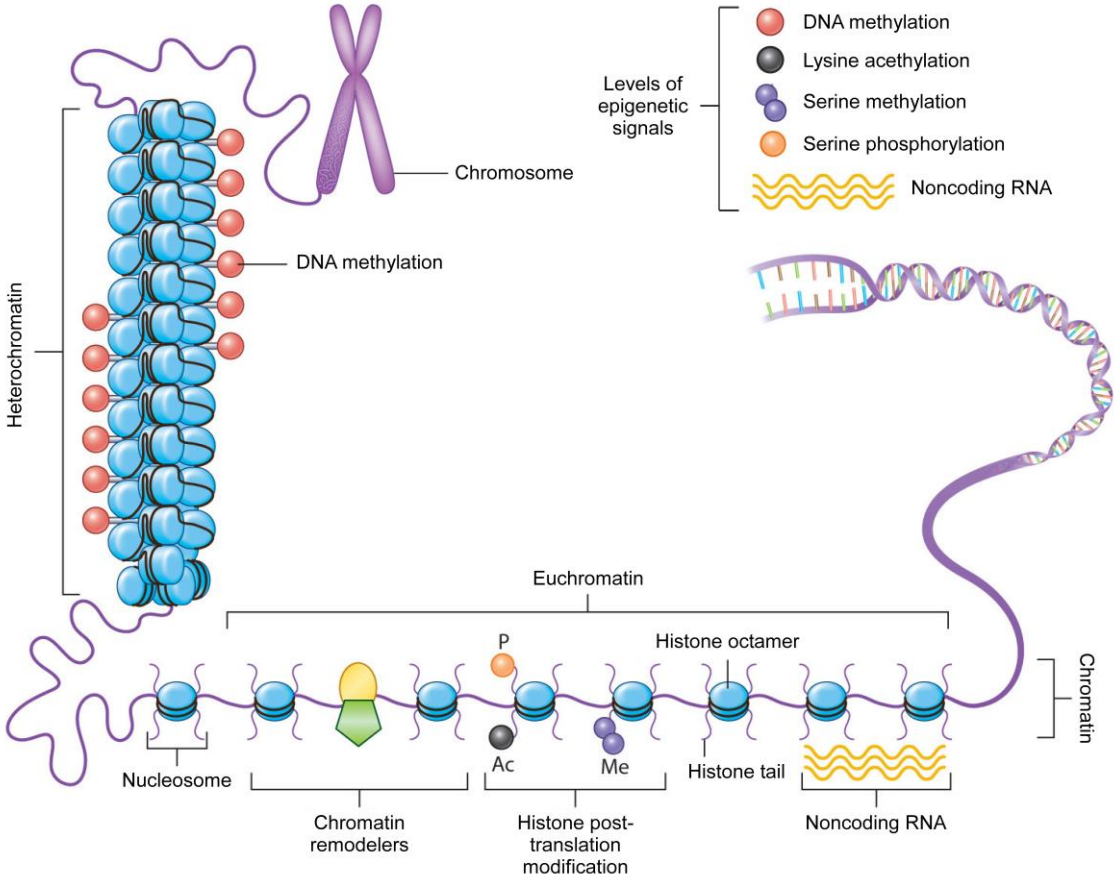

Figure 2. Epigenetic regulation levels. Adapted from Ahuja et al., 2016[31].

1.2.1 Epigenetics in cancer

Epigenetics is determinant in the maintenance of lineage identity of the multiple cell types that constitute the different tissues of an organism, which makes the correct epigenetic programming of cells crucial for the maintenance of tissue homeostasis[28]. Epigenetic aberrations can promote non-programmed loss of cell specialization and identity, disrupting equilibrium between cell types in a tissue, and favoring the initiation and progression of diseases such as cancer. During tissue homeostasis, epigenetic regulators normally function in a tightly coordinated, multilayered manner, but in cancer their dysregulation can sustain the expression of a restricted set of key target genes through specific molecular pathways. Thus, a slight imbalance in basal epigenetic regulation might lead to a catastrophic event that will develop a tumor[32].

The earliest indications of an epigenetic link to cancer were derived from DNA methylation studies, where altered patterns of methylation were observed between the DNA of tumor samples and their corresponding healthy tissues[33,34]. Since then, a general increase in the methylation of promoters has been described in tumor suppressor genes, including relevant genes such as *RB* and *CDKN2A*, which are cell cycle progression inhibitors[35,36]. Conversely, hypo-methylation patterns at promoter CpG islands have also been observed, leading to the aberrant activation of genes that regulate the proliferation capacities of cells[35]. Likewise, dysregulation of histone marks has been reported across multiple tumor types, with both the machinery that establishes these modifications and the downstream chromatin readers and remodelers involved in their interpretation being implicated in oncogenic processes relevant to tumor initiation and progression[37,38]. Indeed, driving mutations are found in genes encoding the enzymes responsible for the synthesis and erasing of histone acetylation or methylation as well as defects on the proteins responsible for their recognition (readers). This miswriting and misreading of histone mark modifications is translated into wide gene expression changes in large sets of genes[37,38].

1.3 Neuroblastoma

1.3.1 Where is neuroblastoma in the childhood cancer landscape?

NB is the most common extracranial solid tumor and the most frequently diagnosed cancer during the first year of life, being very uncommon after 10 years of age[39]. Moreover, it accounts for 12-15% of pediatric cancer-related deaths, making it one of the greatest challenges for clinical practice in hospitals worldwide and a clear target for translational research[40]. Although epidemiologic studies have investigated environmental factors that may be associated with NB, no strong consistent risk factors have been described. Besides that, a family history of NB is present in 1% to 2% of cases, and in fact, children who have siblings with NB are nearly 10 times more likely to also be diagnosed with the disease than those without family history[41].

To understand why NB presents such unique clinical challenges, it is essential to examine its developmental origins and the molecular mechanisms that drive its formation.

1.3.2 Developmental origin of neuroblastoma

NB is an embryonal tumor of the sympathetic component of the peripheral nervous system that develops from sympathoadrenergic progenitors arising from the neural crest (Figure 3)[42]. The neural crest is a transitional embryonic cell population formed during gastrulation and neurulation in fetal development. This embryonic and pluripotent cell population migrates extensively throughout the developing embryo, while differentiating into diverse cell types to develop several tissues including the craniofacial skeleton, adrenal chromaffin cells, melanocytes and the sympathetic and peripheral nervous systems, being the latter, the ones believed to originate NB[43]. Therefore, the development, maintenance and differentiation of this cell population is a highly complex process that must be meticulously controlled by a multifaceted gene regulatory network to be accomplished[44]. These delicate molecular processes involve communication between different cell populations through extracellular gradients of growth and transforming factors, such as BMP, Wnt, MYCN, or Notch signaling pathways. The activation of these pathways initiates the determination of neural crest progenitors, which leads to their delamination through epithelial-mesenchymal transition (EMT) mechanisms, culminating in their migration to various locations and terminal differentiation. Once EMT ends, key regulators of pluripotency (*MYCN*) and EMT (*SOX9, FOXD3, SNAI2, TWIST1*) need to be progressively downregulated, while, for instance, adrenergic determination transcriptional programs must be activated by TFs such as PHOX2B and GATA2/3 to conclude cell differentiation and maturation, suggesting that sympathoadrenal maturation requires low or absent *MYCN* expression[45]. Initiating mutations along with epigenetic or chromosomal derangements during any phase of this process comprising induction, specification, delamination and differentiation may generate

tumor-initiating neuroblasts in different structures of the peripheral nervous system including sympathetic ganglia and the adrenal gland, the two main primary sites of NB[43,46].

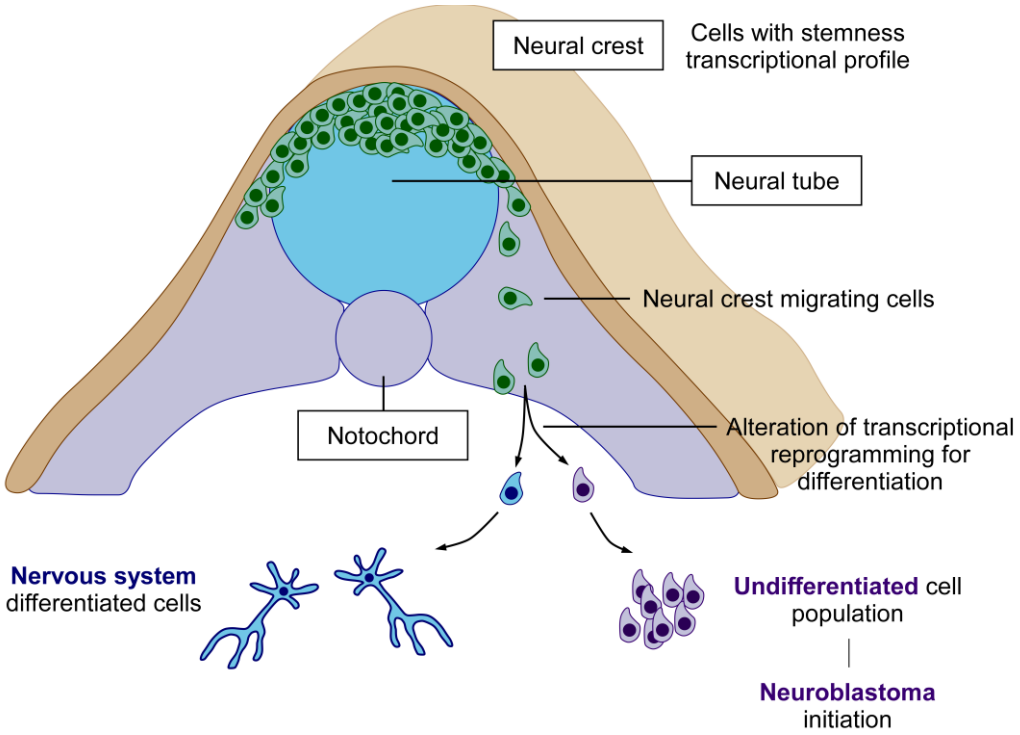

Figure 3. Schematic representation of neuroblastoma origin. Adapted from Marshall et al., 2014[46].

1.3.3 Molecular and epigenetic alterations of neuroblastoma

The origins of NB during development are intrinsically linked to a range of molecular alterations that propel both its initiation and progression. Central to this process are recurrent mutations that disrupt key regulatory factors governing the transformation of neural crest cells into sympathoadrenergic lineages. For example, early in the disease process, dominant-negative, loss-of-function mutations in the *PHOX2B* gene—an essential TF for adrenergic differentiation—have been identified[47,48]. In addition, a small fraction of cases (approximately 1–2%) linked to familial NB have been associated with autosomal dominant germline mutations that exhibit incomplete penetrance[49].

A particularly critical genetic event in NB is the amplification of the *MYCN* oncogene. Tumors are classified as *MYCN*-amplified when they contain over 10 copies of the gene—often reaching the hundreds—resulting in an abnormal surge in MYCN protein levels[50]. As a key member of the MYC TF family, which is associated with maintaining pluripotency, *MYCN* overexpression is detected in approximately 20–30% of NB cases and is used to designate patients as high-risk[51–53]. Under normal developmental conditions, *MYCN* is primarily expressed in neuronal progenitors of the central nervous system (CNS), with only brief expression observed in neural crest cells during dorsolateral migration[43]. However, its abnormal and sustained expression in neural crest precursors appears to maintain a transcriptional program that prevents full terminal differentiation, thereby promoting enhanced proliferation, self-renewal, cellular plasticity, and migratory abilities[54]. This effect may also be compounded by additional, less frequent genetic alterations, such as *TP53* mutations, that can interfere with programmed cell death or cell cycle arrest and thereby contribute to tumor development[55].

In addition to *MYCN*, the *ALK* gene stands out as the second most frequently altered gene in NB[56]. *ALK* encodes a tyrosine kinase receptor that is vital for proper nervous system development. In roughly 10% of NB cases, gain-of-function alterations—encompassing both increased copy numbers and activating point mutations—result in the receptor's hyperactivation[57,58]. This, in turn, stimulates downstream signaling pathways such as the MAP kinase cascade, promoting cell survival and playing a pivotal role in the onset of NB[59,60]. Moreover, more than half of familial NB cases have been linked to germline mutations in *ALK*[61].

While point mutations are generally infrequent in NB, other genes also display recurrent alterations. One such gene is *ATRX*, which encodes a chromatin remodeling protein related to the SWI/SNF complex and functions as a histone chaperone [62]. Loss-of-function mutations in *ATRX* occur in about 10% of cases, with a higher incidence among patients older than 14 years[63]. Similarly, mutations in the

promoter region of the telomerase gene (*TERT*) have been observed, leading to increased expression of telomerase and contributing further to the oncogenic process in NB[64].

NB aggressiveness is also closely linked to the presence of recurrent segmental chromosomal abnormalities. Among the most frequent alterations, gain of chromosome arm 17q is observed in more than half of NB cases, whereas deletion of 1p36 occurs in approximately one quarter of patients. Both lesions have been associated with *MYCN* amplification[65,66]. Another highly recurrent event is loss of heterozygosity at 11q23, which is found in roughly one third of NBs, while unbalanced loss of 11q has been described in nearly 50% of tumors carrying 11q23 LOH. In contrast to 1p36 loss and 17q gain, alterations involving 11q are typically inversely associated with *MYCN* amplification and are nevertheless linked to an unfavorable clinical outcome. The strong relationship between 1p36 or 11q loss and poor prognosis has supported the idea that these chromosomal regions harbor genes with tumor suppressor functions. In the 1p36 locus, candidate tumor suppressors include *CHD5, CAMTA1, KIF1B* and *CASZ1*[67]. Likewise, several genes with putative tumor suppressor roles have been mapped to 11q23, including *H2AFX, ATM* and *CADM1*[68,69]. In addition to these well-established lesions, other recurrent chromosomal abnormalities have also been described in NB, such as gains of 1q and 1p and losses affecting 3p, 4p and 14q[53].

Beyond these genetic and chromosomal events, NB biology is strongly shaped by epigenetic regulation. Even in the absence of highly recurrent coding mutations, changes in chromatin state and transcriptional wiring enforce oncogenic programs, sustain tumor cell identity, and enable cellular plasticity even in the setting of relatively few recurrent coding mutations[70,71]. In particular, super-enhancer-defined regulatory states and their interconversion (adrenergic vs mesenchymal) have emerged as a central framework to explain intratumor heterogeneity and therapy adaptation in NB [72–74], and are discussed in detail below.

This epigenetic plasticity is reflected in the cellular heterogeneity within NB, which mirrors the developmental states of the adrenergic lineage and consists predominantly of two distinct cell phenotypes: mesenchymal-type (MES) cells and adrenergic-type (ADRN) cells[73,74]. MES cells exhibit characteristics of neural crest-derived precursors, whereas ADRN cells are committed to a noradrenergic identity. This dual-cell composition underscores NB's complexity and plasticity, allowing these subtypes to interconvert spontaneously through epigenetic and transcriptional changes in response to environmental stimuli, therapeutic interventions, or intrinsic signaling pathways[73].

The cellular plasticity of NB arises from the co-option of epigenetic mechanisms and lineage-specific transcriptional programs, enabling tumor cells to transition between MES and ADRN states. This process mirrors developmental biology, wherein multipotent precursors in the autonomous nervous system determine their fate through lineage-specific TFs such as PHOX2B, which drives adrenergic identity, or PRRX1, which is essential for mesenchymal lineage commitment[75]. In NB, these lineage-determining mechanisms are hijacked by tumor cells, resulting in intratumoral heterogeneity, therapy resistance, and relapse.

Distinct transcriptional and epigenetic landscapes define ADRN and MES cells, each governed by unique core regulatory circuitries (CRCs) and super-enhancer (SE) networks[71]. SE are extended genomic regions composed of multiple constituent enhancers that are spatially clustered and exhibit unusually high enrichment of transcription factors[76]. ADRN cells, for instance, rely on CRC modules comprising TF such as PHOX2A/B, HAND1/2, GATA2/3, ISL1, TBX2 and ASCL1 which sustain the noradrenergic identity through positive feedback loops within their SE networks[73,74,77–79]. Conversely, MES cells are regulated by PRRX1 and members of the AP1 family, orchestrating a mesenchymal gene expression program that closely resembles human neural crest cell progenitors (hNCCs)[74,75,78].

CRCs serve as robust regulatory networks that amplify the expression of key TF. These TF bind their own SEs and to the SEs of other CRC components, creating interconnected positive feedback loops that sustain the expression of the entire network and reinforce cell identity. The mutual exclusivity of ADRN and MES CRCs underscores their role in maintaining distinct NB cell phenotypes while also enabling transitions when CRC composition is altered[72].

The lack of specific molecular markers has historically hindered studies of cell state transitions by preventing the separation of each cell type[80]. However, advancements in single-cell RNA sequencing (scRNA-seq) and other high-resolution techniques are beginning to bridge this gap, revealing the heterogeneity of NB tumors and the dynamic interplay between cell states[73,81,82]. Indeed, recent studies using scRNA-seq demonstrated that NB cells are not restricted to purely ADRN or MES identities but can also exist in transitional states displaying mixed expression patterns of both phenotypes[83]. Moreover, immunohistochemical analyses and bulk RNA-seq studies have confirmed that MES-like cells may be present in tumors in patients, indicating that MES cells are not merely artifacts of *in vitro* culture conditions but integral components of NB biology that contribute to therapy resistance and disease progression[84,85].

Beyond transcriptional plasticity, additional epigenetic mechanisms may contribute to therapy resistance in NB. For instance, Caspase-8, a member of the mammalian caspase family, has been reported as a frequently inactivated gene by hypermethylation in NB, which may cause defective apoptosis in advanced disease[86–88], resulting in tumor progression and resistance of NB cells against apoptosis-inducing therapies[89]. The methylation status of caspase-8 has been linked to *MYCN* amplification in some studies[86,90] but not in others[91,92], indicating that a direct effect between *MYCN* amplification and caspase-8 inactivation has not been well-described to this day.

1.3.4 Clinical presentation and diagnosis of neuroblastoma

NB is a pediatric cancer with early onset and represents the most common malignancy diagnosed in the first year of life, with an incidence of ~8 cases per million children annually[93]. Ninety percent of NBs are diagnosed in children younger than 10 years, with a median age at diagnosis of 18 months[94].

The most common primary tumor site is the adrenal gland medulla, accounting for 47% of the cases, followed by sympathetic ganglia located at the abdominal (24%) or thoracic (15%) cavities. Other less frequent primary tumor sites include the pelvis and neck[95]. Initial clinical symptoms depend on the primary tumor location and the regional and metastatic dissemination.

In terms of primary tumors, an abdominal tumor may present with discomfort, pain, gastrointestinal disturbances, or a palpable mass, and is associated with poor outcomes. In contrast, thoracic tumors are often discovered incidentally or manifest with respiratory distress and dysphagia. Cervical NBs have the potential to affect the cervical ganglion, resulting in Horner's syndrome, a neurological disorder caused by the interruption of the sympathetic nerves between the brain to one side of the face[96]. Furthermore, dumbbell tumors present in the spinal cord and nerve roots can lead to radicular pain, paraplegia, or bladder or bowel dysfunction. Despite these varied presentations, thoracic, cervical and other extra-abdominal tumors are considered to have better outcomes compared to abdominal masses, particularly those originating in the adrenal gland[97]. Additional systemic symptoms include tachycardia and hypertension due to compromise of renal vasculature, as well as flushing resulting from the release of catecholamines by NB tumors[98].

On the other hand, when it comes to metastatic disease, a different clinical scenario is observed as in 50% of patients metastatic spread is already present at diagnosis. Among patients presenting with metastatic disease, common sites of metastases include bone marrow (70%), bones (60%), lymph nodes (30%) and liver (30%), while

lung, skin and other CNS metastases are less frequent (<5%)[99,100](Figure 4). Metastatic disease to the bone marrow can cause anemia and thrombocytopenia, whereas bone lesions lead to severe pain that may result in limping or refusal to bear weight. Moreover, liver infiltration can cause coagulopathy and jaundice, along with other systemic symptoms such as fever and weight loss. Besides that, paraneoplastic presentations occur in a small percentage of NB patients, including opsoclonus myoclonus syndrome (OMS) and diarrhea caused by the secretion of vasoactive intestinal peptide. Symptoms of OMS include rapid, uncontrolled, horizontal and vertical eye movements, as well as involuntary muscle twitching, occasionally with ataxia[98]. Tumor cell dissemination in the CNS and lungs is not often seen at diagnosis but can occur with progression or relapse[101].

A subset of NB patients presenting a specific pattern of metastasis have a high likelihood of undergoing spontaneous regression without any treatment, as D'Angio et al., first reported in 1971. These patients are typically younger than 2 months and are diagnosed with a small localized primary tumor with possible metastases in liver, skin, or bone marrow that subsequently undergo regression and cell death. Although the exact mechanisms responsible for spontaneous regression remain uncertain, several hypotheses have been proposed, including the action of the immune system or the induction of telomere-mediated senescence, mirroring features of embryonal cells in utero that are not required for organogenesis[46,102]. Moreover, although this phenomenon is reported to occur in approximately 2% of diagnosed NBs, the incidence of subclinical NB may be much higher than the frequency of clinical disease. Autopsies of sympathoadrenal tissues from infants who have died of causes other than cancer have revealed an incidence of neuroblasts nests 40-fold higher than rate of clinical disease[103].

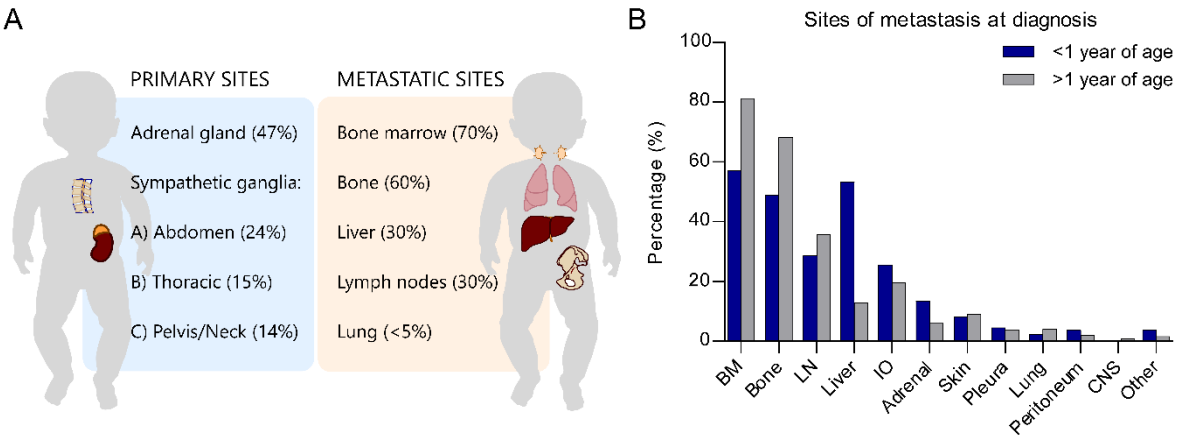

Figure 4. Clinical presentation of neuroblastoma. A. Main neuroblastoma primary and metastatic sites at diagnosis. B. Bar graph representing the most common metastatic sites of NB at diagnosis including > and < 1 years of age patients extracted from DuBois et al., 1999. BM: Bone marrow; LN: Lymph nodes; IO: Intracranial/Orbit; CNS: Central nervous system.

NB diagnosis combines imaging and symptomatic evidence with laboratory analyses of blood, urine, and pathological specimens[53,101]. From a histopathologic perspective, neuroblastic tumors consist of two distinct cell populations: neuroblastic/ganglionic cells, which are tumor cells *per se,* and Schwann cells, which form the Schwannian stroma. The relationship between neuroblastic and Schwann cells has not yet been fully elucidated, and the origin of Schwannian stroma remains unclear. Two different hypotheses propose that Schwann cells are either recruited from adjacent healthy tissues or derived from the same pluripotent neoplastic cell population as neuroblastic cells[104,105].

Despite this uncertainty, the International Neuroblastoma Pathology Committee has morphologically classified neuroblastic tumors into four categories by based on the percentage of Schwannian stroma and grade of morphological differentiation: NB (poor Schwannian stroma), ganglioneuroma (Schwannian stoma-dominant) and ganglioneuroblastoma, which is further subdivided into intermixed (rich Schwannian stroma) or nodular (composites of Schwannian stroma-rich/stroma-dominant and stroma-poor components) subtypes[98,106].

Ganglioneuroma and ganglioneuroblastoma are highly differentiated and well-demarcated tumors that are considered benign forms of NB[53]. Conversely, NB is typically less differentiated and histologically classified as: undifferentiated, poorly

differentiated and differentiating according to the degree of neuroblastic differentiation[106]. Accordingly, histopathological prognosis of patients with NB depends not only on the volume of Schwannian stroma but also on the degree of tumor differentiation and the mitotic-karyorrhexis index (MKI; Table 1), a histological parameter to determine cell turnover by quantifying mitotic cells and cells undergoing nuclear fragmentation[107,108].

Table 1. International neuroblastoma pathology classification.

Category and subtype	Stroma development	MKI	Age (years)	Prognostic
Neuroblastoma				
Undifferentiated	Poor (0<50%)	Any	Any	UH
Poorly differentiated	Poor (0<50%)	H	Any	UH
		Any	>1.5	UH
		L/I	<1.5	FH
Differentiating	Poor (0<50%)	H	Any	UH
		Any	>5	UH
		I	>1.5	UH
		I	<1.5	FH
		L	<5	FH
GNB nodular	Rich/dominant/poor			FH, UH
GNB intermixed	Rich			FH
Ganglioneuroma	Dominant			FH

Abbreviations: GNB: Ganglioneuroblastoma; H: high; I: intermediate; L: low; UH: unfavorable histology; FH: favorable histology.

1.3.5 Risk stratification and clinical management of neuroblastoma

The International Neuroblastoma Staging System (INSS) has traditionally served as the standard consensus framework for classifying NB patients based on the extent of disease at diagnosis and after initial surgery. This system categorizes tumors into stages 1, 2a, 2b, 3, 4, and 4s, with stages 1–3 corresponding to locoregional disease of increasing complexity and stage 4 denoting distant metastatic spread, while stage 4S correspond to the subgroup characterized by the spontaneous regression of

tumors, where the "S" stands for special (Table 1). To harmonize pretreatment risk stratification across clinical trials, the International Neuroblastoma Risk Group (INRG) subsequently developed a new pretherapy staging system (International Neuroblastoma Risk Group Staging System, INRGSS). Unlike the INSS, the INRGSS is assigned before any surgical intervention or systemic treatment and is based on radiological imaging and image-defined risk factors (IDRFs). Within this system, tumors are classified into four stages: L1 and L2 for locoregional disease without or with IDRFs, respectively, and M and MS for metastatic disease, with MS representing the infant pattern analogous to historical stage 4S (Table 2).

Table 2. INSS and INRGSS stages description based in Pudela et al., (2020), Monclair et al., (2009) and Brodeur et al., (1993).

System	Stage	Description
INSS	1	Localized tumor with complete gross excision.
	2a	Localized tumor with incomplete gross excision.
	2b	Localized tumor with or without complete gross excision. Nonadherent lymph nodes positive for tumor.
	3	Unresectable unilateral tumor with or without regional lymph node involvement; or localized unilateral tumor with contralateral regional lymph node involvement; or midline tumor with bilateral extension by infiltration (unresectable) or by lymph node involvement.
	4	Any primary tumor with dissemination to distant lymph nodes, bone marrow, liver, and/or other organs (except as defined for Stage 4S).
	4S	Localized primary tumor (as defined in stage 1, 2a or 2b) with dissemination limited to skin, liver and/or bone marrow (limited to infants <1 year of age).
INRGSS	L1	Localized tumors confined within one body compartment not involving vital structures as defined by the image-defined risk factors (IDRF).
	L2	Loco-regional tumors with presence of one or more IDRF.
	M	Distant metastatic disease (except Stage MS and not contiguous with primary tumor).
	MS	Metastatic disease confined to skin, liver and/or bone marrow in patients <18 y.o.

Following clinical and pathological diagnosis, and prior to initiating treatment, NB patients are classified into different risk groups based on disease stage and molecular alterations to determine specific treatment regimens. According to the INRGSS, these pre-treatment risk groups are subcategorized as very low, low,

intermediate, and high risk. The criteria for patient classification into each group are outlined in Table 3. NB risk groups were established from a cohort of 8,800 patients, with classification based on patient groups exhibiting 5-year event-free survival rates of >85% (very-low), 75-85% (low), 50-75% (intermediate), and <50% (high-risk) (Table 3)[109].

Table 3. INRG risk group stratification system. Extracted from Matthay et al., 2016.

Risk group for treatment	INRG stage	IDRFs in primary tumor	Distant metastases	Age (months)	Grade of differentiation	MYCN status	Hitology
Very-low	L1	Absent	Absent	Any	Any	-	GNBn, NB
Very-low	L1 or L2	Any	Absent	Any	Any	-	GN, GNBi
Low	L2	Present	Absent	<18	Any	-	GNBn, NB
Low	L2	Present	Absent	≥18	Different.	-	GNBn, NB
Low	MS	Any	Present	<12	Any	-	Any
Intermediate	L2	Present	Absent	<18	Any	-	GNBn, NB
Intermediate	L2	Present	Absent	≥18	Different.	-	GNBn, NB
Intermediate	L2	Present	Absent	≥18	Undiff.	-	GNBn, NB
Intermediate	M	Any	Present	<18	Any	-	Any
Intermediate	M	Any	Present	<12	Any	-	Any
Intermediate	MS	Any	Present	12-18	Any	-	Any
Intermediate	MS	Any	Present	<12	Any	-	Any
High	L1	Absent	Absent	Any	Any	+	GNBn, NB
High	L2	Present	Absent	≥18	Any	+	GNBn, NB
High	M	Any	Present	12-18	Any	-	Any
High	M	Any	Present	<18	Any	+	Any
High	M	Any	Present	≥18	Any	Any	Any
High	MS	Any	Present	12-18	Any	-	Any
High	MS	Any	Present	<18	Any	+	Any

Abbreviations: GNBn, 'Ganglioneuroblastoma nodular'; GNBi, 'Ganglioneuroblastoma intermixed'; GN, 'Ganglioneuroma'; NB, 'Neuroblastoma'; Undiff., 'Undifferentiated'; Fav. And Unfav., 'Favourable' and 'Unfavourable', respectively (presence or absence of segmental chromosome alterations).

Patients with very low and low-risk NB are often managed with surgical resection alone, even in cases with incomplete resection[110]. In fact, observational studies have demonstrated that subsets of infants younger than 6 months with localized tumors can be cured without any treatment[111,112].

Intermediate-risk patients are conventionally treated with two to eight cycles of chemotherapy, including carboplatin, cyclophosphamide, doxorubicin and etoposide, combined with surgical resection of the primary tumor[113]. Furthermore, patients with unresectable or disseminated intermediate-risk tumors without *MYCN*

amplification have also shown excellent survival rates when treated with more intensive regimens including radiotherapy. Consequently, both low- and intermediate-risk NBs have excellent outcomes, presenting overall survivals higher than 90%, and recent clinical trials aim to reduce therapy-related toxicities[114].

In contrast, outcomes for high-risk NB patients still remain poor, with long-term survival of approximately 50%[114]. In Europe, high-risk standard-of-care treatment consists of three sequential therapeutic blocks according to SIOPEN (International Society of Pediatric Oncology European Neuroblastoma): Induction, consolidation, and post-consolidation. While the induction phase consists of a regimen of chemotherapeutic agents known as 'rapid COJEC' administered at high-dose intensity with short intervals between cycles (see Table 4)[114], the consolidation phase consists of myeloablative therapy, typically based on busulfan and melphalan, aimed at eliminating residual tumor cells that may persist in reservoirs such as the bone marrow, followed by stem-cell infusions to restore blood cell progenitor levels[115].

Unfortunately, half of the patients who achieve clinical remission after induction and consolidation therapy will relapse, indicating the presence of therapy-resistant minimal residual disease. This necessitates the initiation of the post-consolidation phase, which has been demonstrated to improve both event-free survival and overall survival when immunotherapy is implemented, particularly using an anti-ganglioside 2 (GD2) antibody[116,117] combined with cytokines and retinoic acid.

However, the prognosis at relapse remains dismal, with less than 10% surviving beyond 10 years due to acquired resistance to chemotherapy and radiotherapy[118]. Therefore, new therapeutic strategies to improve survival and reduce long-term toxicities are urgently needed for treating high-risk NB at diagnosis as well as patients with relapsed or refractory disease[98,119].

Table 4. Risk-group treatment regimens followed in Europe based on SIOPEN directions.

Risk group	Induction	Surgery	Consolidation	Post-consolidation
Very low	-	Yes	-	-
Low	-	Yes	-	-
Intermediate	Carboplatin Cyclophosphamide Doxorubicin Etoposide	Yes	-	-
High	**Rapid COJEC:** Cisplatin Vincristine Carboplatin Etoposide Cyclophosphamide	Yes	**Myeloablative** Busulphan Melphalan **Radiotherapy**	**Retinoic acid** **Anti-GD2 therapy**

In recent years, several strategies have been developed for high-risk NB. First, chimeric antigen receptor (CAR) T-cell therapy has been emerging as a promising approach for relapsed or refractory cancers[120]. In particular, the targeting of GD2 with monoclonal antibodies has been associated with a significant survival benefit among high-risk NB patients, which has in turn supported the evaluation of GD2 as a relevant target for CAR-T therapy. In the latest clinical trial (NCT03373097), the use of GD2-CART01 was shown to be feasible and safe in treating high-risk NB, with evidence of antitumor activity[121]. These findings have helped to establish the basis for CAR-T approached in NB and have also encouraged the exploration of additional targets, such as B7-H3 or GPC2[121]. Second, the ALK inhibitors ceritinib and lorlatinib have shown tolerability and antitumor activity as monotherapy in children with relapsed NB harboring ALK alterations[122,123]. Notably, lorlatinib was also evaluated in combination with chemotherapy in a transatlantic trial[123] that incorporated serial ctDNA monitoring, thereby paving the way for the ongoing frontline evaluation of this agent in children with ALK-aberrant tumors. Finally, the phase II BEACON trial showed that the addition of the anti-VEGF monoclonal antibody bevacizumab to three backbone chemotherapeutics regimens used after relapse (irinotecan, topotecan and temozolomide) improved overall response rate and progression-free

survival[124]. However, the use of bevacizumab in combination with temozolomide alone in one of the BEACON trial arms will require further evaluation[125].

1.4 Metastasis

For over a century, researchers have investigated the intricate processes underlying metastasis. In 1889, Stephen Paget introduced the "seed and soil" theory, postulating that metastasis depends on a specific interplay between selected tumor cells (the "seed") and the microenvironment of a particular organ (the "soil")[126]. According to this theory, metastasis occurs only when the seed and soil are mutually compatible. Advances in molecular biology have substantiated this theory through the identification of metastasis-associated genes and the discovery of organ-specific growth factors and chemokines expressed by tissues colonized by tumor cells[127].

Metastasis, defined as the dissemination of malignant cells from a primary tumor to distant organs, is a highly complex and organized process and it encompass multiple interconnected steps. Tumor cells must leave the primary tumor, enter the circulatory system, travel to distant sites, exit the circulation, and proliferate in a new microenvironment (Figure 5)[128,129]. Evidence supports the idea that dissemination can occur early in tumor development, sometimes before clinical diagnosis. The process begins with local invasion, wherein malignant cells lose cell to cell adhesions and acquire motility, enabling them to invade adjacent tissues. Subsequently, during intravasation, tumor cells penetrate the endothelium of blood or lymphatic vessels to enter the systemic circulation[130].

Due to the harsh conditions of circulation, only a small fraction of circulating tumor cells survive, which can fuel heterogeneity among disseminated tumor cells (DTCs) between patients. In fact, although large numbers of cells can be released from the primary mass and detected in blood from patients, forming overt metastases requires further adaptive, colonization and outgrowth steps[131]. These extravasated

cells may form tumor aggregates or emboli with leukocytes and platelets, impairing an immune reaction and facilitating their retention at distant sites[132].

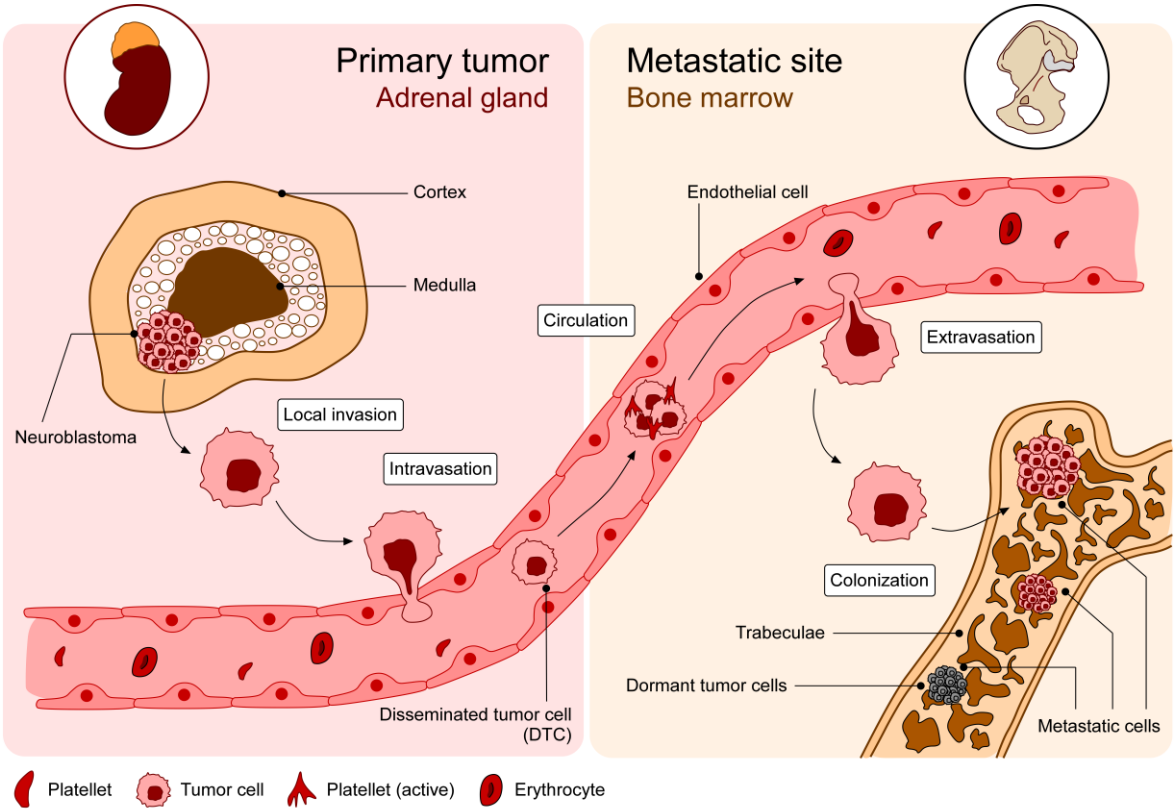

Figure 5. Schematic representation of metastatic cascade. NB cells originating from the adrenal gland (primary tumor) acquire invasive properties that enable local invasion and intravasation into the bloodstream. Once in circulation, tumor cells disseminate to distant organs, where they extravasate, invade the surrounding tissue, and proliferate to establish metastatic lesions. Common metastatic sites in NB include the bone marrow, where disseminated tumor cells may persist in a dormant state before reactivating and contributing to disease progression or relapse.

Following this retention, some tumor cells mechanically entrapped in capillaries can follow different paths. In some settings, they may proliferate within the vessel lumen, forming an intravascular cluster that can damage the vessel wall and lead to rupture[133]. Alternatively, they can exit the circulation by crossing the endothelium and the underlying matrix. Importantly, vascular structure varies by organ, which can shape where extravasation is more likely to happen. Liver and bone marrow capillaries are sinusoidal and feature fenestrated endothelial cells with a discontinuous basal lamina[134], features that may lower the physical barrier to transmigration and are aligned with the high frequency of liver and bone marrow involvement observed in NB metastasis[128,135]. By contrast, lung capillaries have

tighter endothelial junctions and a more continuous basement membrane, potentially limiting tumor cell extravasation and contributing to the relatively low frequency of lung metastases in NB. In the case of the central nervous system, the brain microvasculature is further stabilized by pericytes and astrocytic end-feet, forming the blood–brain barrier[128,134].

Following successful extravasation, the ability of tumor cells to establish metastatic lesions depends critically on their adaptation to the new microenvironment. Once in this environment, tumor cells are subjected to numerous environmental pressures that promote further transcriptional and epigenetic adaptations, thereby supporting tumor cell proliferation and the induction of an angiogenic response, which is essential for the development of metastasis[127]. In fact, tissue structure and composition vary widely across organs, therefore successful outgrowth in each site depends on distinct, organ-specific features[136]. Many pro-metastatic stromal components including cancer-associated fibroblasts and hematopoietic stem cells activate stem-cell support pathways including Wnt, TGF-β, bone morphogenetic protein (BMP), Notch and STAT3. Moreover, these stromal cells are also able to activate cell metabolism and survival pathways such as phosphoinositide 3-kinase–protein kinase B (PI3K–AKT), mitogen-activated protein kinase (MAPK) and hypoxia-inducible factor (HIF)[137]. It is known that some of these pathways also drive development and tissue regeneration; however, in metastatic settings, cancer cells frequently overactivate these pathways to sustain oncogenic signaling despite weak microenvironmental stimulation. Eventually, owing to the high energy demands associated with this process, some cells can survive in a dormant or slow-cycling state as disseminated tumor cells, forming a reservoir that may later drive metastatic outgrowht[130]. Reactivation from this quiescent state is thought to be influenced by microenvironmental cues, including changes in extracellular matrix composition, inflammatory signals, and the availability of growth factors, as well as systemic conditions and intrinsic cellular programs that reinitiate proliferation[138].

In many adult epithelial cancers, tumor progression usually follows a recognizable sequence from hyperplasia and dysplasia to in situ tumor and invasive disease[10], allowing lesion evolution to be monitored over time in some cases. By contrast, pediatric tumors often show rapid clinical progression and limited symptomatology during early stages, often hindering early detection. This results in a delayed diagnosis, frequently occurring when the disease has already reached an advanced stage where systemic symptoms appear aggressively[139]. NB illustrates this pattern, as approximately 50% of patients present with metastatic disease at the time of diagnosis[101].

Over the past decades, extensive research on NB has uncovered a variety of factors influencing tumor progression and overall prognosis, such as patient age, disease stage, tumor histology, molecular markers, and genetic abnormalities. While these advances have enhanced our knowledge of the heterogeneous characteristics of primary NB, metastasis—the primary driver of mortality in this cancer—remains poorly understood[140].

1.4.1 Bone marrow metastases in neuroblastoma

The bone marrow is one of the most common sites to be involved by tumors that metastasize via the bloodstream. In adults, the tumors that most frequently metastasize to the bone marrow are prostate, lung and breast carcinomas, although any tumor that is characterized by blood-borne metastases can infiltrate this niche[141,142]. In children, rhabdomyosarcoma, Ewing sarcoma, retinoblastoma and NB account for the majority of bone marrow metastases[53,143,144].

Bone marrow infiltration may be suspected based on several clinical and diagnostic findings: (1) bone pain, (2) pathological fractures or lesions demonstrated by radiology, (3) unexplained hot spots on isotopic bone scans or positron emission tomography (PET), (4) abnormal magnetic resonance imaging (MRI) findings, (5) hypercalcemia or elevated serum alkaline phosphatase activity or (6) unexplained

hematological abnormalities[145]. When bone marrow involvement is suspected, physical examination of the bone marrow through aspiration or trephine biopsy is performed to establish a definitive diagnosis and support complementary clinical findings[146].

Aspiration and trephine biopsy are most commonly performed from the ilium, particularly from the posterior iliac crest. Under local anesthesia, a fine needle is used to minimize risk and discomfort. In bone marrow aspiration, marrow material is aspirated through the needle, whereas in trephine biopsy, a small cylindrical sample of bone marrow is obtained within the needle[147].

Examination of the bone marrow by aspiration or trephine biopsy is an established part of NB staging. Rosettes of tumors cells around bone marrow material are found in up to two thirds of patients, and approximately half of patients present with a positive biopsy at the time of initial diagnosis, evidencing that the disease might have already spread to other sites[139,148,149]. However, evaluating bone marrow infiltration becomes particularly challenging in patients who have undergone chemotherapy, therefore performing trephine biopsy is crucial for accurate assessment in these cases[150,151].

A growing body of evidence indicates that tumor cells inhabit a specialized niche within the bone marrow, which not only facilitates their colonization but also supports their long-term survival[152,153]. The interaction between newly arrived tumor cells and this microenvironment plays a crucial role in helping cells adapt to their new environment. This adaptation reduces sensitivity to therapy through molecular and phenotypic changes, including the adoption of a prolonged dormant state.[153,154].

After tumor cells leave the primary tumor site, bone marrow hematopoietic cells contribute to tumor inflammation, vascularization and subsequent metastasis. Interestingly, this phenomenon may be explained by the fact that hematopoietic cells are developmentally related to endothelial progenitors, with both potentially

arising during embryonic development from a common hemangioblast[155]. VEGFR1-positive hematopoietic precursor cells can colonize the tumor where they contribute to inflammation, and they can also prime distant organs for the establishment of metastatic cells[156]. In addition, VEGFR2-positive hematopoietic precursor cells contribute to vasculogenesis by providing an additional source of endothelial cells that merge with mature endothelial cells originating from surrounding tumor tissues[127].

There is clear evidence that cytokines (IL-6, IL-7, IL-11, TNF-α, M-CSF, LIF) and growth factors (IGF-1, EGF, TGF-β and BNDF) released from the bone matrix play an important role in promoting the survival and proliferation of NB cells in the bone marrow upon arrival[127]. Particularly, the majority of NB cells express IGF-1 receptor, which activates MAPK and PI-3K pathways and inhibits Caspase-3 activation upon ligand binding[157]. This results in an increased trans-endothelial cell migration and adherence of tumor cells, as well as a protective state in front of apoptosis activation[158,159]. Moreover, NB cells also express *EGFR1* and *TrkB*, which are activated by EGF/TGF-α and BDNF, respectively. These activations trigger stimulation of cell proliferation and survival through the activation of MAPK, PI-3K/Akt and PKC pathways, allowing tumor cells to proliferate in this organ and evade chemotherapy-induced cell death[160–163].

In summary, the bone marrow provides a supportive metastatic niche for NB cells, promoting survival, proliferation, and resistance to therapy. A better understanding of the mechanisms underlying bone marrow colonization and dormancy may reveal new therapeutic targets in metastatic NB.

1.4.2 Liver metastases in neuroblastoma

Hepatic metastases occur in approximately 30% of patients with metastatic NB, with age-dependent distribution patterns[99,100]. In infants younger than 12 months, liver involvement is substantially more common, affecting 40% of cases, compared to

only 11% in children 18 months or older[100]. This age-related pattern is most pronounced in stage 4S disease, where hepatic metastases are present in over 80% of cases[100].

Within stage 4S NB, infants with non-amplified *MYCN* and hepatic metastases without bone or orbital involvement usually show a favorable course, often characterized by spontaneous regression or limited therapeutic requirements. This distinctive metastatic pattern, designated as stage 4S by D'Angio, Evans, and Koop in 1971[164], has been validated in subsequent studies, with up to 50% of cases resolving without cytotoxic therapy[165–167]. Therefore, liver involvement in stage 4S NB does not negatively impact event-free survival in this age group[166].

However, this favorable prognosis is age-dependent and influenced by the presence of other metastases. While infants with isolated liver metastases generally have excellent outcomes, the presence of concomitant bone or orbital involvement predicts poor survival even in this age group[168]. Moreover, in children 18 months or older, hepatic metastases represent the metastatic site with the highest negative impact on survival[100] and correlate with aggressive tumor biology. Indeed, in this older age group, liver metastases are significantly associated with *MYCN* amplification (40% vs. 29% in patients without hepatic involvement), 1p chromosomal deletion, and markedly elevated serum LDH levels at diagnosis[100]. Additionally, the presence of hepatic metastases is higher in patients with primary tumors in the adrenal gland (69% of cases) and frequently co-occur with pulmonary metastases, suggesting shared biological mechanisms of hematogenous dissemination[100]. This age-dependent prognostic shift, observed in large patient cohorts, demonstrates that both tumor biology and patient age critically determine metastatic behavior.

Emerging evidence suggests that organ-specific adhesion mechanisms may influence NB liver colonization. Studies on hematogenous metastasis demonstrate that metastatic cells adhere preferentially to cryostat sections of their target

tissues[169–171172]. This phenomenon suggests that tumor cell-host adhesion contributes significantly to organ-specific metastatic tropism[173,174].

These biological insights have important therapeutic implications. Given the favorable natural history of stage 4S disease, treatment de-escalation strategies have been proposed for infants with hepatic metastases, even in the presence of limited bone involvement[175]. Multiple reports document long-term survival in infants with hepatic metastases who received minimal or no chemotherapy, supporting individualized therapeutic approaches based on tumor characteristics and patient age[175]. Nevertheless, in cases with rapidly progressive hepatomegaly or clinical deterioration, chemotherapy remains effective and should be continued until regression of liver metastasis is achieved[176]. Radiotherapy is generally avoided in these young children due to risks of nephrotoxicity and impaired bone growth[177,178].

Importantly, recent data suggest that treatment intensification has mitigated the historically poor prognosis associated with hepatic metastases in older children. Morgenstern et al. (2016)[100] demonstrated that the adverse prognostic impact of liver involvement in patients ≥18 months is neutralized when treated with stem cell transplantation (SCT)-inclusive regimens, suggesting that aggressive multi-modal therapy can overcome the therapeutic resistance traditionally associated with hepatic disease. This finding underscores the importance of risk-adapted treatment stratification based on both metastatic pattern and patient age.

Despite these clinical observations, the molecular mechanisms underlying age-dependent hepatic metastatic behavior in NB remain incompletely understood. Elucidating these mechanisms—particularly the interplay between tumor intrinsic factors (*MYCN* amplification, 1p deletion), age-related hepatic microenvironmental changes, and cell adhesion molecules—could refine risk stratification and optimize treatment strategies for patients with hepatic metastases.

1.4.3 Lymph node metastases in neuroblastoma

Lymph node (LN) involvement occurs in approximately 30% of stage 4 NB patients at diagnosis[99,100]. LN metastasis can be classified as regional (ipsilateral or contralateral to the primary tumor) or distant, with distinct prognostic implications. While regional LN involvement in localized disease correlates with worse outcomes, distant LN metastasis without extranodal organ involvement—designated as 4N disease—has been associated with more favorable prognosis in selected patient subgroups[179–181], although this survival advantage appears influenced by patient age and treatment intensity[100].

Notably, patients with distant LN metastasis exhibit distinct biological features including absence of *MYCN* amplification, elevated urinary HVA levels, and unique catecholamine profiles[181]. These findings suggest that LN metastasis may represent a biologically distinct entity with different mechanisms of colonization.

Despite these well-documented clinical observations, the molecular mechanisms governing LN colonization in NB remain poorly understood. Whether the favorable prognosis associated with distant LN involvement reflects intrinsic tumor biology, organ-specific microenvironmental factors, or host immune responses is unclear. The transcriptomic and epigenetic adaptations enabling NB cells to colonize lymphoid tissue—and the factors determining progression from regional to distant LN spread—have not been systematically investigated, warranting further research to refine risk stratification and treatment strategies.

1.4.4 Lung metastases in neuroblastoma

Although almost all metastatic NB tumors are found throughout the bone marrow, lymph nodes and liver, lung metastases indicate the most advanced disease and confer the worst prognosis with a 5-year survival rate of less than 40%[182]. This statement confirms the previously reported low incidence (<4%) of lung metastasis at initial diagnosis in patients with stage 4 NB[99,183,184], which represents a unique

characteristic, as the lung is the most common site of metastasis in most other pediatric extra-cranial solid tumors. Thus, the etiology for this low incidence of lung metastasis in NB remains unclear, particularly since an early analysis of the metastatic pattern in NB concluded that metastasis does not passively follow the pattern of blood flow[185].

These observations suggest that specific features of the pulmonary microenvironment are hostile to NB growth upon arrival, which may result in dormant micrometastases that are initially cell-cycle arrested by viability-inhibitory factors in the lung[186]. These dormant cells may subsequently progress to actively growing macrometastatic lesions, causing late metastatic relapse[187,188]. Critically, the ability of dormant cells to become activated is largely determined by their interaction with the microenvironment at the secondary site[129,189,190]. However, the specific mechanisms that maintain dormancy and regulate the transition to progressive growth remain largely unknown[189,191], and this activation may represent a late event in disease progression due to the aggressive features of reactivated clones[182].

In clinical practice, among children with documented pulmonary metastasis, lung disease correlates with MYCN amplification and is associated with LDH elevation, metastasis to the CNS, and poor outcome[99]. However, detecting pulmonary involvement presents diagnostic challenges. One problem is the distinction between extension of a primary tumor into the thorax, which has favorable biological features, and discrete pulmonary metastases[192]. Without biopsy confirmation, this distinction may be difficult or impossible[184]. Consequently, the reported 4% incidence may be underestimated, as not all patients undergo detailed chest imaging in routine clinical practice for non-thoracic primary tumors[182].

Altogether, patients with stage 4 NB rarely have detectable lung metastasis at initial diagnosis. However, those diagnosed with lung metastases present a more aggressive clinical course, with increased risk for early disease progression and early

death. Considering all the aforementioned reasons, future investigations should focus on the impact of interactions between factors in the pulmonary microenvironment and tumor cells, given that the mechanisms of microenvironmental control remains incompletely understood and tumor cells presence may alter its natural behavior[193].

1.4.5 Metastatic models in neuroblastoma

Several experimental models have been used to study metastatic NB over the past decades. These approaches include systemic injection models, orthotopic xenografts, genetically engineered mouse models (GEMMs), direct organ injection strategies, and, more recently, patient-derived xenografts (PDXs). Each of these systems reproduces distinct aspects of metastatic disease, and their use depends largely on the biological or therapeutic question being addressed (Table 5)[194].

Table 5. Models for development of metastatic neuroblastoma in mice.

	Systemic injections	Orthotopic/ subcutaneous	GEMMs	Direct injection	PDXs
TUMOR SPECIES	Human/Mouse	Human/Mouse	Mouse	Human/Mouse	Human
ADVANTAGES	-Resembling latter phases of metastatic cascade -Targets are human	- Resembling full metastatic cascade -Targets are human	-Immune competent -Native tissue microenvironment -Spontaneous tumor development	-Tumor growth in desired organ -Rapid tumor growth -Targets are human	-Tumor retains original histological and molecular human features -Represents diversity and complexity of human disease
LIMITATIONS	-Omits primary tumor and intravasation -Restricted to existent NB cell lines	-Time consuming -Restricted to existent NB cell lines	-Limited tumor heterogeneity -Targets are murine -Expensive and time consuming -Lack of metastasis in relevant metastatic sites	-Not resembling metastatic cascade -Restricted to existent NB cell lines	-Non-immune system environment -Ethical constrains -Expensive and time consuming

Among the most widely used approaches, systemic delivery of tumor cells through tail-vein or intracardiac injection allows the study of metastatic colonization after entry into the circulation[195–197]. In mice, both injections have been commonly used to introduce tumor cells into the bloodstream and to evaluate their ability to survive in circulation, arrest in distant organs, and generate metastatic lesions. Because these approaches bypass primary tumor formation, local invasion and intravasation, it is mainly suited to the analysis of late metastatic events such as organ colonization and metastatic burden rather than the full metastatic cascade[194]. Indeed, given that approximately half of NB patients already present with metastatic disease at diagnosis, current research has increasingly focused on understanding the

proliferative and adaptive capacities of metastatic cells within distant organs, rather than on the full sequence of metastatic events.

Other models aim to provide a more disease-relevant anatomical context. In particular, GEMMs have been generated based on modeling some of the clinically relevant NB features including MYCN amplification[54] or ALK mutations[59]. However, spontaneous dissemination to clinically relevant metastatic sites are infrequent in this setting[198]. Orthotopic xenografts, in contrast, have been described to metastasize to clinically relevant metastatic organs[199]. Alternatively, direct injection of NB cells into bone marrow cavity or the liver parenchyma can be used to investigate tumor-microenvironment interactions at metastatic locations, although these approaches do not model dissemination itself[200].

PDX-based models, although reported as early as 1984, have recently emerged as a promising alternative because they may retain key human biological features of the original tumor such as chromosome 1p or 11q losses and 17q gains that would be particularly challenging to models using GEMMs. Moreover, they have been described to be patient-replicative models, particularly when implanted orthotopically[201]. These models may therefore offer improved clinical relevance for studying tumor behavior and preclinical testing of new drugs to be evaluated, including the identification of predictive biomarkers of response and mechanisms of drug resistance[202,203]. However, their application remains limited by the requirement for immune-deficient mice, limiting the ability to test immunotherapies, and the availability of suitable patient samples[204].

Overall, current NB metastasis models should be considered as complementary systems that provide distinct but equally relevant insights into different aspects of the disease.

2.HYPOTHESIS AND OBJECTIVES

Given that approximately half of NB patients present with metastatic disease at diagnosis, and that metastasis remains the leading cause of mortality, there is a critical need to better understand the mechanisms underlying disease progression and metastatic colonization. In this context, epigenetic deregulation may play a fundamental role not only in tumor initiation but also in adaptative processes that enable tumor cells to survive, disseminate and establish proliferative growth in distant organs.

Deciphering the chromatin and transcriptional programs associated with metastatic colonization is therefore essential to characterize the molecular features that support NB adaptation to distant microenvironments. Identifying genes and regulatory pathways that are indispensable for this process may reveal vulnerabilities whose perturbation could impair metastatic growth and provide new opportunities for therapeutic intervention.

We therefore hypothesize that epigenetically driven chromatin and transcriptional programs acquired during metastatic colonization are required for NB adaptation to distant microenvironments, and that their perturbation will impair metastatic growth and uncover therapeutic vulnerabilities. Based on this rationale, three main objectives were defined to guide the development of this thesis:

1. To develop clinically representative metastatic neuroblastoma mouse models

2. To characterize the epigenetic reprogramming associated with metastatic neuroblastoma

3. To identify therapeutic targets through the epigenetic profiling of neuroblastoma metastases

3. MATERIALS AND METHODS

3.1. Cell lines and tissue culture

Ten different NB cell lines were used during the course of this work: SK-N-BE(2), SH-SY5Y, SK-N-AS, CHLA-90, NBL-S, LAN-6, LAI-5S, KELLY, IMR-32 and SK-N-FI cell lines (Table 6). Cell line features are listed in Table 4. SK-N-BE(2), SH-SY5Y, SK-N-AS and IMR-32 cell lines were purchased from American Type Culture Collection (ATCC, Manassas, VA, USA); LAI-5S and KELLY cell lines were procured from the Public Health England Culture Collection (Salisbury, UK); NBL-S and LAN-6 cell line were obtained from Leibniz Institute DMSZ (Braunschweig, DE). CHLA-90 cell line was obtained from the Children's Oncology Group Cell Culture and Xenograft Repository (Lubbock, TX, USA) and SK-N-FI cell lines was delivered by the Memorial Sloan Kettering Cancer Center (MSKCC, New York, NY, USA). All NB cell lines were cultured, as suggested by Children's Oncology Group Cell Culture and Xenograft Repository, in Iscove's modified Dulbecco's medium (IMDM, Gibco, Amarillo, TX, USA) except KELLY that was cultured in Roswell Park Memorial Institute 1640 (RPMI, Thermofischer Scientific, Waltham, MA, USA), supplemented with 10% heat-inactivated fetal bovine serum (FBS; South America Premium, Biowest, Nuaillé, France), 1% insulin-transferrin-selenium supplement (Gibco), 100 U/mL penicillin, 100 µg/mL streptomycin (Gibco), and 5 µg/mL plasmocin (InvivoGen, San Diego, CA, USA).

All cultures were maintained at 37 °C in a 5% CO_2 saturated atmosphere, and biannually tested for mycoplasma contamination. All cell lines grew in adhesion as monolayer. Before reaching confluence, cells were rinsed once with phosphate-buffered saline (PBS; Hyclone Laboratories, Logan, UT, USA) and detached using 0.05% trypsin (Gibco) or non-enzymatic cell dissociation buffer (Gibco), collected with fresh medium, centrifuged for 3 minutes at 800 rpm, resuspended and cultured in new plates or flasks with fresh medium.

Cell counting was performed by mixing a 10 µl sample of cell suspension with 10 µl of 0.4% trypan blue and loading 10 µl of the mixture onto Cell Counting slides (NanoEntek, Seoul, South Korea); viable cell number was determined using Cell Counter EVE (NanoEntek).

For cell line storage, cells were cryopreserved in FBS with 10% dimethyl sulfoxide (DMSO) by slow freezing using an isopropanol freezer container at -80ºC, prior to immersion into liquid nitrogen. Resuscitation of frozen cells was performed by rapid thawing at 37ºC, dilution of cells into fresh medium, centrifugation, resuspension and plating in fresh medium.

Table 6. Neuroblastoma cell lines molecular features extracted from ExPASy's Cellosaurus data base.

Cell line	Origin	Stage	MYCN status	TP53 status	Gender	*11q*
SK-N-BE (2)	Bone marrow	4	Amplified	Not functional	M	WT
SHSY-5Y	Unknown	4	Non-amplified	WT	F	WT
SK-N-AS	Brain	4	Non-amplified	Not functional	F	Loss
CHLA-90	Bone marrow	4	Non-amplified	Not functional	M	WT
NBL-S	Adrenal gland	3	Non-amplified	WT	M	Loss
LAN-6	Bone marrow	4	Non-amplified	Deleted	M	WT
LAI-5S	Bone marrow	4	Amplified	Not functional	M	WT
KELLY	Brain	Unk.	Amplified	Not functional	F	WT
IMR-32	Abdominal mas	4	Amplified	WT	M	WT
SK-N-FI	Bone marrow	Unk.	Non-amplified	Not functional	M	WT

11q column refers to Chromosomal 11q status. WT: Wildtype.

3.1.1 Vector transduction

NB cells were transduced with a lentiviral vector referred to as FLUC, which contains a constitutively expressed mCherry reporter gene and the firefly luciferase gene. FLUC plasmid (CSCW2-Fluc-ImC) was kindly provided by Dr. Rana Moubarak (New York University)[205]. The latter encodes an enzyme that catalyzes the oxidation of luciferin, enabling bioluminescent detection of tumor cells in vivo. Lentiviral particles carrying the FLUC construct were produced in HEK293T cells during 48-72h after lipofectamine 2000 transfection and used to infect NB cell lines, allowing for stable

genomic integration and constitutive expression of both reporter genes. This dual-reporter system enables simultaneous visualization by fluorescence microscopy and quantitative monitoring of tumor burden through bioluminescence imaging.

3.2. Development of in vivo neuroblastoma mouse models

Experimental procedures involving animals were performed at the Rodent Platform of the Laboratory Animal Service of Vall d'Hebron Institute of Research (LAS, VHIR, Barcelona, Spain). All animal protocols were reviewed and approved according to regional Institutional Animal Care and Ethical Committee of Animal Experimentation (CEEA: 39/20).

SK-N-BE(2), SH-SY5Y, SK-N-AS, CHLA-90, NBL-S, LAN-6, LAI-5S, KELLY, IMR-32 and SK-N-FI cell lines were used to develop primary and NB metastatic mouse models. The metastatic experimental models were generated by the intravenous injection of 2×10^6 NB-FLUC cells in 200 µL of PBS into 5-week old Fox Chase SCID beige mice (Charles River, Wilmington, MA, USA). This mouse strain was developed by intercross of C.B-17 SCID/SCID to C57BL/6 bg/bg mice, and carries both autosomal recessive SCID and beige mutations, which produce severe combined immunodeficiency affecting both the B and T lymphocytes, and defective natural killer (NK) cells, respectively.

Mice were monitored at two levels. On the one hand, luciferase activity was used for in vivo bioluminescence imaging (IVIS) at the indicated time points. Mice were anesthetized by isoflurane inhalation and intraperitoneally injected with D-luciferine (Invitrogen, Waltham, MA, USA). Luciferase signal was acquired using an IVIS SpectrumCT In Vivo Imaging System (PerkinElmer, Waltham, MA, USA), and visualized and quantified using Living Image Software 4.5.2 (Perkin Elmer). Average photon counts from same-duration expositions were calculated for the whole body of each mouse and normalized by extraction of background signal. On the other hand, mice were routinely monitored for symptomatology such as suffering signs or

apparition of palpable metastatic lesions, marking the ending point of the experiment for the individual mouse, which was euthanized. This follow-up also allowed the performance of survival analyses between groups.

When euthanized, macro-metastatic lesions were identified and extracted. Moreover, other potential metastatic loci were also extracted to detect micrometastatic niches such as: brain, tongue, heart, lungs, kidneys, adrenal glands, ovaries, phallopian tubes and uterus, leg bones and muscle, liver, stomach, spleen, pancreas and gut. To characterize both macro- and micrometastatic focuses, organs were fixed in formaldehyde 3,7-4% pH=7 (Labbox Labware, Barcelona, ES) for 48-72h and then maintained in PBS until embedded in paraffin.

For primary tumor formation, $5x10^6$ cells from each cell line were injected subcutaneously into the flank in Matrigel (Corning, NY, USA) in a 1:1 ratio to generate primary tumors (n = 5 per cell line). Subcutaneously injected mice were monitored at two levels. First, luciferase activity was used for in vivo bioluminescence imaging (IVIS) at the indicated time points, as explained above. Second, tumor measurements were performed twice or three times per week using a caliper in order to monitor tumor volume. End point criteria was determined by tumor volume >1000 mm^3.

3.2.1 Immunohistochemistry

Tissues were dehydrated by applying different alcohol (VWR Chemicals, Radnor, PA, USA) and xylene (PanReac Applichem, Barcelona, ES) cycles at different timings and concentrations. Next, samples were covered with liquid paraffin (50 to 70ºC) and left to dry. For tissue sectioning, tissues were cut to a thickness of 3-4 µm of using a microtome (Epredia HM, PHC Holdings, Tokio, JPN) before placing them on glass slides (Epredia HM, PHC Holdings).

3.2.1.1 Haematoxylin-Eosin staining

Hematoxylin & Eosin staining was carried out with the platform Tissue-Tek Prisma Plus automated slide stainer (Sakura Finetek USA, Torrance, CA, USA) harboring 5 different steps: Heat up, removal of paraffin, hematoxylin (Merck KGaA, Darmstadt, GE) staining, eosin (PanReac Applichem) staining and assembly (Table 7).

Table 7. Haematoxylin-Eosin staining protocol.

Step	Reagent/Action	Duration
Sample heating	Heat in oven	20 minutes
Deparaffinization	Xylene, 2 baths	10 minutes each
	Absolute alcohol, 2 baths	5 minutes each
	95º Alcohol, 2 baths	5 minutes each
	Distilled water	5 minutes
Hematoxylin staining	Hematoxylin, 2 dips	3 minutes each
	Running water	1 minute
	Hydrochloric acid	9 seconds
	Distilled water	30 seconds
	Ammoniacal water	1 minute
	Running water	1 minute
Eosin counterstaining	Eosin	30 seconds
	95ºAlcohol, 2 baths	6 seconds each
	Absolute alcohol	6 seconds
	Xylene, 2 baths	6 seconds each
Mounting	Automated mounting	---

3.2.1.2 Chromogranin A staining

Immunohistochemical staining was performed using the Benchmark Ultra staining module (Ventana Medical Systems, Oro Valley, AZ, USA) and the ultraView Universal DAB Detection Kit (Ventana Medical Systems).

The process began with deparaffinization using EZ Prep™ solution (10x, Ventana Medical Systems). Antigen retrieval was then performed with Cell Conditioning Solution 1 (CC1, Pre-diluted, pH 8, Ventana Medical Systems). The primary antibody, Anti-Chromogranin A (LK2H10), Mouse Monoclonal (Pre-diluted, Ventana Medical Systems), was applied and incubated for 15 minutes.

Following primary antibody incubation, the antigen-antibody complex was detected using the Universal HRP Multimer secondary antibody. The resulting complex was visualized using hydrogen peroxide as the substrate and 3,3'-tetrachlorodiaminobenzidine (DAB) as the chromogen. A counterstaining was performed with hematoxylin (Ventana Medical Systems), followed by Bluing Reagent (Ventana Medical Systems) to enhance nuclear contrast.

Upon completion of the automated staining protocol, the tissue samples were dehydrated and mounted for observation under a light microscope.

3.2.2 Isolation of NB cells from primary and metastatic tissues

Mice were euthanized once they reached the predefined humane endpoint criteria. Given the different biological and clinical features of the models used, humane endpoint criteria were defined separately for the metastatic and primary tumor settings. When euthanized, subcutaneous primary tumors along with livers and leg bones including tibia, peronei and femur were collected for posterior procedures.

Primary tumors and livers were mechanically dissociated and, after one PBS wash step, incubated with 2 mL of 1X Accutase dissolved in Dulbbecos PBS (Fisher Scientific, Waltham, USA) during 5-10 min at 37ºC. Next, each homogenate containing one dissociated liver or primary tumor was filtered through a 100 µm cell strainer (Corning Inc., Corning, NY, USA), diluted in 5 mL of media and centrifuged for 5 minutes at 1500 rpm. Supernatant was discarded and pellet resuspended in 2 mL erythrocyte lysis buffer (Qiagen, Hilden, Germany) and incubated for 10 minutes on ice. Homogenates were centrifuged again for 5 minutes at 1500 rpm and pellets resuspended in 10 mL of media. The resulting single cell suspension containing a mix of mouse hepatocytes and human NB cells (for liver samples) or other mouse cells and human NB cells (for primary tumor samples) was counted using Cell Counter EVE (NanoEntek).

After that, human cell populations present in the liver and primary tumor were enriched with the Mouse Cell Depletion Kit, following manufacturer's instructions, using one purification LS column for each liver or primary tumor in a QuadroMACS magnetic cell separator (Miltenyi Biotec, Bergisch Gladbach, Germany). Final purified cell eluates were counted again in Cell Counter EVE (NanoEntek).

Leg bone tissues were mechanically dissociated to extract bone marrow cells. Next, each homogenate containing bone and bone marrow cells was washed in PSB, centrifugated at 1500 rpm for 5 min, resuspended in media and then filtered through a 100 µm cell strainer (Corning). After that, cell suspension was centrifuged for 5 minutes at 1500 rpm. Supernatant was discarded and pellet resuspended in 2 mL erythrocyte lysis buffer (Qiagen) and incubated for 10 minutes on ice. Homogenates were centrifuged again for 5 minutes at 1500 rpm and pellets resuspended in 3 mL of media. The resulting single cell suspension containing a mix of mouse bone cells and human NB cells was counted using Cell Counter EVE (NanoEntek).

3.2.3 Cell sorting

Liver, primary tumors and bone cell suspensions were then centrifugated for 5 minutes at 1500 rpm, resuspended in 200 µL of PBS stained with a 1:2000 dilution of Live/Dead Violet fluorescent viability marker (Invitrogen), and incubated during 5 minutes at room temperature. Afterwards, cells were centrifugated again and resuspended in PBS 1X supplemented with 5% FBS and 2 mM EDTA (Merck).

Finally, these cell populations were analyzed and sorted using an Aurora CS (Cytek Bioscience, Fremont, CA) flow cytometer for mCherry, and Live/Dead Violet detection at the Flow Cytometry facility of Vall d'Hebron Institute of Research. Among the viable and single cell population, mCherry positive and Live/Dead negative were identified as alive human NB cells and sorted for posterior analyses, in contrast with the residual mouse hepatocytes or mouse bone cells, negative for mcherry, that were rejected.

3.3 Genomic analyses

3.3.1 RNA-sequencing

Cell pellets after 5 min centrifugation at 1500rpm were obtained after Aurora CS sorting of mCherry positive and Live/Dead negative cells and stored at -80ºC until processing. RNA extraction was performed after -80ºC storage by resuspending cells in 700 µL of Qiazol lysis buffer (Qiagen) and total RNA was extracted using the miRNeasy mini extraction kit (Qiagen), following the manufacturer's instructions. An additional in-column step of DNAse I treatment (Qiagen) was performed for 15 minutes at room temperature to minimize the contamination with genomic DNA. Total RNA was eluted in 20 to 25 µL of RNAse-free water and then stored a -80ºC until processing.

RNA-seq experiments were performed with three biological replicates of primary tumors and liver metastases per each cell line. Samples were quantified using Qubit fluorometric quantification (Thermo Fisher Scientific) and the quality was evaluated using Bioanalyzer (Agilent). Libraries were prepared at the Institute for Research in Biomedicine (IRB Barcelona) and sequencing was performed at the Centre for Genomic Regulation (CRG) Genomics Unit using the Illumina HiSeq2500 sequencer.

Raw RNA-seq reads were subjected to adapter and quality trimming using Trim Galore v0.3. Cleaned reads were then aligned to the human reference genome hg38 using STAR v2.7.10a with default alignment parameters. Gene-level read counts were obtained for each sample using the feature.

Counts function from the Rsubread R package v2.8.2 with default settings. Differential gene expression analysis was performed with DESeq2 v1.34.0. The package was used to estimate log2 fold changes and assess the statistical significance of contrasts between conditions. Expression values were normalized using the variance stabilizing transformation (VST) implemented in DESeq2 for downstream analyses such as clustering and visualization.

3.3.2 ATAC-sequencing

Cells for ATAC-seq were obtained after Aurora CS sorting of mCherry positive and Live/Dead negative cells. Cells were centrifugated for 5 minutes at 1500rpm and then resuspended in the following cryopreservation medium: FBS 50%, IMDM 40% and DMSO 10% before storage in liquid nitrogen until processing at the Institute for Research in Biomedicine (IRB Barcelona). Cryopreservation medium was selected according to Fujiwara et al., (2019) protocol. Briefly, 10,000-50,000 primary tumor or liver/bone marrow metastatic cells were collected in triplicates and treated with transposase Tn5 (Nextera DNA library preparation kit, Illumina). DNA was purified using a PureLink quick gel extraction and PCR purification combo kit (Introgen). All samples were PCR-amplified using NEBNextHigh-Fidelity 2x PCR Master Mix (New England Biolabs, Ipswich, MA, USA) with primers containing a barcode to generate libraries and a C1000 Touch Thermal Cycler (BioRad). The DNA was purified again using a PureLink quick gel extraction and PCR purification combo kit. Samples were quantified using Qubit fluorometric quantification (Thermo Fisher Scientific) and the quality was evaluated using Bioanalyzer (Agilent). Sequencing was performed at the Centre for Genomic Regulation (CRG) Genomics Unit, using the Illumina HiSeq2500 sequencer.

Raw sequencing reads were pre-processed and quality-controlled prior to downstream analysis. Adapter trimming and quality filtering were performed with NGmerge v0.3. Trimmed reads were aligned to the human reference genome hg38 using Bowtie2 v2.3.5 with the --very-sensitive option. PCR and optical duplicates were identified and removed with sambamba markdup v1.0.0. Insert size metrics were calculated using Picard tools v1.98. Per-sample TSS enrichment scores were computed following ENCODE TSS enrichment standards (see ENCODE guidelines HTML).

Peaks were called on each sample group (side × type × cell line combination) using Genrich v0.6.1. Peak annotation to nearest genes and genomic features was

performed with HOMER v5.1 (hg38, v7.0 annotation). A set of consensus peaks was defined as the union of all Genrich-called peaks across conditions; these intervals were merged (reduced) using the reduce function from the IRanges R package v2.28.0. For each sample, read counts per consensus peak were obtained with the featureCounts function from the Rsubread R package v2.8.2, explicitly ignoring duplicated reads.

Differential chromatin accessibility between pairwise conditions was assessed using DESeq2 v1.34.0 on raw counts. Unless otherwise stated, analyses did not include covariate adjustment.

3.4 Data and statistical analysis

3.4.1 Principal component analysis (PCA)

Principal component analysis (PCA) of metastatic cell lines was performed using the web-based tool ClustVis: a web tool for visualizing clustering of multivariate data (BETA) - custom edition, version 2.0 (Metsalu, Tauno and Vilo, Jaak. Clustvis: a web tool for visualizing clustering of multivariate data using PCA and heatmap. Nucleic Acids Research, 43(W1):W566–W570, 2015. doi: 10.1093/nar/gkv468.). The analysis utilized engraftment frequencies by metastatic organ and cell line, which were subsequently clustered according to genetic background.

3.4.2 ATAC-seq

For multivariate exploration, PCA was applied to the variance-stabilizing transformed (VST) count matrix. No adjustments for potential confounding variables were performed prior to PCA.

Gene ontology (GO) analyses were performed using The Database for Annotation, Visualization, and Integrated Discovery (DAVID) platform[206,207]. GO annotations presenting FDR<0.05 were used for this analysis.

3.4.3 RNA-seq

For multivariate exploration, PCA was applied to the VST count matrix. No adjustments for potential confounding variables were performed prior to PCA.

Gene ontology (GO) analyses were performed using The Database for Annotation, Visualization, and Integrated Discovery (DAVID) platform[206,207]. GO annotations presenting FDR<0.05 were used for this analysis.

3.4.4 ATAC-seq and RNA-seq integration

To integrate epigenomic and transcriptomic data, thresholds were adjusted to allow a broader inclusion of candidates. For ATAC-seq, liver-associated peaks showing a p-value<0.05 in comparison versus primary tumor were selected independently for each cell line. All peaks categories were considered. Gene annotations corresponding to peaks overlapping in three or more cell lines were further selected. For RNA-seq, significantly deregulated genes were defined using a p-value<0.05 in liver versus primary tumor comparisons for each cell line. To overlap gene lists, Multiple List Comparator from Molbiotools was used. Genes overlapping in at least three cell lines were selected to be integrated to filtered ATAC-seq peak-associated genes. Subsequently, overlap of ATAC- and RNA-seq genes that were present in three or more cell lines allowed the analysis of correlation between epigenomic and transcriptomic modulations in liver metastases as well as the identification of potential targets for the treatment of metastatic NB.

For ATAC-seq peaks visualization of potential candidates, the UCSC Genome Browser[208] website was used. To prioritize candidate targets, gene expression data and Kaplan-Meier curves were explored using the R2 platform[209] (including NBAtlas platform). Particularly, two different datasets were used: GSE45547 and GSE253865. Single cell analysis of healthy tissues was performed using the CELLxGENE Discover plaform from Tabula Sapiens[210] and dependency analysis was performed using the CRISPR (DepMap Public 26Q1+Score, Chronos) data from DepMap[211].

4. RESULTS

4.1 Neuroblastoma cell lines recapitulate distinct metastatic patterns of human metastatic dissemination

With the goal of developing an experimental mouse model that recapitulates the pattern of metastasis in NB patients, we selected a panel of 10 NB cell lines stably-transduced with a lentiviral vector encoding the firefly luciferase reporter gene. This panel comprises cell lines representing major genetic features of NB including *MYCN* status, 11q deletion and *p53* mutation, thereby broadening the genetic scope of the study (see Table 6). These cells were injected in the tail vein of immunosuppressed SCID beige mice, followed by monitoring of tumor growth using in vivo luminescence imaging monitoring and clinical assessment by palpation. For all established models, bioluminescence imaging was performed 2 hours after cell injection to confirm the successful injection of viable cells (Figure 6). IVIS acquisition confirmed the presence of tumor cells in the lungs, consistent with the lungs being the first capillary bed reached following entry into the venous circulation.

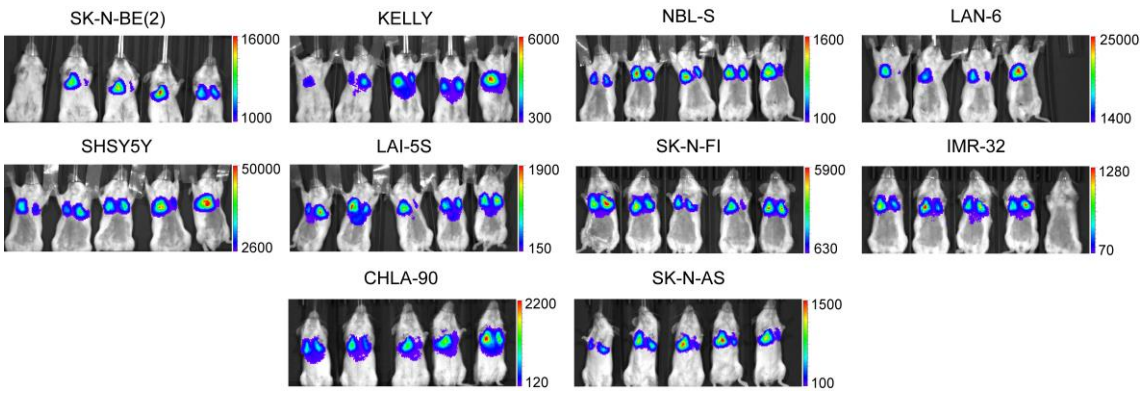

Figure 6. *In vivo* luminescence imaging 2h post-injection of tail-vein metastatic models. A panel of 10 different NB cell lines (SK-N-BE(2), KELLY, NBL-S, LAN-6, SHSY5Y, LAI-5S, SK-N-FI, IMR-32, CHLA-90 and SK-N-AS) was injected intravenously in 5 mice per group.

All injected cell lines, with the exception of LAI-5S and SK-N-FI, resulted in an increased luminescence signal over time (Figure 7A). Some cell lines, like SK-N-BE(2), SHSY-5Y, NBL-S, and CHLA-90, displayed a clear pattern of accumulation in the mid-ventral area (Figure 7A), consistent with preferential involvement of central visceral

organs. In contrast, KELLY, SK-N-AS, LAN-6, and IMR-32 exhibited a more dispersed distribution of signal across multiple anatomical sites, indicative of broader metastatic dissemination (Figure 7A). Three cell lines—SK-N-BE(2), SK-N-AS, and CHLA-90—showed an additional strong luminescent signal in the leg bones (Figure 7A). Despite differences in luminescence distribution across cell lines, all lines except LAI-5S and SK-N-FI proliferated progressively, reflected by increasing luminescence over time. We quantified this signal increase as measure of tumor growth (Figure 7B).

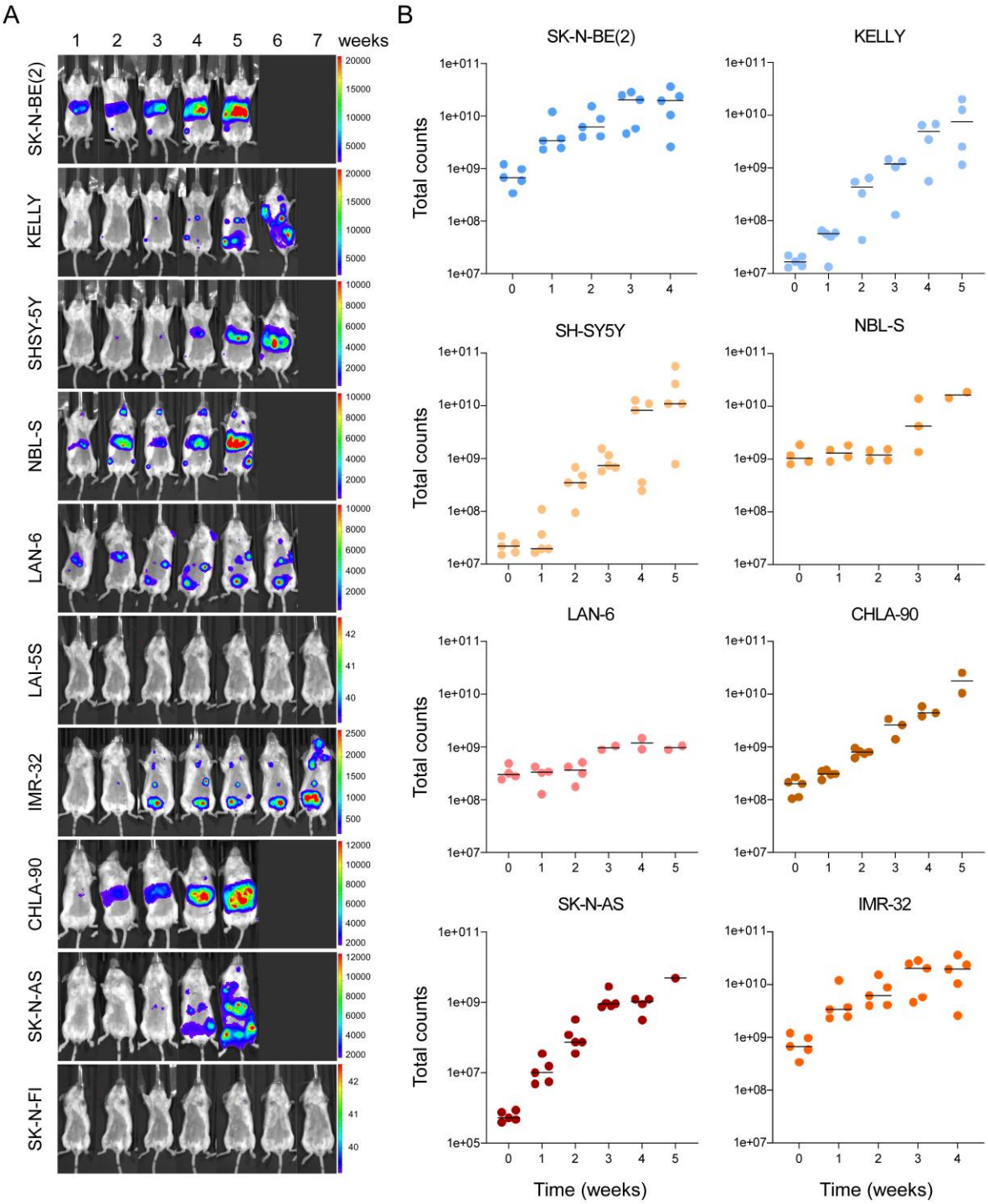

Figure 7. *In vivo* bioluminescence imaging of metastatic neuroblastoma models. A. Representative mouse for each NB cell line injected intravenously via tail vein, monitored weekly by IVIS imaging. Color scale indicates total photon flux (counts). B Quantification of photon flux for each cell line; each point representing an individual mouse and bars denoting the median.

4.2 Bioluminescence imaging combined with clinical parameters enables longitudinal assessment of metastatic progression

Following intravenous injection, bioluminescence imaging (IVIS) allowed for longitudinal monitoring of tumor growth. Complementary assessments were performed to support accurate evaluation of disease progression. Tumor palpation and body weight were recorded at least twice weekly, along with routine monitoring of overall health status. This combined approach allowed the identification of cell line-specific symptoms associated with metastatic NB in mice (Table 8). Large, distended, and inflamed abdomens were detected by palpation in mice injected with SK-N-BE(2), CHLA-90, NBL-S and SHSY-5Y after 3–4 weeks. These findings were consistent with liver metastases and hepatomegaly, and correlated with increases body weight. In contrast, mice injected with SK-N-AS, NBL-S and IMR-32 showed weight loss (Figure 8A). These animals also displayed reduced hind limb mobility and developed intraperitoneal and paraspinal lesions detectable by palpation, a phenotype also observed in mice injected with the KELLY cell line (Table 8).

Detection of tumoral cells in intraperitoneal and paraspinal regions is consistent with dissemination to distant lymph nodes and may contribute to impaired mobility through compression of motor nerves. In mice injected with LAN-6 and SH-SY5Y, symptoms were generally mild, apart from non-specific signs of declining health. Across all models, a bristly hair, reduced mobility, and eye closure were common indicators of stress and weakness, typically emerging after the onset of the initial disease-specific symptoms. Altogether, organ-specific tumor growth was associated with characteristic clinical signs that informed disease evolution and supported the definition of humane endpoint criteria. These endpoints enabled evaluations of overall survival for each model and the generation of survival curves linking metastatic burden to survival outcomes (Figure 8B).

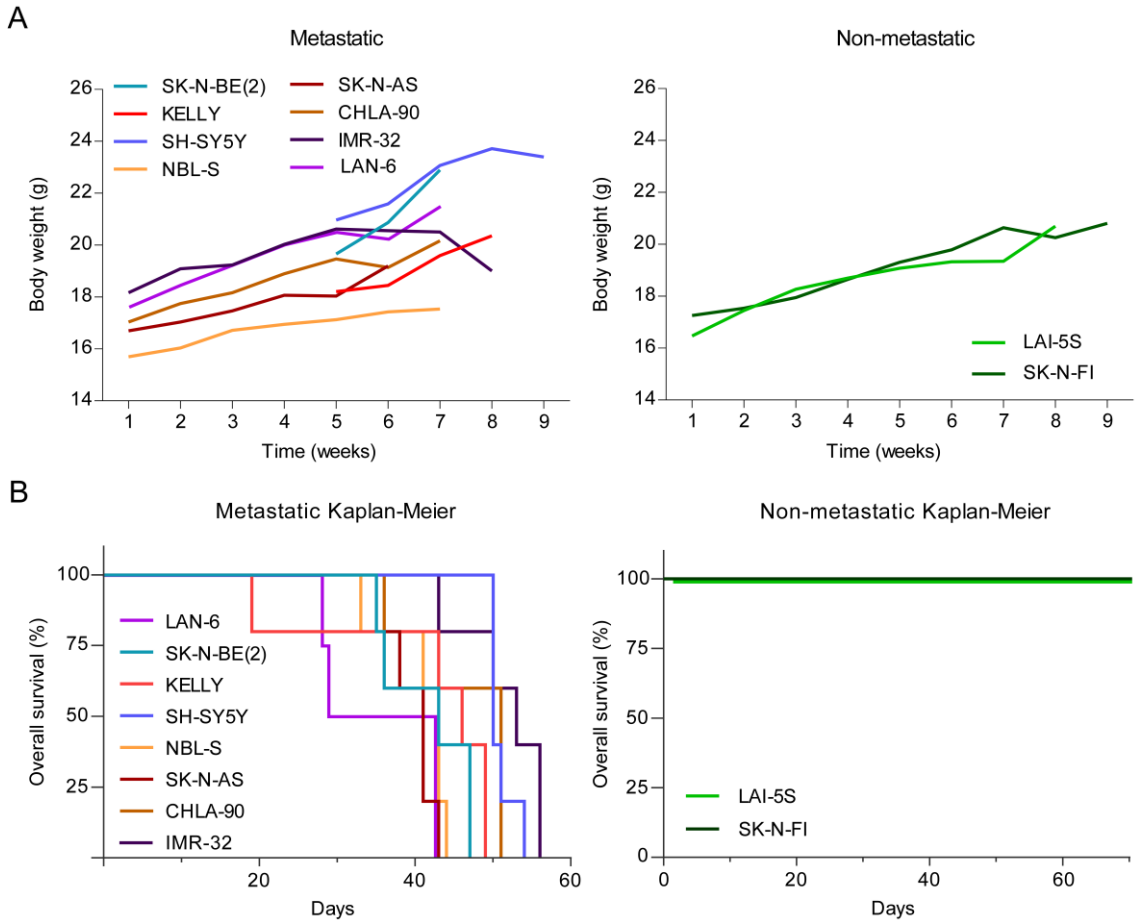

Figure 8. Body weight trajectories and Kaplan-Meier survival analyses of metastatic NB mouse models. A. Body weight over time in mice injected with NB cell lines. Left: cell lines generating detectable metastases (n=8). Right: poorly metastatic cell lines (n=2). Each cell line is represented in a distinct color. Body weight was recorded weekly throughout the study. B. Kaplan-Meier survival curves for mice injected with NB cell lines. Left: cell lines generating detectable metastases (n=8). Right: cell lines defined as non-metastatic (n=2).

Table 8. Clinical features of disease progression in mice injected with NB cell lines.

Cell line	Mean sacrifice (days)	Symptomatology
SK-N-AS	39.6 ± 1.4	Weight loss, hind mobility loss
NBL-S	40.8 ± 2.0	Abdominal distension, weight loss and poor mobility
SK-N-BE(2)	41.6 ± 2.6	Abdominal distension and poor mobility
LAN-6	41.8 ± 4.8	Poor general aspect
CHLA-90	45.0 ± 3.7	Abdominal distension
KELLY	46.8 ± 1.7	Weight loss, neck masses
SHSY-5Y	51.0 ± 0.8	Abdominal distension
IMR-32	51.6 ± 2.4	Hind mobility loss, poor mobility and weight loss

4.3 Liver, bone marrow, kidney and adrenal glands are the predominant metastatic sites in mice

At humane endpoints, mice were euthanized and subjected to necropsy for metastatic characterization. Large metastatic foci were identified macroscopically and confirmed by hematoxylin and eosin (H&E) staining, whereas micrometastatic lesions were detected only by histological analysis (Figure 9).

The liver, bone marrow and adrenal gland constituted the predominant metastatic sites across nearly all tested cell lines (Table 9). However, the frequency of organ involvement differed substantially between models. SK-N-BE(2), SK-N-AS, CHLA-90 and NBL-S showed particularly consistent liver involvement, with metastases detected in 100% of mice. Adrenal gland metastases were also frequent in SK-N-BE(2), SK-N-AS and CHLA-90, occurring in 80% of mice, whereas bone marrow involvement was consistent in SK-N-BE(2) and SK-N-AS, affecting 80% and 100% of mice, respectively. In contrast, KELLY, SHSY-5Y, and IMR-32 displayed a different distribution pattern, with lower frequencies of metastases in these organs (<60%) and developed additional intraperitoneal and supraspinal tumors not observed in the other models. This is consistent with the IVIS imaging bioluminescence, which revealed a more diffuse bioluminescent distribution in these cell lines, supporting larger heterogeneity in metastatic spread. Additional metastatic sites included the lungs and ovaries, with frequencies of 80% or higher in SK-N-AS, KELLY and NBL-S. IMR-32 showed a particularly high number of lymph node and ovarian metastases, each observed in 80% of mice. In LAN-6 cell line, although bioluminescent signal was detected and quantified, no macro- or micrometastastatic lesions were identified after histological analysis. Taken together, these findings indicate that the different models reproduce distinct but complementary aspects of metastatic NB organotropism.

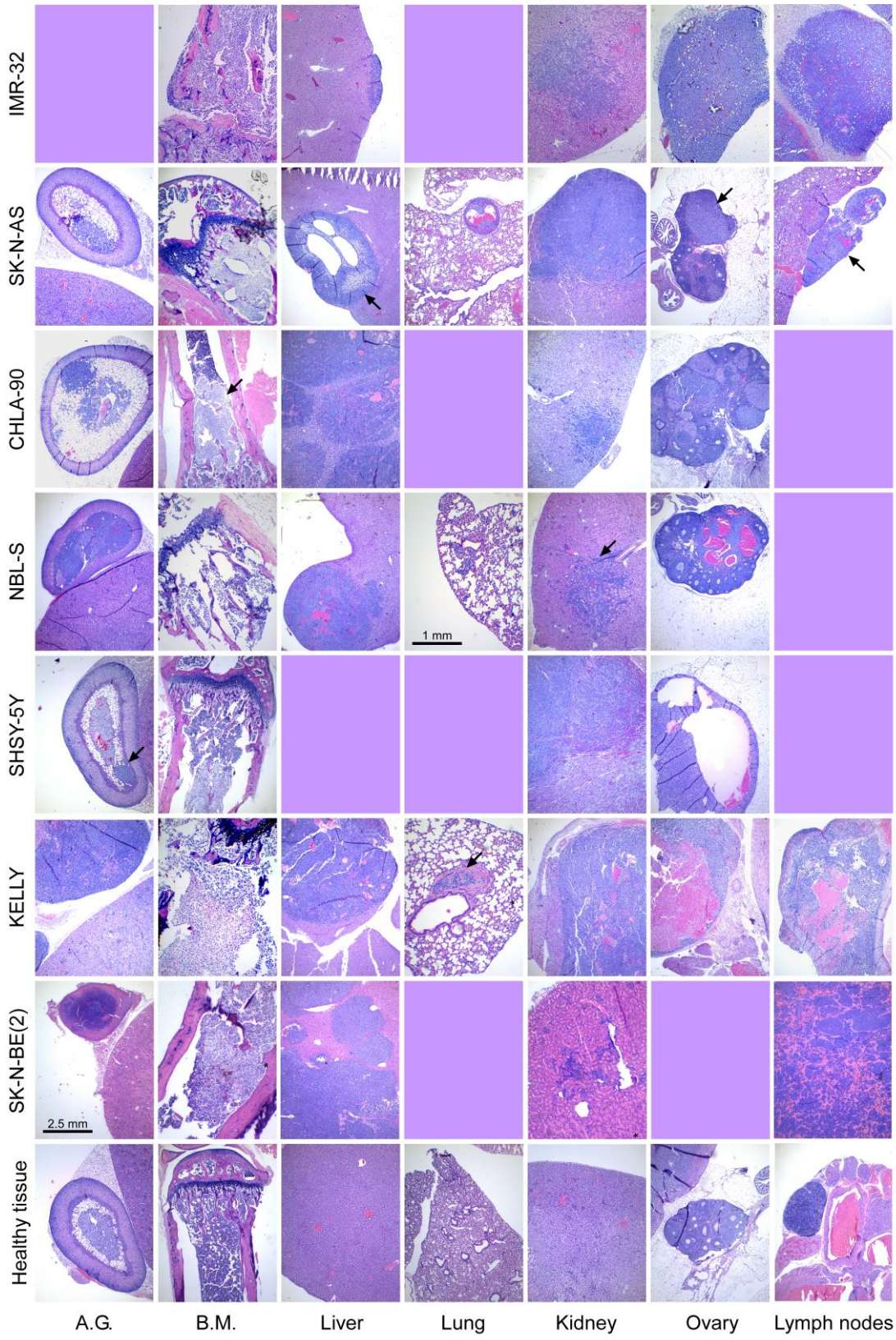

Figure 9. Representative hematoxylin and eosin staining of metastatic lesions. Rows correspond to NB cell lines (n=7) and columns correspond to organs where metastases were found. All pictures were acquired at 4x magnification (scale bar = 2.5 mm) except lung, acquired at 10x (scale bar = 1 mm). Arrows show one representative metastasis per organ and purple panels indicate no presence of metastasis. A.G: adrenal gland; B.M: bone marrow.

To confirm that the detected luminescence signal corresponded to metastatic lesions, we performed immunohistochemical (IHC) hematoxylin and eosin tissue staining and staining for chromogranin A (CgA). CgA is a well-established marker of neuroendocrine differentiation and is routinely used in the pathological assessment of NB due to its broad expression in tumors of neuroendocrine origin. In our models, CgA IHC was used to confirm or exclude micrometastatic foci in cell lines such as NBL-S, SHSY-5Y and SK-N-FI that were inconspicuous or undetectable by H&E staining alone (Figure 10). CgA staining was particularly useful in organs of NBL-S injected mice by enabling clear discrimination of small NB cell clusters in lungs and ovaries from surrounding stromal tissue (Figure 9A). In contrast, in organs of SHSY-5Y (ovaries) and SK-N-FI (liver and spleen) injected mice, no micrometastasis were detected after CgA staining. Overall, combining conventional histology with IHC validation improved the accuracy and robustness of macro- and micrometastasis detection, strengthening the translational relevance of our metastatic NB models.

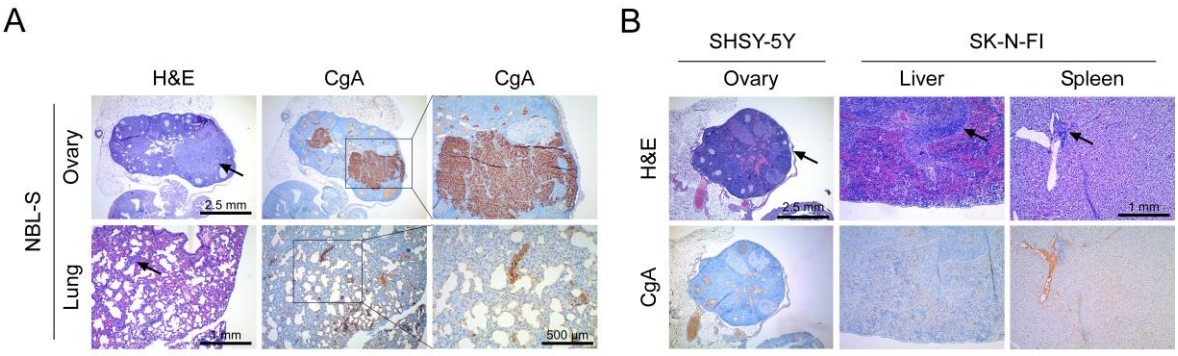

Figure 10. Chromogranin A immunohistochemistry of potential micrometastatic lesions. A. Representative histological sections from NBL-S injected mice showing hematoxylin and eosin staining (H&E; left) and the corresponding chromogranin A (CgA) immunohistochemistry (middle and right), highlighting the neuroendocrine marker expression consistent with NB. B. Negative controls for chromogranin A staining, including tissues from SHSY-5Y injected mice (ovary) and SK-N-FI injected mice (liver and spleen). H&E and CgA immunohistochemical staining were performed on serial consecutive sections from the same tumor sample. Arrows indicate representative metastases.

Table 9. Metastasis engraftment frequencies per organ and cell line.

	SK-N-BE(2)	KELLY	SHSY-5Y	NBL-S	IMR-32	CHLA-90	SK-N-AS
Lymph nodes	1/5	3/4	0/5	0/5	4/5	0/5	1/5
Lung	1/5	3/4	0/5	4/5	0/5	0/5	4/5
Liver	5/5	1/4	2/5	5/5	1/5	5/5	5/5
Adrenal gland	4/5	3/4	3/5	2/5	0/5	4/5	4/5
Kidney	0/5	3/4	1/5	4/5	1/5	2/5	5/5
Bone marrow	4/5	1/4	2/5	1/5	2/5	3/5	5/5
Ovary	0/5	3/4	2/5	4/5	4/5	2/5	4/5

LAI-5S, LAN-6 and SK-N-FI cell lines were not included.

4.4 Metastatic patterns across neuroblastoma cell lines correlate with molecular and phenotypic features

To assess whether genetic background contributes to the metastatic behavior of human NB cell lines, we quantified organ-specific engraftment frequencies as a proxy for metastatic dissemination across multiple target tissues (Figure 11A). This analysis revealed substantial inter-line variability in metastatic distribution, highlighting pronounced heterogeneity in organ tropism across the panel. To test whether these patterns relate to intrinsic molecular or biological features, we integrated metastatic engraftment profiles with genomic and phenotypic annotations and performed PCA (Figure 11B). The annotation set used for clustering included the following NB attributes: *MYCN* amplification status, 11q deletion status, TP53 functional status, sex, adrenergic (ADRN) versus mesenchymal (MES) lineage identity, and the clinical origin of each cell line.

PCA revealed a structured organization of the cell lines, with the first two principal components (PC1 and PC2) accounting for 40% and 27.7% of the total variance, respectively (Figure 11B). Notably, cell lines harboring 11q deletion formed a distinct cluster, separated from 11q wild-type models (Figure 11B i), consistent with an association between this alteration and metastatic patterns. Notably, SK-N-AS and

NBL-S, both characterized by 11q loss, showed remarkably similar metastatic patterns, with frequent dissemination to the ovaries, lungs, and liver. Cells also segregated by p53 status along PC2, with p53-functional and p53-non-functional models occupying distinct regions in the PCA (Figure 11B ii), suggesting divergence in metastatic behavior linked to p53. In line with this observation, p53-non-functional cell lines, including SK-N-BE(2), SK-N-AS, and CHLA-90, showed similar metastatic spread patterns, with high frequencies of involvement in the adrenal glands, liver, and bone marrow. Stratification by clinical origin showed a similar separation along PC2, indicating that tissue of origin features may also contribute to variability in dissemination profiles (Figure 11B vi). In contrast, *MYCN*-amplified and non-amplified cell lines did not show clear separation (Figure 11B iv). Likewise, no consistent clustering emerged when cell lines were grouped by ADRN versus MES lineage state or by sex (Figure 11B iii, v), suggesting that these features are not uniformly associated with metastatic distribution in this experimental setting. Altogether, while not all traits explain the variance across cell lines, 11q status and p53 status show clustering patterns, indicating that these features may contribute to the observed stratification.

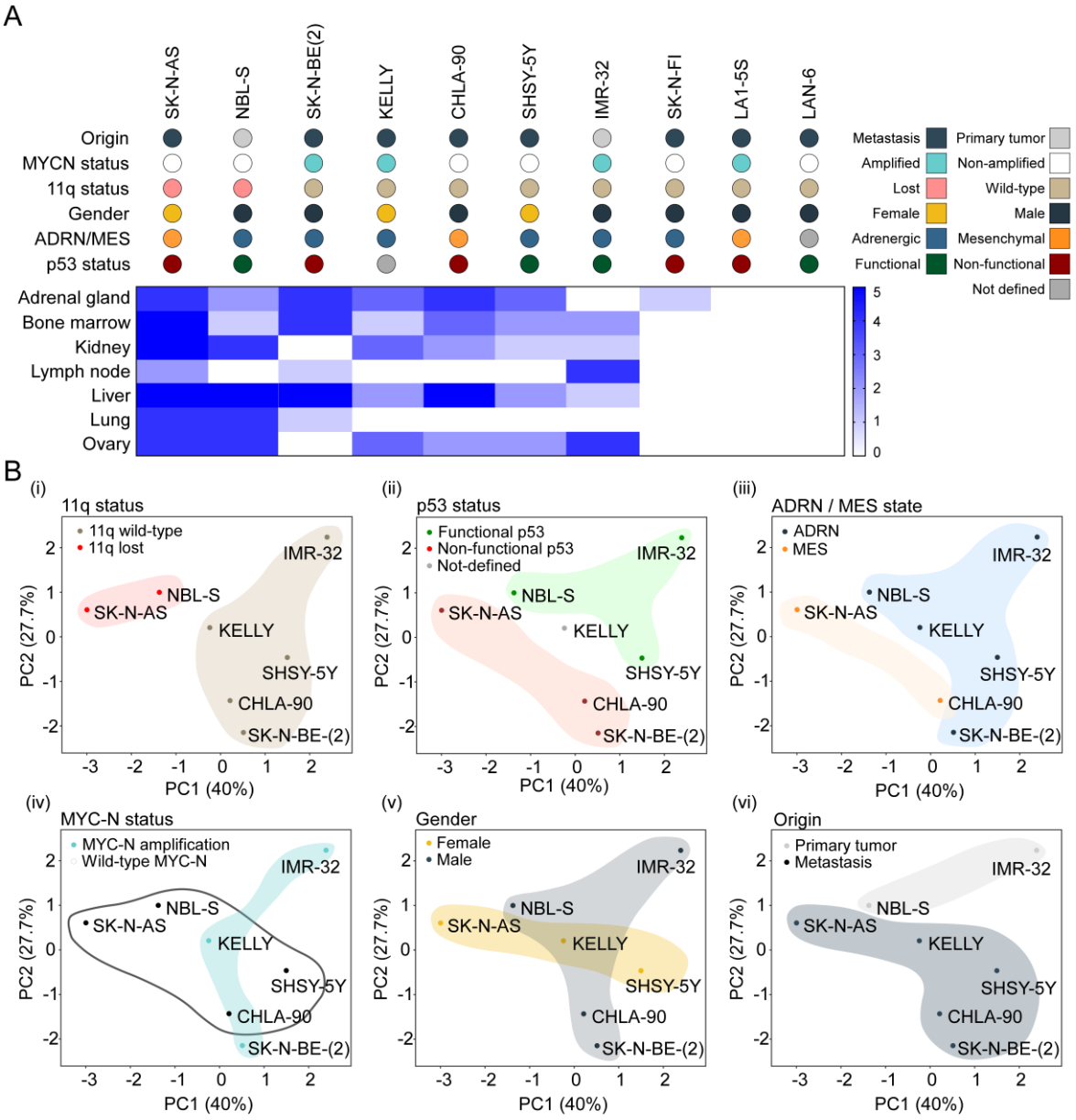

Figure 11. Characterization of neuroblastoma cell line panel used for metastatic modeling. A. Heatmap showing metastatic tropism of ten NB cell lines across seven anatomical sites. Color intensity indicates the number of mice with metastases in each organ (0-5). B. PCA of cell lines colored by genetic and clinical features: 11q status, p53 status, ADR/MES state, MYCN amplification, gender, and origin. PC1 and PC2 explain 40% and 27.7% of variance, respectively.

4.5 Epigenetic remodeling in metastatic neuroblastoma is cell-line and niche-dependent

The assay for transposase-accessible chromatin using sequencing (ATAC-seq) is a genome-wide approach that enables the identification of accessible chromatin regions and the characterization of chromatin states across different biological conditions. By profiling chromatin accessibility, this technique provides insights into regulatory elements potentially involved in transcriptional control. Furthermore, changes in chromatin accessibility can reveal alterations in gene regulatory programs associated with specific cellular phenotypes or biological processes.

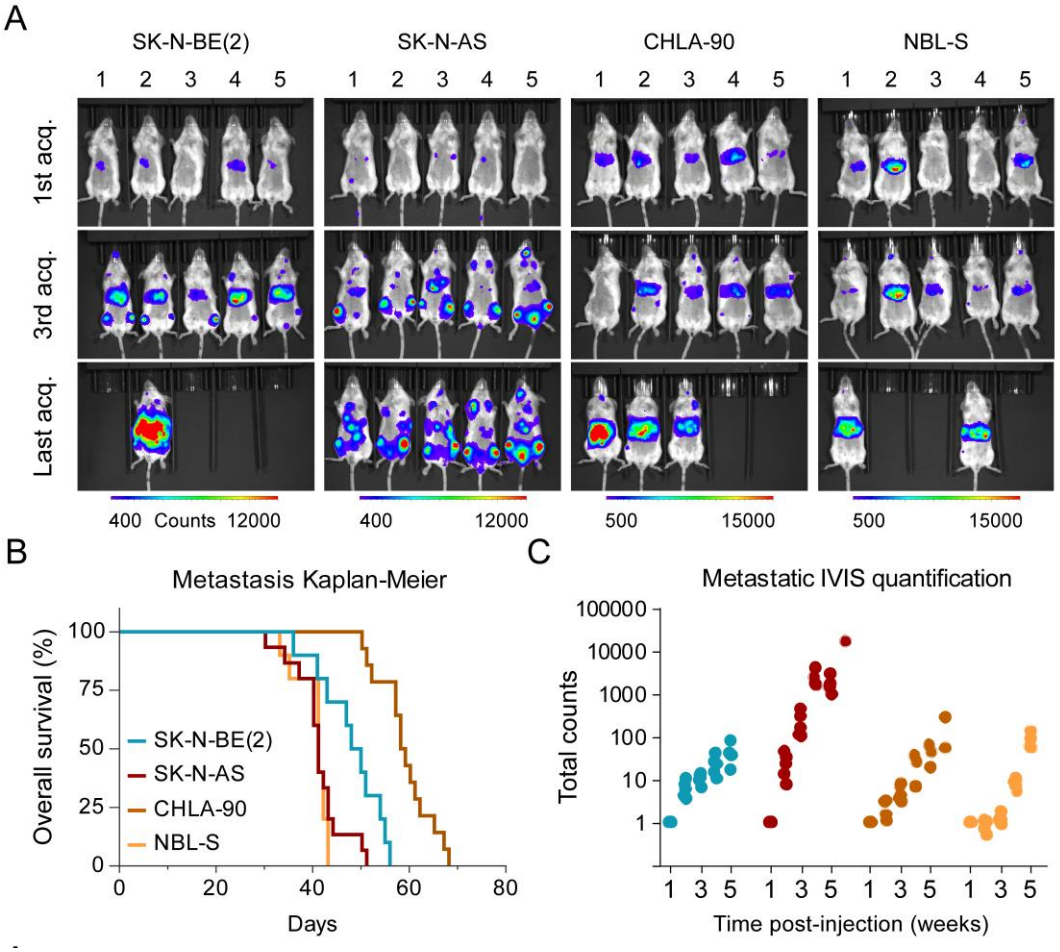

Figure 12. Metastatic tumor growth. A. Representative image of 5 metastatic mice per cell line at the indicated time-points. B. Kaplan-Meier survival curve of metastatic mice represented in overall survival (%). C. Metastatic IVIS quantification over time. Scale bar indicates bioluminescence signal in total counts.

To characterize epigenetic reprogramming associated with metastatic NB, we selected the four NB cell lines with higher frequency of bone marrow and/or liver

metastases (SK-N-BE(2), SK-N-AS, CHLA-90, and NBL-S) to generate matched metastatic (intravenous injection; Figure 12) and primary (subcutaneous injection; Figure 13) tumors in independent mice. Tumor progression was using IVIS imaging to track metastatic lesions (Figure 12A) and both IVIS and caliper measurements for subcutaneous tumors. Mice were sacrificed according to humane endpoint criteria: IVIS signal in combination with clinical symptoms and body weight variations for metastatic disease (Figure 12C) and tumor volume >1500 mm^3 for primary tumors (Figure 13C). Based on these criteria, overall survival was assessed for mice injected with each cell line (Figure 12B and 13B).

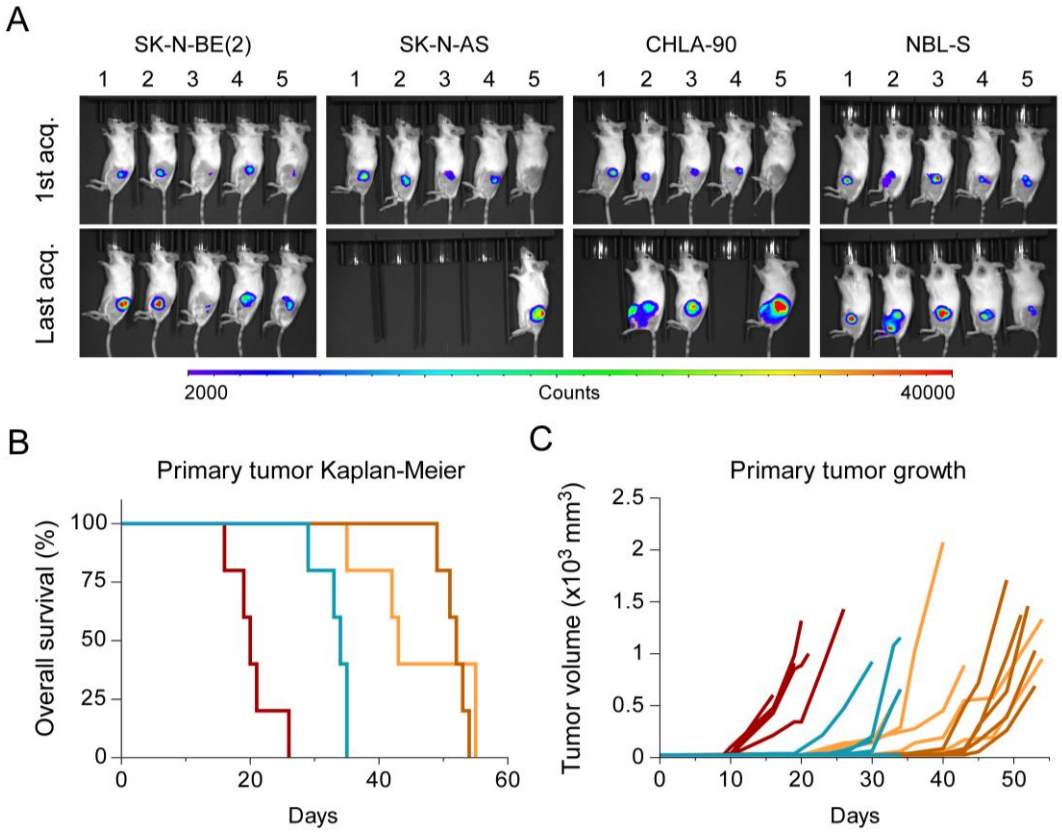

Figure 13. Subcutaneous tumor growth. A. Representative image of 5 subcutaneously injected mice per cell line at the indicated time-points. B. Kaplan-Meier survival curve of metastatic mice represented in overall survival (%). C. Graphical representation of subcutaneous tumor growth measurements (mm^3). Scale bar indicates bioluminescence signal in total counts.

After establishment of the metastatic mouse model and upon reaching the predefined humane endpoint criteria, mice were euthanized and livers, hind limb bones, and primary tumors were harvested for tumor cells collection and nuclei isolation to perform ATAC-seq. All samples were plotted in a PCA to identify the

major sources of variation. The PCA indicated that intrinsic cell line identity was the dominant driver of variance across all metastases (Figure 14A). Notably, when analyses were stratified by cell line, samples clustered by metastasized organ, consistent with metastasis-specific chromatin accessibility changes (Figure 14B).

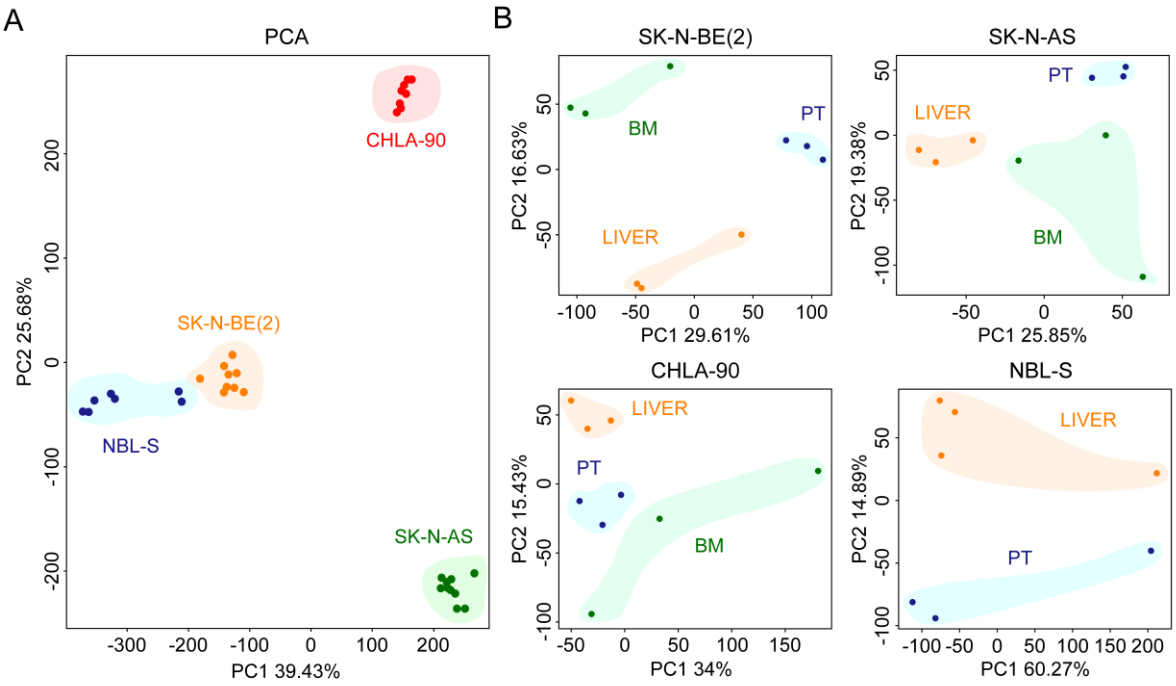

Figure 14. Principal component analyses (PCA) for ATAC-seq samples. A. PCA including all cell lines, each represented in a different color. B. PCA plots of each individual cell line clustered by metastatic organ. BM: Bone Marrow (green); PT: Primary Tumor (blue); Liver (orange).

Overall, chromatin accessibility changes detected in ATAC-seq predominantly affected sites associated to protein-coding genes (~65-70%) across all cell lines and metastatic sites ($p<0.05$; $FC>|1.25|$, except CHLA-90: $p<0.1$; $FC>|1.25|$), whereas ncRNA loci-related sites accounted for approximately 30-35% of differentially-regulated regions (Figure 15A and 16A).

Both the magnitude (number of peaks) and directionality (open vs close) of these epigenetic modifications varied substantially between cell lines and metastatic tissues, revealing cell line and site-specific chromatin remodeling patterns. These differences are collected in the heatmaps represented in Figures 15B and 16B, together with their respective median peak coverage quantifications.

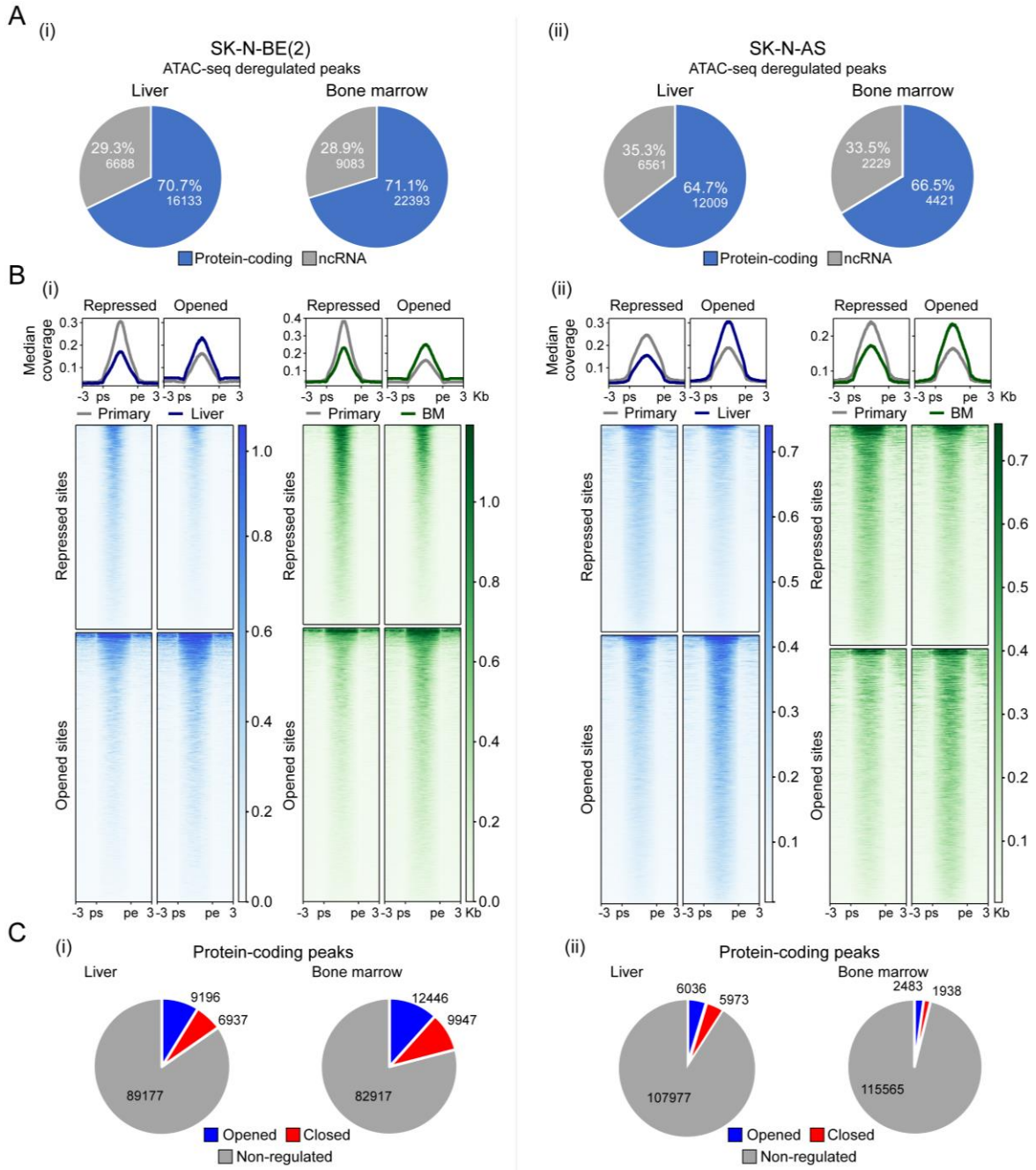

Figure 15. Epigenetic landscape of metastatic neuroblastoma models generated with SK-N-BE(2) (i) and SK-N-AS (ii) cell lines. A. Schematic representation of gene-type classification of ATAC-seq deregulated peaks for liver and bone marrow metastases (p-value<0.05 and FC>|1.25|). B. Median coverage representation of ATAC-seq differential opened and closed areas in liver and bone marrow metastases (p-value<0.05 and FC>|1.25|) and their corresponding heatmap. ps: Peak start; pe; Peak end. C. Schematic representation of opened and closed ATAC-seq peaks annotated as protein-coding genes (p-value<0.05).

Notably, the magnitude of epigenetic remodeling differed among the four models. SK-N-BE(2) injected mice showed the most pronounced chromatin accessibility changes (Figure 17A), with >20,000 deregulated peaks in both metastatic organs and a pronounced response in the bone marrow niche (31,922 changes: 17,651 opened; 14,271 closed) compared to liver (23,852 changes: 12,892 opened; 10,960 closed). In contrast, SK-N-AS displayed a more modest remodeling landscape (Figure 17B), especially in bone marrow (9,439 changes: 4,938 opened; 4,501 closed), whereas in liver metastases it showed nearly twice as many changes (17,566: 8,591 opened; 8,975 closed). CHLA-90 exhibited the lowest remodeling in liver (16,659 changes: 8,903 opened; 7,756 closed), and a comparable extent in bone marrow (15,159 changes: 9,301 opened; 5,858 closed) (Figure 17C). NBL-S also showed substantial chromatin plasticity in the hepatic microenvironment, with 18,345 deregulated sites (7,546 opened; 10,799 closed) (Figure 17D).

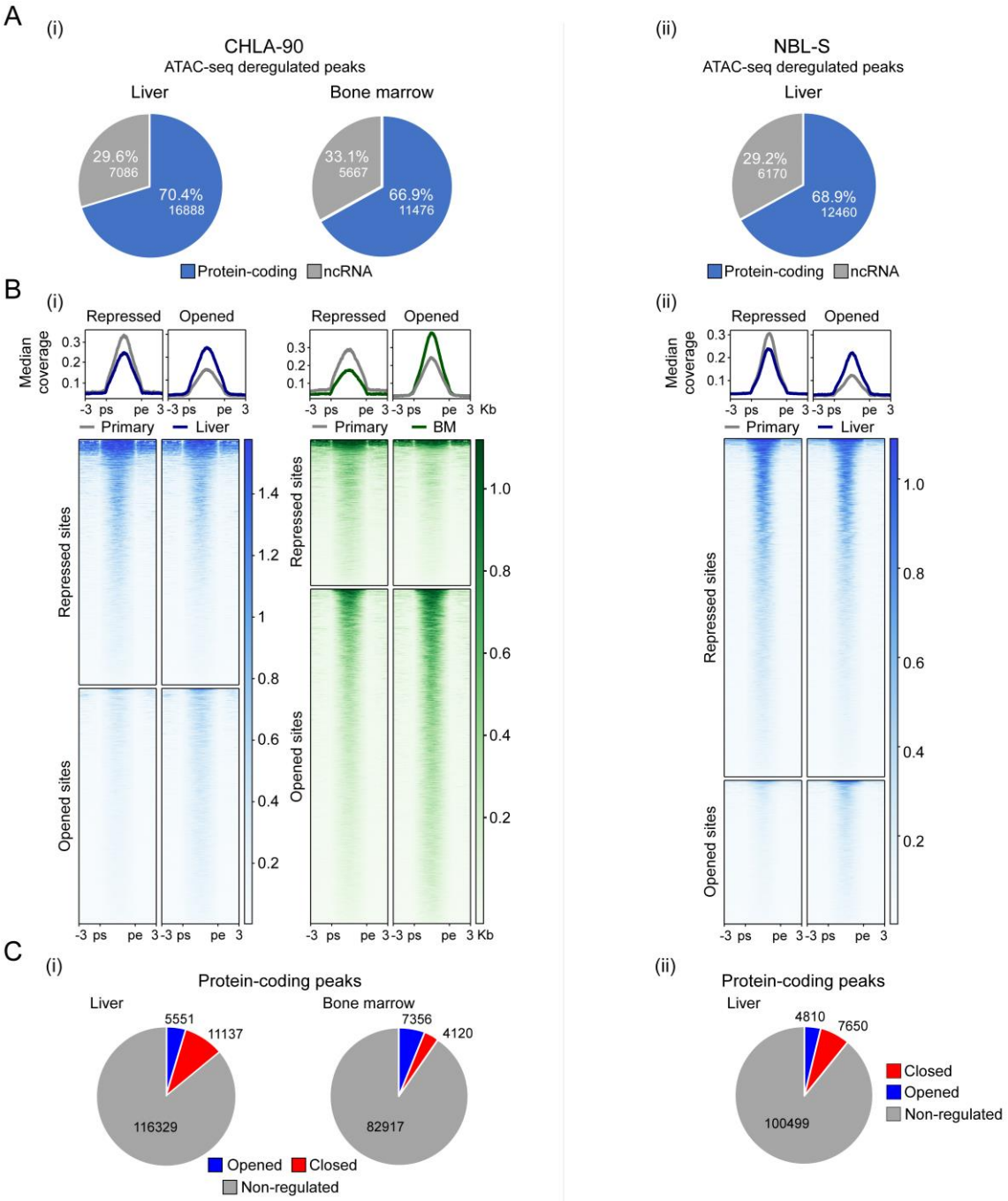

Figure 16. **Epigenetic landscape of metastatic neuroblastoma models generated with CHLA-90 (i) and NBL-S (ii) cell lines.** A. Schematic representation of gene-type classification of ATAC-seq deregulated peaks for liver and bone marrow metastases (p-value<0.05 and FC>|1.25|). B. Median coverage representation of ATAC-seq differential opened and closed areas in liver and bone marrow metastases (p-value<0.05 and FC>|1.25|) and their corresponding heatmap. ps: Peak start; pe; Peak end. C. Schematic representation of opened and closed ATAC-seq peaks annotated as protein-coding genes (p-value<0.05).

Beyond magnitude, the directionality of these modifications revealed distinct niche-specific and cell line-dependent adaptation patterns. In liver metastases, SK-N-BE(2), SK-N-AS and CHLA-90 conditions maintained a balanced or slightly open chromatin profile compared to primary tumors (Figure 17A i; Figure 17B i; Figure 17C i), whereas NBL-S cells exhibited a predominantly repressive landscape, representing the strongest chromatin closure response observed (Figure 17D). Conversely, bone marrow metastases showed a consistent bias toward chromatin opening across cell lines: SK-N-BE(2) showed the most pronounced accessibility increase, followed by CHLA-90 and SK-N-AS (Figure 17A ii; Figure 17B ii; Figure 17C ii). This pattern in the bone marrow niche contrasted with the more heterogeneous remodeling patterns observed in liver metastases.

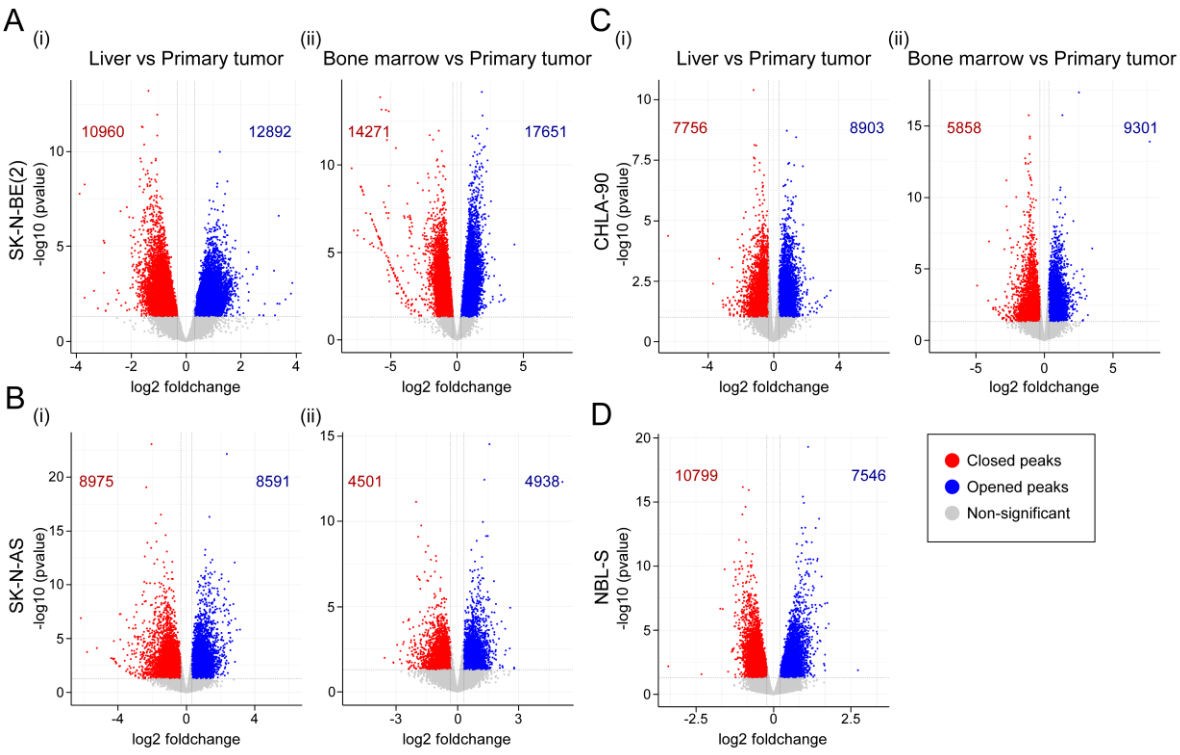

Figure 17. Volcano plots for ATAC-seq deregulated peaks across cell lines. Liver (p-value <0.05 except CHLA-90 p-value <0.1; FC>|1.25|) and bone marrow metastases (p-value <0.05; FC>|1.25|) were shown for SK-N-BE(2), SK-N-AS and CHLA-90 cell lines. Liver metastases (p-value<0.05; FC>|1.25|) were shown for NBL-S model.

4.6 Distinct epigenetic reprogramming converges on common biological processes across models

To identify biological programs potentially shaped by chromatin remodeling in liver or bone marrow metastases, differentially accessible ATAC-seq peaks linked to protein-coding genes were subjected to Gene Ontology (GO) Biological Process enrichment analysis.

Among regions with increased chromatin accessibility in liver metastases, several biological processes were recurrently enriched across cell lines (Figure 18A). Notably, neuronal-related pathways were consistently represented, alongside neural crest–associated features compatible with changes in morphology, motility, and colonization capacity. These included processes such as cell migration, axon guidance, and actin cytoskeleton organization.

In addition, pathways associated with proliferation and tumor progression were enriched in some models, including PI3K/AKT, Kit and FGFR signaling (see Table 10). Notably, positive regulation of the MAPK cascade was repeatedly enriched across cell lines (Figure 18A), suggesting that it may represent a common component of the chromatin accessibility landscape in liver metastases. Additional biological processes such as angiogenesis and protein phosphorylation, were identified in most but not all models (see Table 10).

Conversely, regions with reduced chromatin accessibility were enriched for genes involved in cell adhesion and nervous system development (Figure 18B). Interestingly, several GO processes—such as cell migration, axon guidance, and actin cytoskeleton organization—exhibited bidirectional accessibility changes, with some genes losing accessibility while others gained it. This pattern suggests a modular reconfiguration of pathway components rather than uniform activation or repression, indicating that chromatin remodeling selectively tunes gene modules within the same biological program according to context-specific requirements.

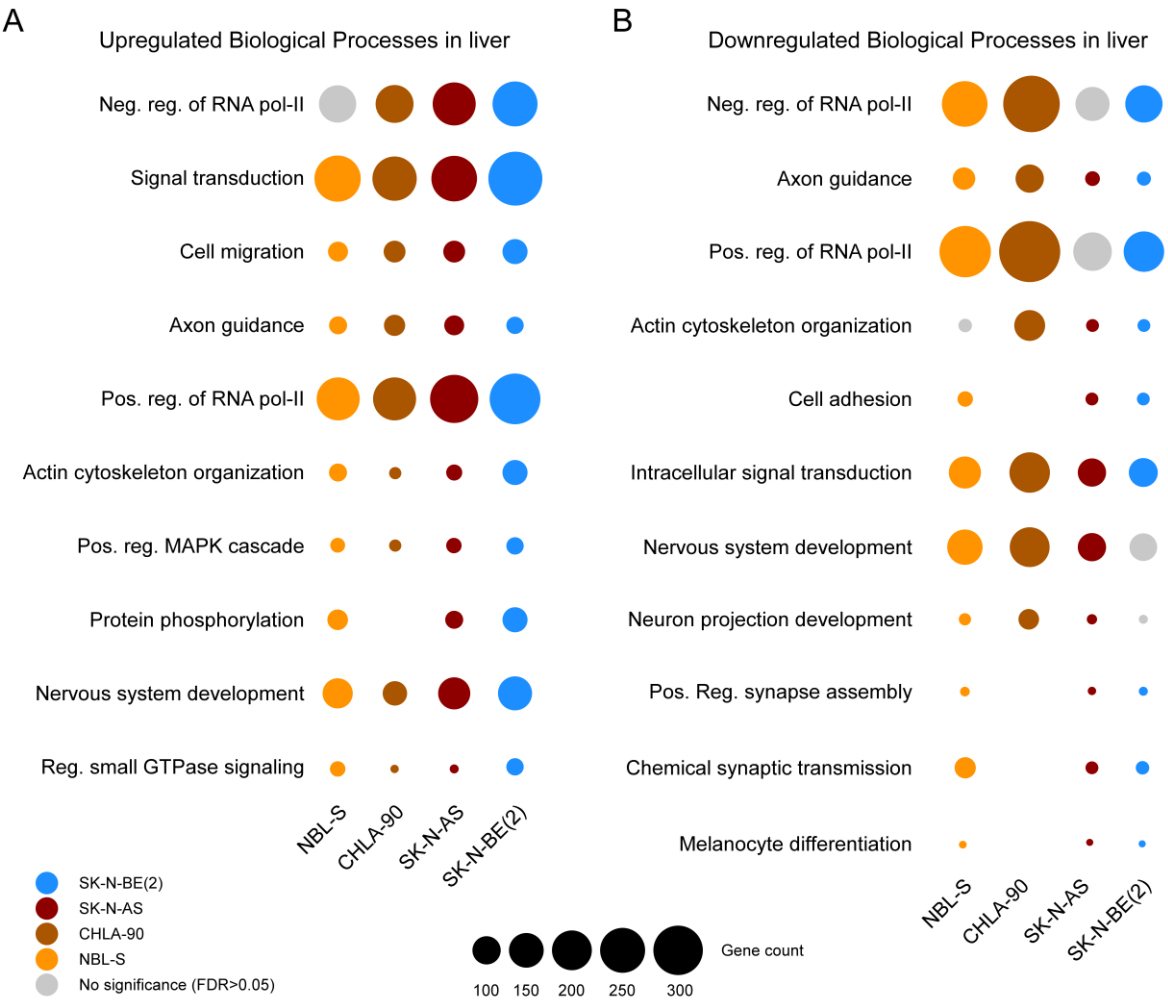

Figure 18. Bubble plot showing enriched Gene Ontology Biological Processes associated with upregulated (A) and downregulated (B) pathways in liver metastases. Pathways were considered if significantly enriched at FDR<0.05 in at least three cell lines. Each cell line is denoted by a distinct color, grey indicating no significance and bubble size reflects the number of genes contributing to each biological process.

In bone marrow metastases, regions with increased chromatin accessibility were enriched for neuronal-related programs, including axon guidance, alongside motility- and morphology-associated processes such as cell migration and actin cytoskeleton organization (Figure 19A). Notably, no single specific signaling pathway was consistently enriched across all cell lines, indicating that accessibility remodeling in the bone marrow context is, at least in part, cell line–dependent.

Regions with decreased accessibility were enriched for genes involved in cell adhesion, including cell–cell adhesion across all cell lines, as well as genes associated with nervous system development (Figure 19B).

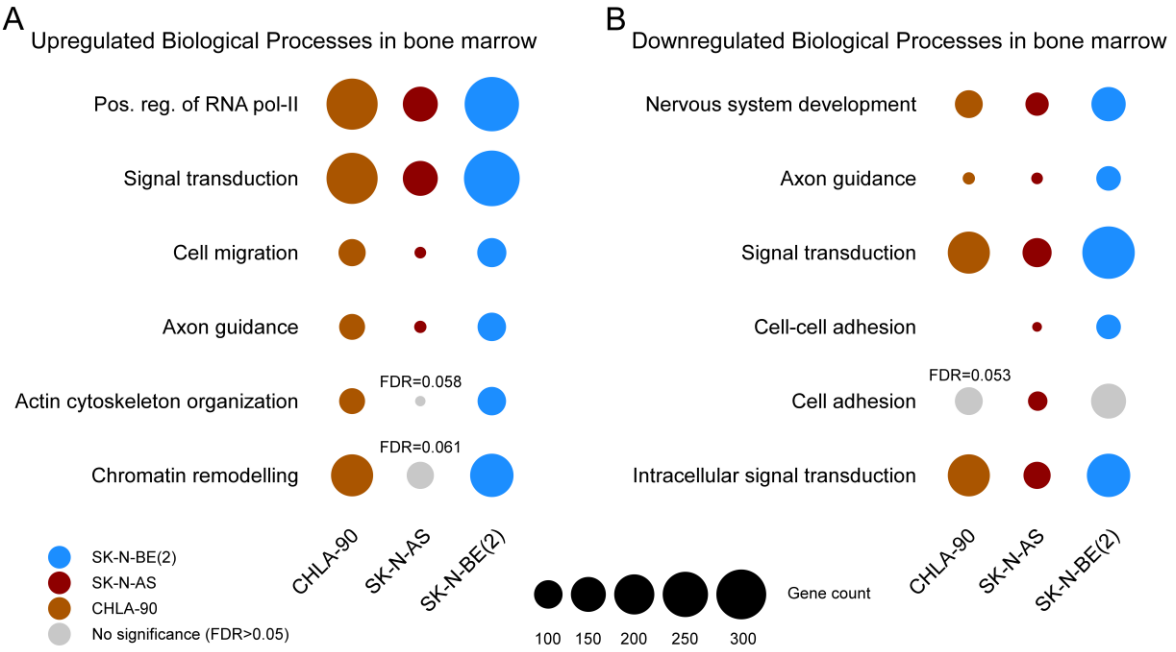

Figure 19. Bubble plot showing enriched Gene Ontology Biological Processes associated with upregulated (A) and downregulated (B) pathways in bone marrow metastases. Pathways were considered if significantly enriched at FDR<0.05 in at least two cell lines. Each cell line is denoted by a distinct color, grey indicating no significance and bubble size reflects the number of genes contributing to each biological process.

Collectively, ATAC-seq profiling revealed extensive chromatin remodeling in both liver and bone marrow metastases. Neuronal, migration-related and cytoskeletal gene programs showed increased accessibility, whereas adhesion-related programs displayed reduced accessibility. Signaling pathways exhibited more variable patterns; MAPK signaling was consistently enriched in liver metastases, whereas signaling changes in bone marrow metastases were cell line–dependent.

Table 10. Additional biological processes recurrently enriched in liver metastases across neuroblastoma models after ATAC-seq analysis and their corresponding FDR per cell line.

Biological process	SK-N-BE(2)	SK-N-AS	CHLA-90	NBL-S
Pos. reg. of PI3K/AKT signaling	n.d.	<0.01	<0.01	<0.01
FGFR signaling pathway	0.22	<0.01	<0.01	0.16
Kit signaling pathway	0.41	0.08	<0.01	0.12
Angiogenesis	0.08	<0.01	<0.01	<0.01
Protein phosphorylation	0.01	0.05	n.d.	<0.01

4.7 Chromatin accessibility changes in liver metastases are not consistently mirrored by transcriptional alterations

To determine whether the chromatin accessibility differences identified by ATAC-seq were accompanied by corresponding transcriptional changes, we performed RNA-seq in matched primary tumors and liver metastases. Across all four RNA-seq datasets, PCA revealed a clear separation between primary tumors and liver metastases, confirming that metastatic lesions adopt a reproducible transcriptional state (Figure 20). In each model, both tissues segregated primarily along PC1 or PC2, indicating that the primary and secondary components driving variance in RNA-seq samples are explained by organ origin, with primary tumors clustering tightly while liver metastases were more dispersed.

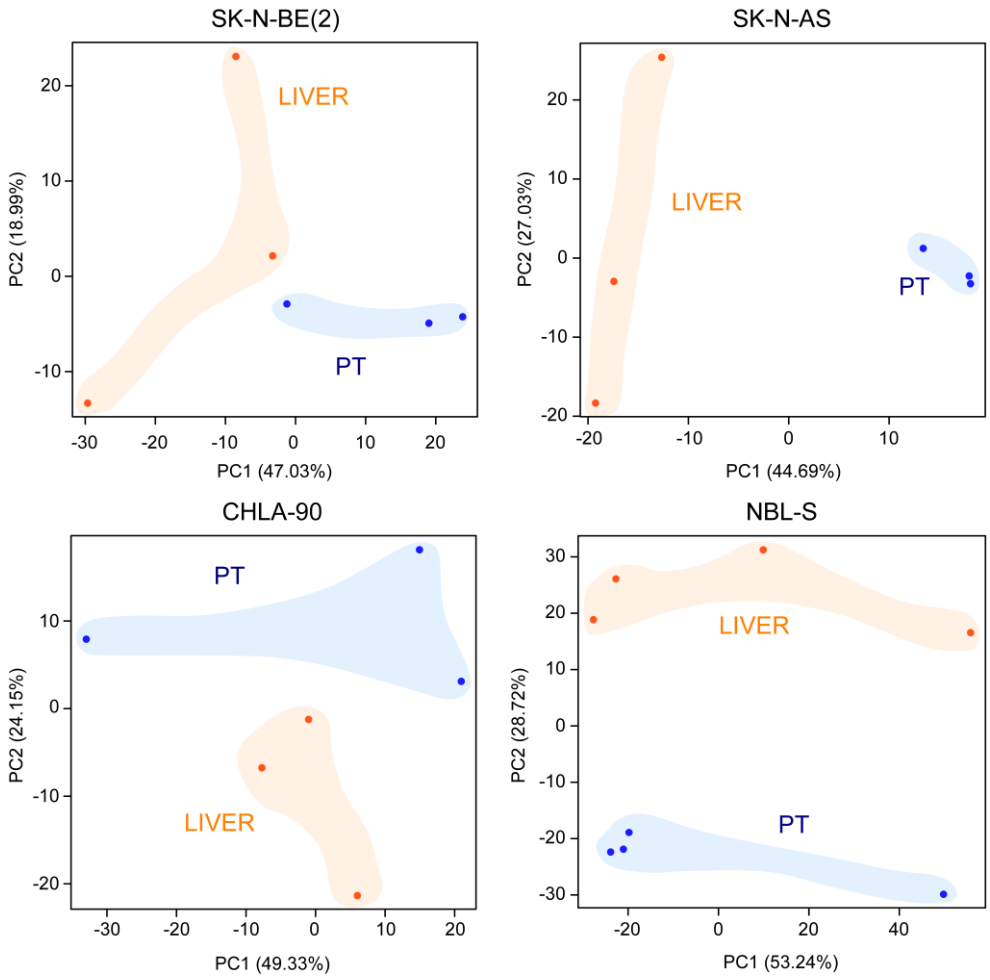

Figure 20. Principal component analysis for RNA-seq samples. Each panel represents an independent cell line model comparing primary tumors (blue) and liver metastases (orange).

To characterize the transcriptomic adaptations occurring during metastatic colonization, RNA-seq was performed on liver metastases derived from the four NB cell lines and compared with those of their corresponding primary tumors.

Both the magnitude (number of genes) and directionality (upregulated and downregulated) of these transcriptomic modifications varied substantially between cell lines, revealing line-specific gene expression patterns. These differences are collected in the volcano plots represented in Figures 21A-D.

Of note, the magnitude of transcriptomic changes differed among the four models. NBL-S injected mice showed the most pronounced gene expression plasticity (Figure 21D), with more than 1,400 upregulated and 1,400 downregulated genes in liver metastases. Similarly, SK-N-AS also displayed a broad transcriptomic alteration, showing more than 1,000 and 800 upregulated and downregulated genes, respectively (Figure 21B). Conversely, CHLA-90-injected mice exhibited the lowest level of gene expression changes in liver metastases, while SK-N-BE(2) also showed a reduced transcriptional remodeling (Figure 21C). CHLA-90 showed 458 upregulated and 526 downregulated genes, whereas SK-N-BE(2) showed 733 upregulated and 585 downregulated genes (Figure 21A).

Beyond their magnitude, the directionality of these changes revealed distinct cell line-dependent adaptation patterns. SK-N-BE(2) and SK-N-AS liver metastases showed a predominant pattern of gene upregulation relative to their corresponding primary tumors (Figure 21A and 21B). In contrast, CHLA-90 cell line showed a higher number of downregulated genes in liver metastases (Figure 21C). NBL-S liver metastases, by comparison, displayed a more balanced profile of gene deregulation compared to primary tumor (Figure 21D).

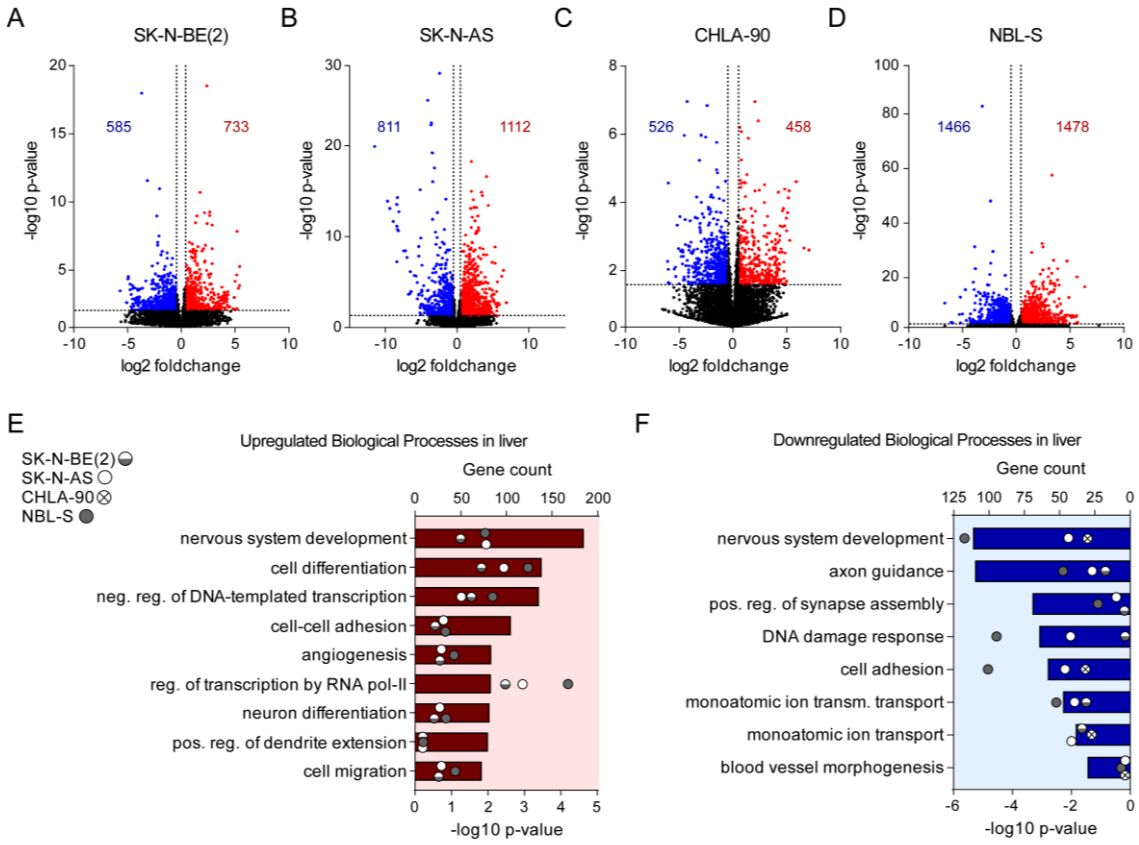

Figure 21. Transcriptomic landscape of liver metastases. A-D. Volcano plots for RNA-seq deregulated peaks across cell lines for liver metastases (p-value <0.05 except; FC>|1|). E-F. GO analysis showing upregulated and downregulated biological processes modulated in three or more cell lines in liver metastases (p-value<0.05). Bars represent significance (-log10 p-value) and dots represent gene count for each cell line.

To identify biological programs associated with transcriptional reprogramming in liver metastases, differentially expressed RNA-seq genes (p-value<0.05) were subjected to Gene Ontology Biological Process enrichment analysis. Among upregulated genes in liver metastases, several biological processes were recurrently enriched in at least three cell lines (Figure 21E). These included neuronal-related pathways such as nervous system development, neuron differentiation and positive regulation of dendrite extension, consistent with the concomitant presence of the enrichment of cell migration. Additional biological processes linked to cell differentiation, angiogenesis and global transcriptional regulation were also detected. Moreover, other biological processes were enriched only in selected cell lines and are therefore presented separately in Table 11. These included processes such as cell population proliferation and wound healing, reflecting transcriptional

programs that were not consistently shared across all models. Conversely, downregulated genes were also enriched for neuron-related processes, including nervous system development, axon guidance and positive regulation of synapse assembly. Particularly, long-term synaptic potentiation and regulation of membrane potential were only downregulated in certain cell lines shown in Table 11. Pathways related to ion transport, DNA damage response and cell adhesion were likewise downregulated (Figure 21F).

Table 11. Additional biological processes recurrently upregulated or downregulated in liver metastases across neuroblastoma models after RNA-seq analysis and their corresponding FDR per cell line.

Biological processes	SK-N-BE(2)	SK-N-AS	CHLA-90	NBL-S
Upregulated				
Notch signaling pathway	n.d.	<0.01	n.d.	<0.01
Pos. reg. cell population proliferation	<0.01	0.09	n.d.	<0.01
Wound healing	n.d.	0.02	n.d.	<0.01
Downregulated				
Long-term synaptic potentiation	0.01	n.d.	<0.01	n.d.
Reg. of membrane potential	n.d.	0.02	n.d.	<0.01

ATAC-seq genes derived from differentially accessible peaks ($p<0.05$; except CHLA-90 $p<0.1$) were cross-referenced with RNA-seq differentially expressed genes ($p<0.05$; except CHLA-90 $p<0.1$). Genes were considered overlapping if they were associated with at least one differentially accessible ATAC-seq peak and were also significantly differentially expressed in RNA-seq. Overall, only a limited fraction of ATAC-associated genes showed transcriptional alterations (Figure 22A-D).

In SK-N-BE(2) and CHLA-90, only ~1.5–3% of genes associated with differential chromatin accessibility were also differentially expressed in RNA-seq (Figure 22A, C). In contrast, SK-N-AS and NBL-S showed a markedly higher number of common genes, with ~10–12% of ATAC-associated genes also exhibiting significant transcriptomic changes (Figure 22B, D). Notably, although SK-N-BE(2) displayed the highest number of differentially accessible peaks, it showed one of the lowest overlap rates with RNA-seq transcriptional alterations. For CHLA-90, this lower overlap is less surprising given that it also displayed one of the lowest numbers of

ATAC-associated changes overall. Conversely, despite having a lower number of differentially accessible peaks, SK-N-AS exhibited the strongest overlap with RNA-seq, suggesting tighter coupling between chromatin accessibility remodeling and transcriptional adaptation in this context. Finally, NBL-S combined a large number of differentially accessible peaks with high RNA-seq transcriptional alteration, also indicating a stronger relationship between accessibility changes and transcriptional output.

Altogether, these findings suggest that cell line-specific factors like genetic background influence substantially the extent of chromatin accessibility remodeling and its relation to the transcriptional landscape, contributing to a differential adaptation to the metastatic microenvironment.

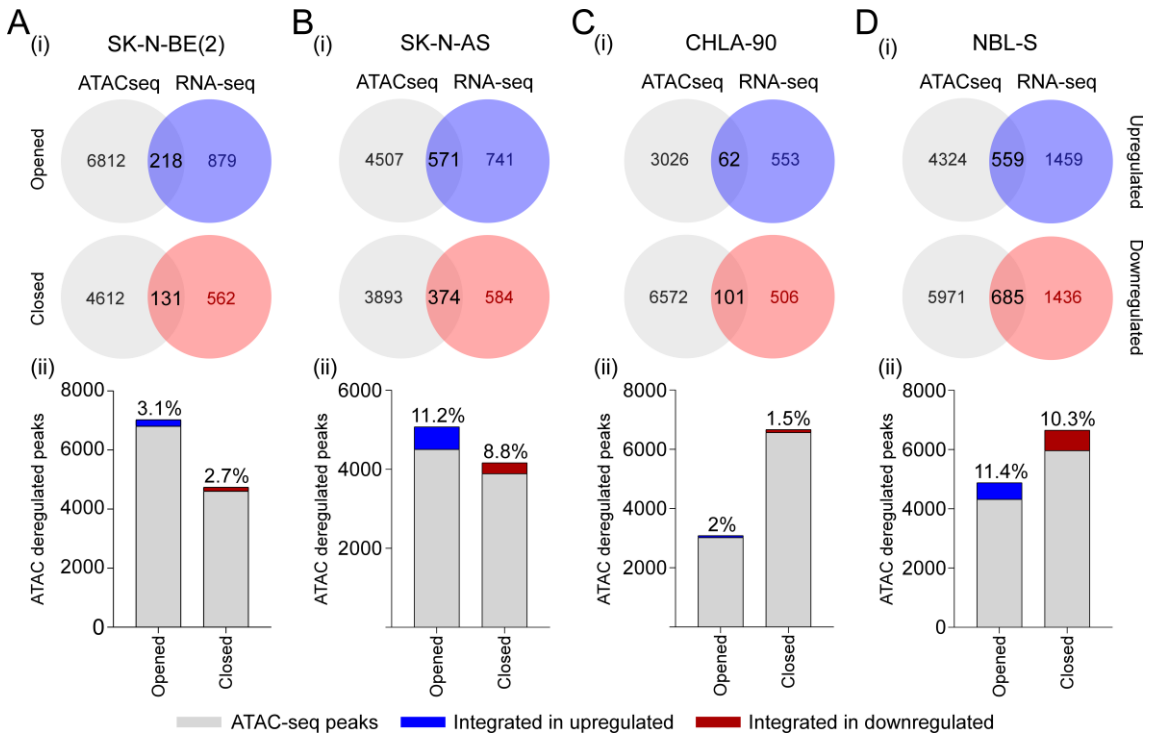

Figure 22. Graphical representation of ATAC- and RNA-seq integration. A-D. Upper panel: Venndiagrams showing ATAC-seq (p—value<0.05) and RNA-seq (p-value<0.05) overlap. Blue indicates RNA-seq upregulated and red RNA-seq downregulated. Lower panel: bar graph indicating percentage of overlapped RNA-seq gene expression with total ATAC-seq gene annotated peaks.

4.8 Integrated chromatin accessibility and gene expression reveals shared Gene Ontology Biological Processes across neuroblastoma models

To delineate the biological processes (BP) underlying tumor cell adaptation to the hepatic microenvironment, ATAC- and RNA-seq profiles were integrated for each cell line, and BP-level enrichment analysis was performed on overlapping gene sets. Enriched terms were then intersected across cell lines to identify programs consistently modulated in liver metastases (Figure 23).

Integration of more accessible regions with transcriptional upregulation highlighted several recurrent processes across cell lines (Figure 23A). These processes were mainly related to membrane-associated signaling including enzyme-linked receptor signaling, positive regulation of signaling, and regulation of transport.

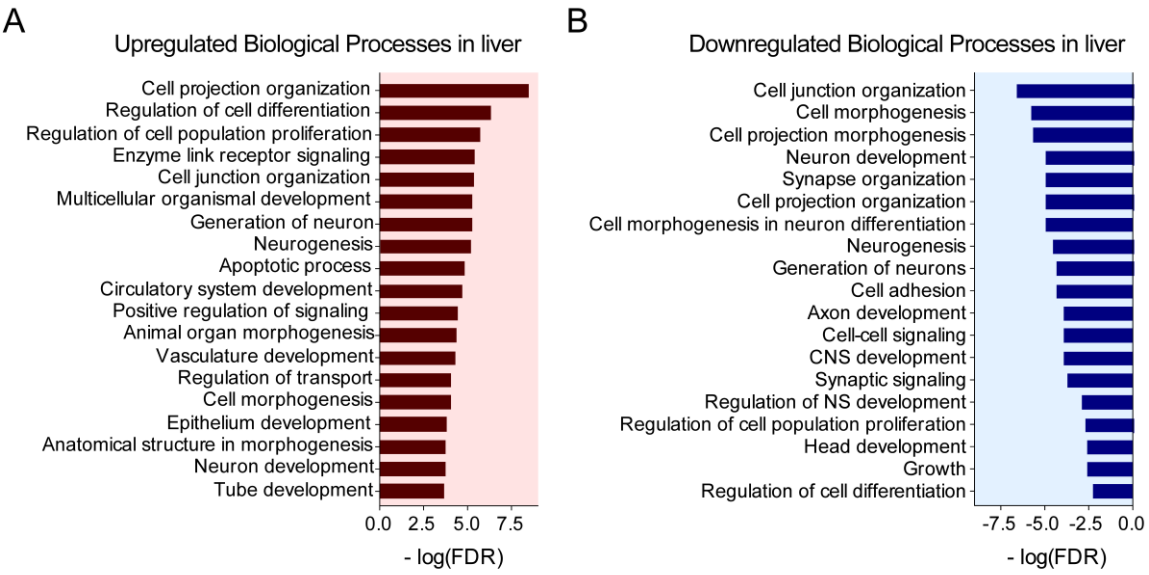

Figure 23. Identification of functional GO Biological Processes after ATAC- and RNA-seq integration. A. Upregulated biological processes in three or more cell lines. B. Downregulated biological processes in three or more cell lines.

In parallel, multiple genes related to phenotypic remodeling were enriched, upregulating processes such as cell projection organization, cell junction organization, regulation of multicellular organismal development and organ morphogenesis (Figure 23A).

Neural-lineage–associated processes such as neurogenesis and tube development were also enriched, suggesting engagement of neuronal differentiation–related gene modules. In addition, genes involved in vascular and angiogenesis programs such as circulatory system development and vasculature development, together with processes related to differentiation, proliferation, and apoptosis, were repeatedly enriched among genes showing coupled increases in accessibility and expression across models.

Conversely, integration of chromatin-closing events with transcriptional downregulation highlighted reduced activity of synapse-associated programs as well as cell–cell interaction pathways, particularly cell adhesion and cell–cell signaling (Figure 23B). Notably, neural-related terms appeared in both concordant upregulated and downregulated sets, indicating that these processes exhibit non-uniform regulation: within the same annotated BP, distinct gene modules showed opposing patterns.

Collectively, these results indicate that although individual cell lines displayed distinct chromatin accessibility and transcriptional changes in liver metastases, conserved biological processes can be identified across models, consistent with shared programs required for metastatic niche adaptation.

4.9 Identification of potential therapeutic targets against neuroblastoma metastases

To identify genes with potential therapeutic relevance in NB metastasis, we used an integrative multi-omic approach combining ATAC-seq and RNA-seq (Figure 24), followed by candidate prioritization based on clinical relevance through bioinformatic analyses and interrogation of publicly available datasets.

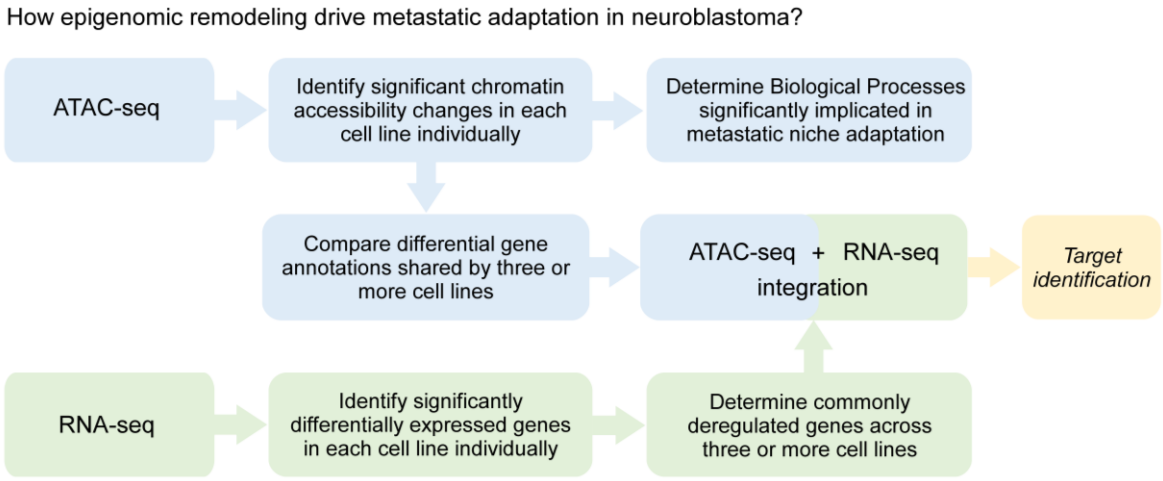

Figure 24. ATAC- and RNA-seq integrated target identification workflow.

First, chromatin accessibility (ATAC-seq) and gene expression (RNA-seq) were analyzed independently for each cell line. We then prioritized shared genes with increased (n = 1,206) or decreased accessibility (n = 1,887) that were observed in at least three cell lines (Figure 25A). In parallel, we applied an analogous strategy to the transcriptomic data, selecting genes that were consistently upregulated (n = 55) or downregulated (n = 27) across three or more cell lines (Figure 25B). Schematic workflow of ATAC-seq and RNA-seq analyses was represented in Figure 25C. Next, we integrated both layers by intersecting accessibility-associated candidates with concordant expression changes, identifying 20 candidate genes: 15 with increased accessibility and upregulated expression, and 5 with decreased accessibility together with downregulated expression (Figure 25D).

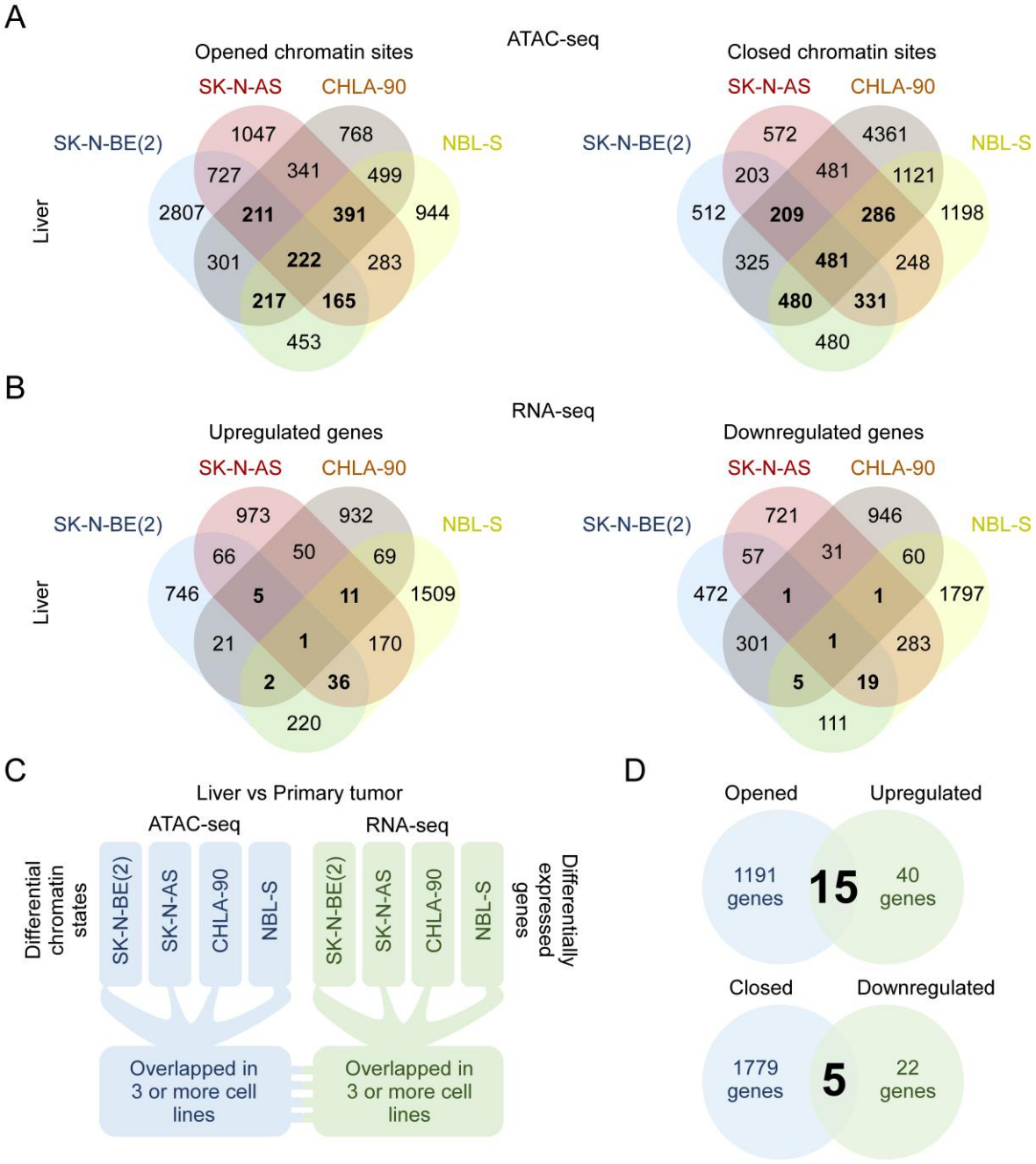

Figure 25. Integrated analysis of ATAC- and RNA-seq data across cell lines (p-value<0.05). A. Overlapping annotated ATAC-seq opened and closed genes for liver metastases. B. Overlapping upregulated and downregulated genes for RNA-seq. C. Schematic representation of ATAC- and RNA-seq analyses. D. ATAC- (blue) and RNA-seq (green) integration for target identification.

4.10 Prioritization of upregulated metastatic candidate targets

From the 20 genes identified through the integrative ATAC-seq/RNA-seq analysis, we prioritized the 15 genes displaying concordant transcriptional upregulation together with increased chromatin accessibility in at least three cell lines. This prioritization was motivated by the rationale that this epigenetic and transcriptional pattern in metastatic contexts may offer more confident candidates for therapeutic intervention, as they reflect actively engaged regulatory programs. Accordingly, this subset of upregulated candidates was selected for initial follow-up and characterization (Table 12). Moreover, two alternative candidates marked with an asterisk in Table 12 were included due to clear significance in RNA-seq data, supported by near significant ATAC-seq chromatin accessibility in some models.

Table 12. Potential upregulated targets after ATAC-seq and RNA-seq gene integration. Alternative candidates are marked with an asterisk. Fold change express mean across significant cell lines.

Gene	Protein function	Subcellular location	Fold change	Inhibitor
ADAMTS1	Metalloproteinase	Extracellular matrix	2.71±0.7	-
AFAP1	Cytoskeleton	Cytoplasm	1.38±0.03	-
**ASCL1*	Transcription factor	Nucleus	3,21 ± 1,04	-
BEND4	Protein-DNA interaction	Cytoplasm and nucleus	2.83±1.2	-
**DLL3*	Notch ligand	Cell membrane	3,16 ± 1,2	Inhibitory antibody
DUSP10	Phosphatase	Cytoplasm and nucleus	1.49±0.14	-
GFRA2	GPI-anchored receptor	Cell membrane	9.27±6.17	Small molecule
GRK5	Ser/Thr-Kinase	Cell membrane, cytoplasm and nucleus	1.71±0.23	Yes
KCNIP1	Subunit K+ channel	Cell membrane and cytoplasm	9.62±2.49	-
MSX2	Transcription factor	Nucleus	4.44±2.42	-
NOL4	RNA-binding	Nucleus	1.26±0.09	-
PRAG1	Tyrosine-Kinase	Cytoplasm and nucleus	1.1±0.05	-
RFTN1	Lipid-raft	Cell membrane and cytoplasm	2.73±0.74	-
SCHIP1	Cytoskeleton	Cytoplasm	1.27±0.08	-
SEZL6	Transmembrane	Endoplasmic reticulum	3.02±1.37	-
STK3	Ser/Thr-Kinase	Cytoplasm, nucleus and cell membrane	1.31±0.19	Yes
TBX3	Transcription factor	Nucleus	2.48±0.56	-

4.11 Metastasis-associated candidates are dispensable for neuroblastoma cell viability in DepMap

Using DepMap CRISPR-Cas9 loss-of-function screens, we evaluated whether the metastasis-associated candidates prioritized from our multi-omic analyses were also required for NB cell viability *in vitro* (Figure 26). Chronos gene-effect scores were extracted from 14 NB cell lines available in the platform (SK-N-BE(2), SK-N-AS, CHLA-90, KELLY, SK-N-FI, SK-N-DZ, SK-N-SH, COG-N-278, COG-N-305, LS, IMR-32, NGP, NB69 and SHSY-5Y). Across this panel, STK3, ASCL1, TBX3, BEND4 and *DLL3* genes presented a negative chronos gene score. However, none of them achieved a median -1-threshold considered to indicate a major dependency. Particularly, only *ASCL1* displayed marked negative outliers in a small subset of cell lines, consistent with a context-restricted dependency rather than a broadly essential gene in this context. *SHIP1, GFRA2, ADAMTS1, DUSP10, KCNIP1,* and *GRK5* showed gene-effect values clustered close to 0, indicating little to no viability dependency under standard culture conditions. Moreover, the subset of *NOL4, PRAG1, RFTN1* and *AFAP1* genes, showed an increased gene effect after CRISPR/Cas9, indicating higher proliferation rates when the gene is not present. Overall, these data indicate that the prioritized candidates are not captured as common DepMap "core viability" dependencies in NB, supporting the notion that their relevance may be scenario-specific (e.g., metastatic adaptation, niche interactions, or state-dependent programs) rather than universal requirements for proliferation *in vitro*.

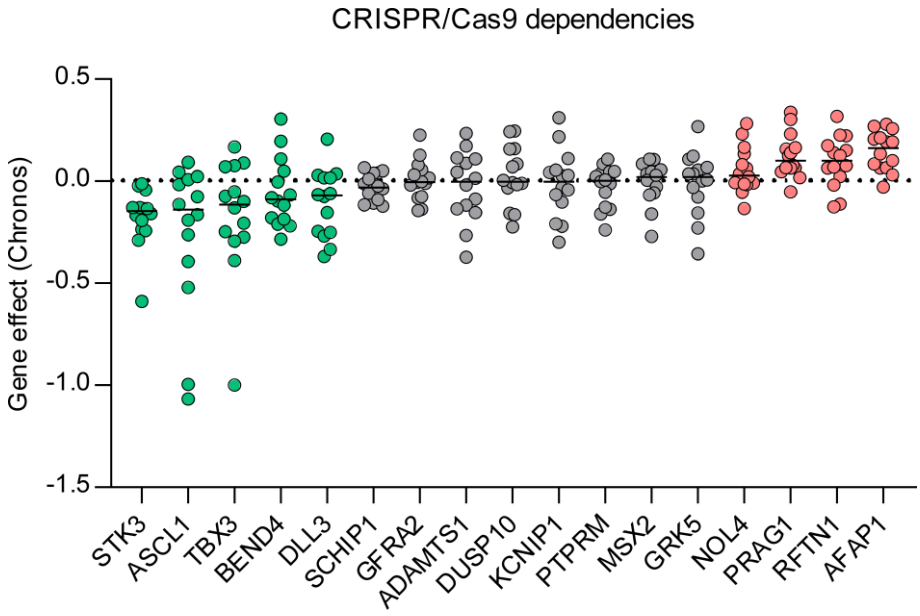

Figure 26. DepMap dependency analysis for upregulated candidates and alternative candidates.

4.12 Selection of metastasis-associated candidates based on biological, transcriptional, and therapeutic features

Given that DepMap dependency scores alone were not sufficient to prioritize therapeutic targets in metastatic NB, as functional dependency screens may not capture the full spectrum of therapeutically relevant vulnerabilities, we next applied additional selection criteria to enrich for candidates with either (1) potential clinical relevance or (2) features suggesting novelty in the cancer field. For each candidate, we reviewed intrinsic protein features and relevance within our models, including protein function, subcellular localization, reported links to cancer biology, RNA-seq fold-change, and the availability of inhibitors (Table 12). Based on this multi-parameter prioritization, six genes—*ADAMTS1, ASCL1, DLL3, GFRA2, GRK5,* and *KCNIP1*—emerged as the most promising candidates for deeper investigation.

The characterization of the prioritized genes followed two complementary levels of analysis. First, we examined the epigenetic and transcriptional profiles of selected candidates in liver metastases using ATAC- and RNA-seq data. *GFRA2* and *GRK5* are shown here as representative examples of targets that were ultimately selected (Figure 27 and 28), illustrating the type of coordinated chromatin and expression

changes associated with metastatic lesions. We then evaluated the clinical relevance of the candidate genes through bioinformatical analyses including gene expression in metastatic patients, their correlation to overall survival, tumor-cell specificity, and comparison with healthy tissue expression.

To first characterize the epigenomic and transcriptomic profile regulation of these prioritized targets, ATAC-seq signal was visualized across each gene locus, highlighting in grey differentially accessible peaks (hereafter referred to consensus peaks) identified in each cell line and organ, together with the corresponding RNA-seq expression changes (Figure 27 and 28).

For *GFRA2*, in all models showing significant *GFRA2* upregulation (SK-N-BE(2), SK-N-AS, and NBL-S; Figure 27E, F and H), expression changes were accompanied by chromatin accessibility modulations across the locus (Figure 27A, B and D). These modulated regions included promoter-proximal as well as intronic and intergenic consensus peaks. Particularly, in SK-N-BE(2), liver-associated accessibility changes did not reach the nominal significance threshold ($p = 0.07$) but was retained for visualization (Figure 26A). Moreover, significant increase of chromatin accessibility in bone marrow was observed in this model (Figure 27A). The specific consensus peaks affected across cell lines were partly shared and partly cell line–specific (Figure 27A-B and 27D). However, accessibility changes for *GFRA2* were more frequently organ-dependent within a given model, with several consensus peaks modulated in only one metastatic site (Figure 27A-B and 27D). Conversely, liver metastases derived from the CHLA-90 cell line did not show significant *GFRA2* gene deregulation (Figure 27G) or alterations in chromatin accessibility (Figure 27C).

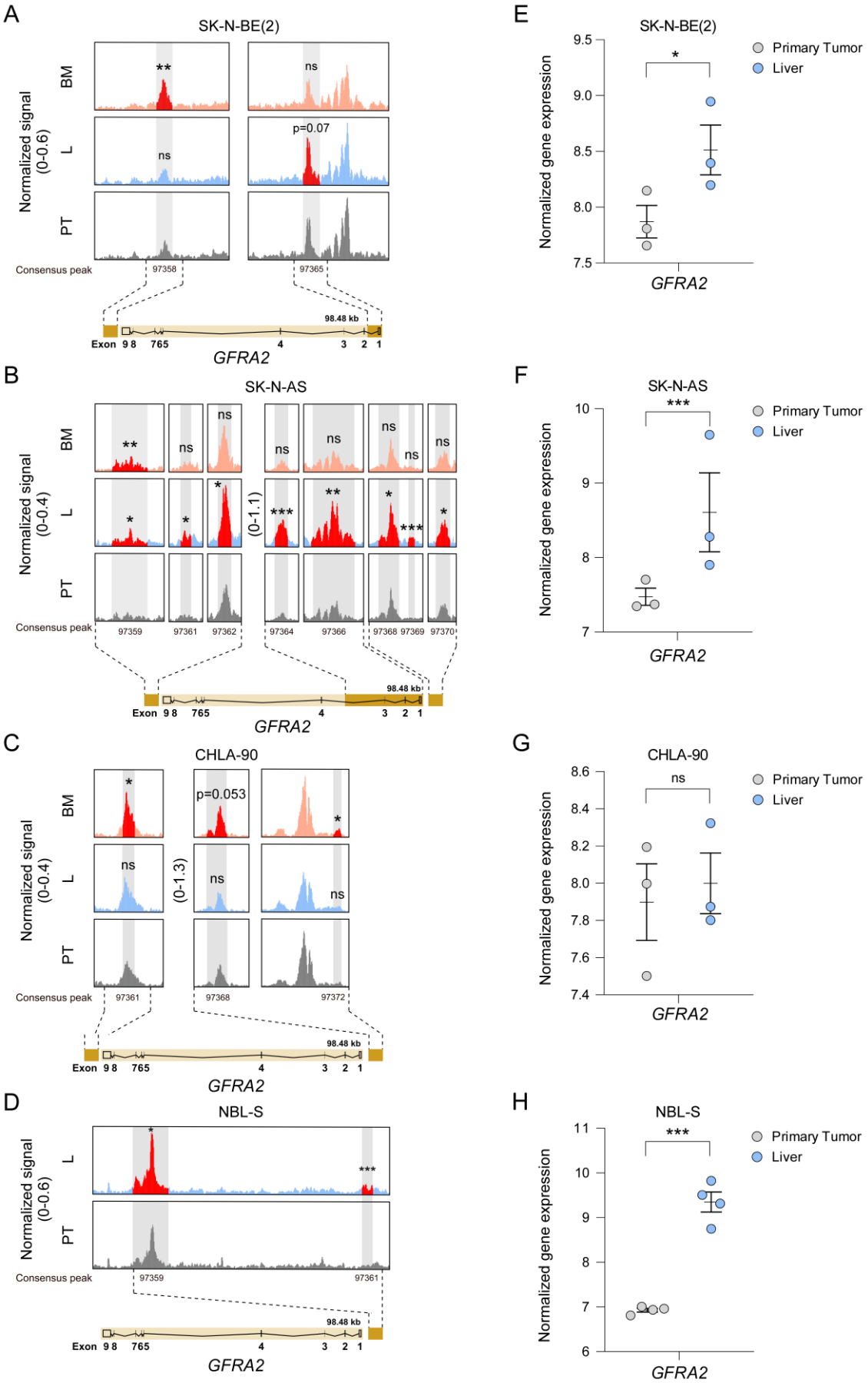
A
SK-N-BE(2)
Normalized signal (0-0.6)
BM
L
PT
**
ns
ns
p=0.07
Consensus peak
97358
97365
98.48 kb
Exon 9 8 765 4 3 2 1
GFRA2
B
SK-N-AS
Normalized signal (0-0.4)
(0-1.1)
Consensus peak
97359
97361
97362
97364
97366
97368 97369
97370
C
CHLA-90
Normalized signal (0-0.4)
(0-1.3)
p=0.053
Consensus peak
97361
97368
97372
D
NBL-S
Normalized signal (0-0.6)
Consensus peak
97359
97361
E
SK-N-BE(2)
Normalized gene expression
Primary Tumor
Liver
GFRA2
F
SK-N-AS
***
G
CHLA-90
H
NBL-S

Figure 27. Epigenetic and transcriptomic modulation of *GFRA2* gene. A-D. ATAC-seq modulated peaks normalized signal. E-H. RNA-seq normalized gene expression modulation. BM: Bone marrow; L: Liver; PT: Primary tumor.

For *GRK5*, concordant increases in accessibility and expression were observed in SK-N-BE(2) (Figure 28A and 28E) and SK-N-AS (Figure 28B and 28F), involving promoter-proximal regions and intronic consensus peaks. In contrast, CHLA-90 exhibited differential accessibility changes across the *GRK5* locus in liver metastases without a significant expression change (Figure 28C and 28G). Conversely, NBL-S showed significant *GRK5* overexpression in liver metastases despite the absence of differentially accessible peaks meeting the applied thresholds in the *GRK5* locus (Figure 28D and 28H). Across models with both organs available, and in contrast to *GFRA2*, several *GRK5* consensus peaks modulated in liver metastases were also modulated in bone marrow within the same cell line (Figure 28A–C). However, the specific consensus peaks affected differed between cell lines, consistent with strong model-dependent accessibility patterns also observed in *GFRA2*. In addition, some accessibility changes were organ-associated, as not all liver changes were detected in bone marrow and vice versa (Figure 28B and 28C).

This analysis showed that chromatin accessibility at a given gene can be modulated through distinct consensus peaks across cell lines, consistent with heterogeneity in epigenetic regulation among NB metastatic models. In addition, increased accessibility was not uniformly associated with transcriptional upregulation across models.

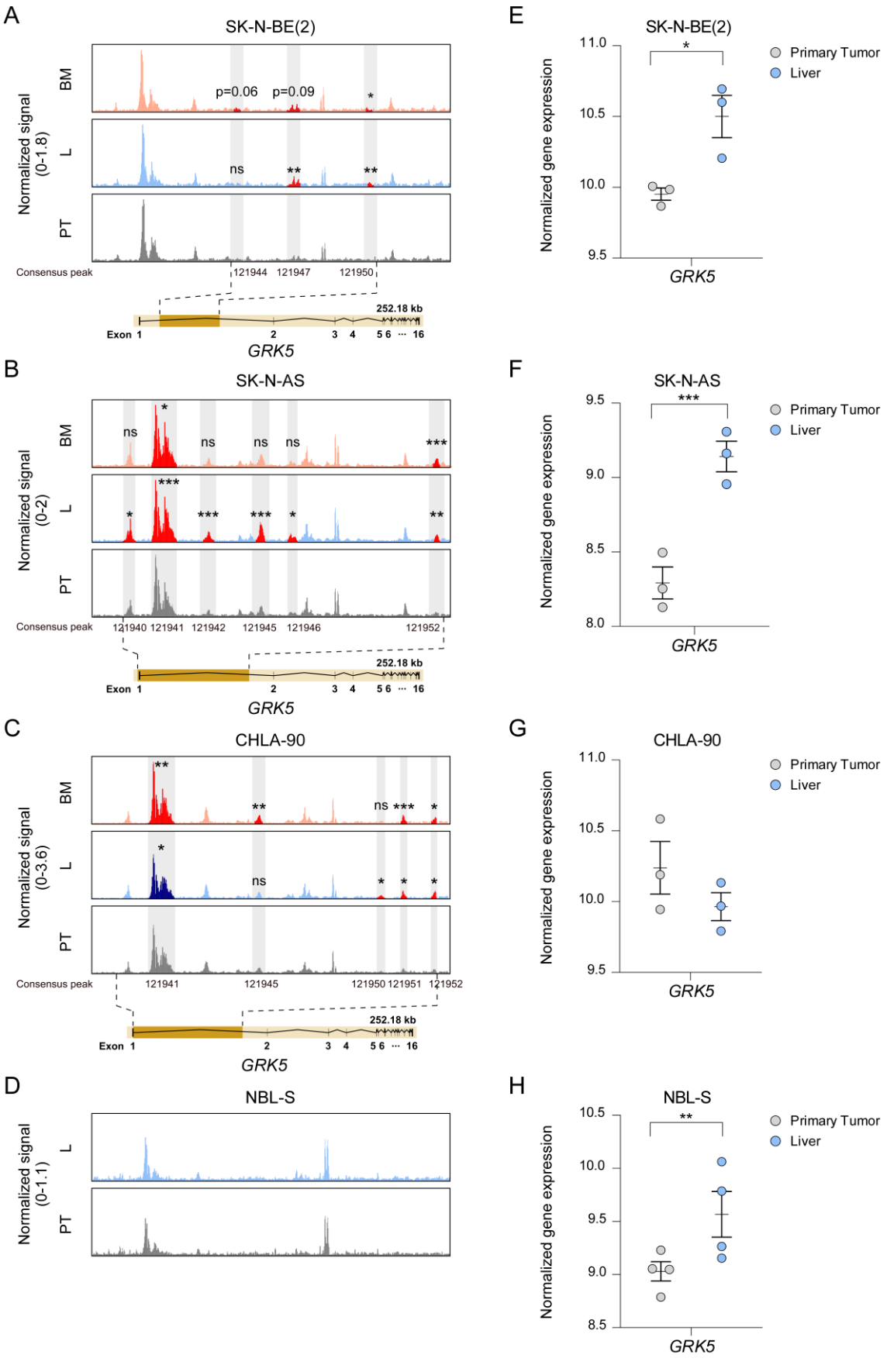
A
SK-N-BE(2)
Normalized signal (0-1.8)
BM
L
PT
p=0.06
p=0.09
*
ns
**
**
Consensus peak
121944
121947
121950
252.18 kb
Exon 1
2
3
4
5 6 ··· 16
GRK5
B
SK-N-AS
Normalized signal (0-2)
BM
L
PT
ns
*
ns
ns
ns
***
***
*
***
***
*
**
Consensus peak
121940
121941
121942
121945
121946
121952
252.18 kb
Exon 1
2
3
4
5 6 ··· 16
GRK5
C
CHLA-90
Normalized signal (0-3.6)
BM
L
PT
**
**
ns
***
*
*
ns
*
*
*
Consensus peak
121941
121945
121950
121951
121952
252.18 kb
Exon 1
2
3
4
5 6 ··· 16
GRK5
D
NBL-S
Normalized signal (0-1.1)
L
PT
E
SK-N-BE(2)
Normalized gene expression
11.0
10.5
10.0
9.5
*
Primary Tumor
Liver
GRK5
F
SK-N-AS
Normalized gene expression
9.5
9.0
8.5
8.0
***
Primary Tumor
Liver
GRK5
G
CHLA-90
Normalized gene expression
11.0
10.5
10.0
9.5
Primary Tumor
Liver
GRK5
H
NBL-S
Normalized gene expression
10.5
10.0
9.5
9.0
8.5
**
Primary Tumor
Liver
GRK5

Figure 28. Epigenetic and transcriptomic modulation of *GRK5* gene. A-D. ATAC-seq modulated peaks normalized signal. E-H. RNA-seq normalized gene expression modulation. BM: Bone marrow; L: Liver; PT: Primary tumor.

After defining the epigenomic and transcriptomic landscapes of the selected candidates, we assessed their clinical relevance using public patient datasets.

At the expression level, *GFRA2* was significantly upregulated in metastatic patient group (stage 4) across two NB datasets, including the Kocak cohort (Figure 29A) and the SEQC cohort (data not shown), both available through the R2 platform. In survival analyses, higher *GFRA2* expression was associated with poorer prognosis in the Kocak dataset (Figure 29B), with the separation between groups becoming more evident at longer follow-up times (up to 200 months). To further characterize its cellular distribution, we interrogated single-cell transcriptomic data from the R2 NBAtlas, including tumor cells, immune populations (B and T lymphocytes, myeloid progenitors, and NK cells), fibroblasts, Schwann cells, endothelial cells, and other stromal populations (Figure 29C). *GFRA2* showed marked tumor-cell specificity, with only minimal expression in non-malignant cell populations. To complement this analysis, we examined *GFRA2* expression in the Tabula Sapiens single-cell atlas, which enabled the assessment of baseline transcriptional distribution across multiple healthy organs and cell types at single-cell resolution. *GFRA2* showed very low expression across most analyzed tissues (Figure 29D), with only sparse and highly restricted expression in specific cellular subsets. This pattern was further supported by comparative analyses across healthy tissues and four independent NB tumor datasets, in which *GFRA2* displayed a strong contrast between tumor and normal samples (Figure 29E). Expression was consistently elevated in all NB datasets, whereas healthy tissues generally showed low *GFRA2* levels, with relatively higher expression detected in brain. Notably, the association between high expression and poor overall survival was maintained when the analysis was restricted to stage 4 patients (Figure 29F).

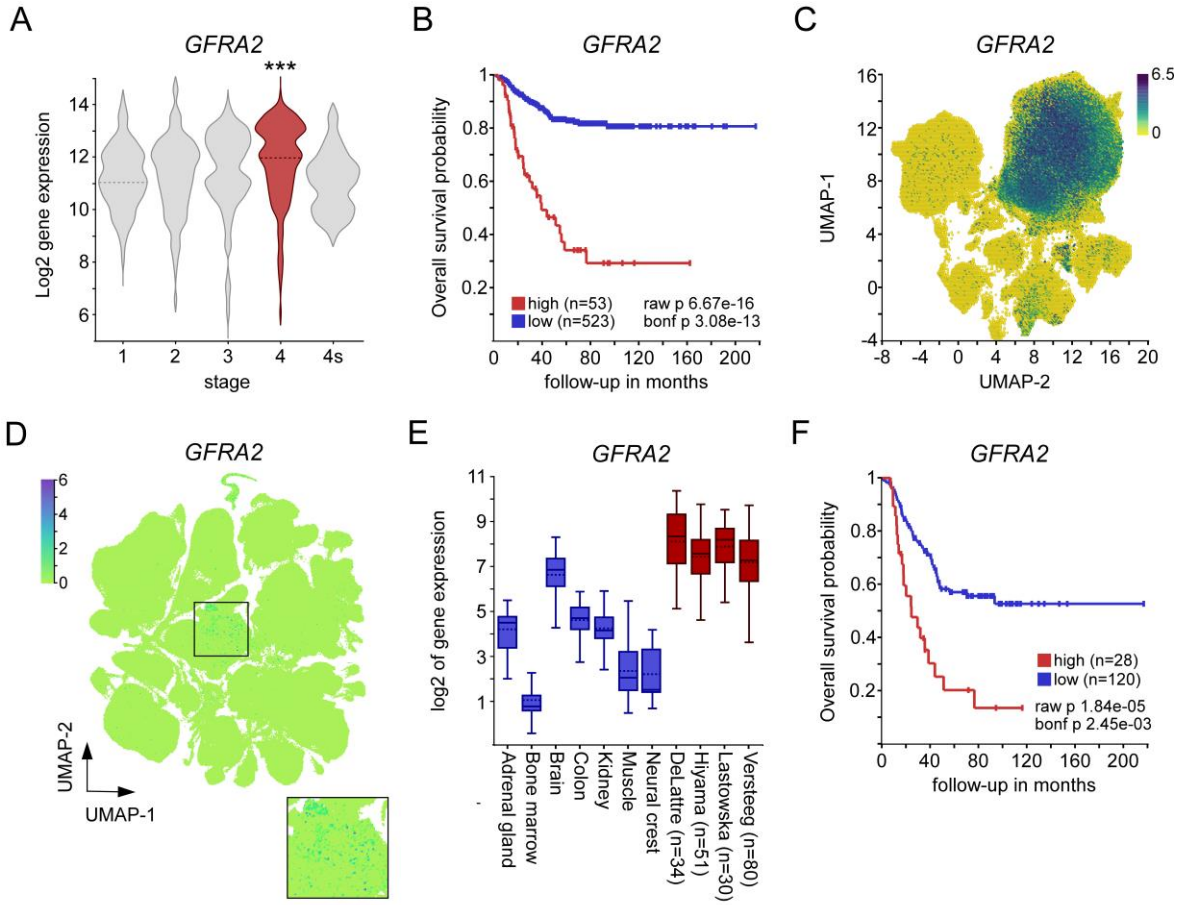

Figure 29. *GFRA2* clinical relevance analysis. A. Log2 gene expression for *GFRA2* in R2 platform (Kocak) across disease stages. Significance refers to the comparison between Stage 4 and Stage 1 patients. B. Kaplan-Meier curves showing prognosis in high and low *GFRA2* expression patients (Kocak). C. scRNA-seq *GFRA2* gene expression data from NBAtlas NB patients (de Preter, n=68 patients) across cell types. D. Tabula sapiens UMAP of scRNA-seq gene expression in healthy tissues. E. Healthy tissues (purple) gene expression compared to four different NB datasets (Red; DeLattre (n=34), Hiyama (n=51), Lastowska (n=30) and Versteeg (n=80). F. Kaplan-Meier curved showing prognosis in high and low *GFRA2* expression stage 4 patients (Kocak).

GRK5 was also significantly upregulated in metastatic patient group (stage 4) across both the Kocak (Figure 30A) and SEQC (data not shown) NB cohorts. Higher *GRK5* expression was associated with poorer overall survival in the Kocak dataset (Figure 30B), again with a more evident separation at longer follow-up. In the NBAtlas single-cell data, *GRK5* expression was predominantly detected in tumor cells, although moderate expression was also observed in endothelial and fibroblast populations (Figure 30C). In Tabula Sapiens, *GRK5* showed detectable expression in selected cell populations, particularly within cardiovascular-associated and colorectal-related cell types (Figure 30D). When compared across healthy tissues

and NB datasets, *GRK5* retained a marked tumor-versus-normal contrast (Figure 30E), with consistently higher expression in NB and lower expression in most healthy tissues, except for relatively elevated levels in the adrenal gland. After restricting the Kaplan–Meier analysis to St4 patients, the direction of the effect remained consistent with that observed in the full cohort, although statistical significance was lost (Figure 30F). This likely reflects the very small number of stage 4 patients with low *GRK5* expression rather than a true reversal of the association.

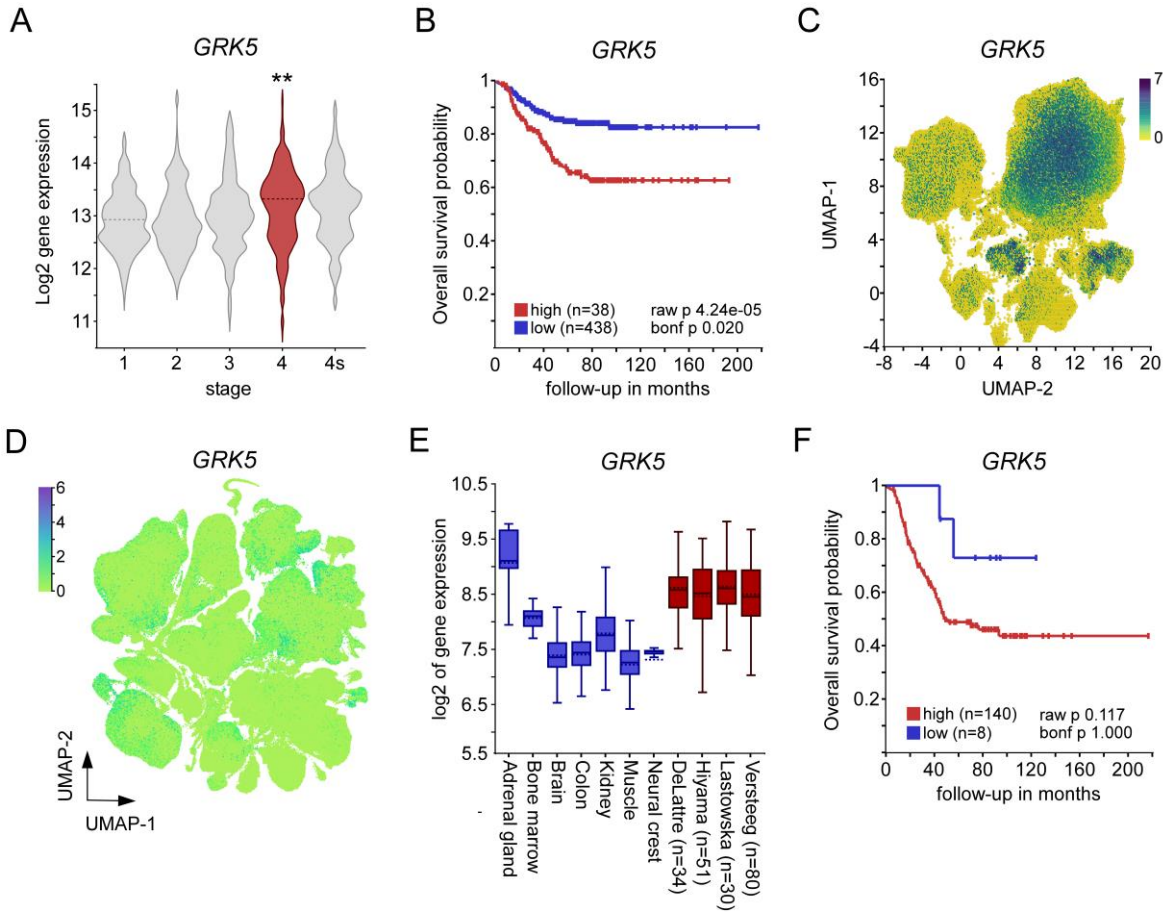

Figure 30. *GRK5* clinical relevance analysis. A. Log2 gene expression for *GRK5* in R2 platform (Kocak) across disease stages. Significance refers to the comparison between Stage 4 and Stage 1 patients. B. Kaplan-Meier curves showing prognosis in high and low *GRK5* expression patients (Kocak). C. scRNA-seq *GRK5* gene expression data from NBAtlas NB patients (de Preter, n=68 patients) across cell types. D. Tabula sapiens UMAP of scRNA-seq gene expression in healthy tissues. E. Healthy tissues (purple) gene expression compared to four different NB datasets (Red; DeLattre (n=34), Hiyama (n=51), Lastowska (n=30) and Versteeg (n=80). F. Kaplan-Meier curved showing prognosis in high and low *GRK5* expression stage 4 patients (Kocak).

Similarly, *KCNIP1* was significantly upregulated in stage 4 patients across both the Kocak (Figure 31A) and SEQC (data not shown) datasets. Higher *KCNIP1* expression

was associated with poorer prognosis in the Kocak cohort (Figure 31B). In the NBAtlas, *KCNIP1* expression was also largely restricted to tumor cells, although at lower levels than those observed for *GFRA2* and *GRK5* (Figure 31C). Consistent with this, Tabula Sapiens showed very low *KCNIP1* expression across most healthy tissues (Figure 31D), again with only minimal and localized expression in selected cellular subsets. However, when healthy tissues were compared against NB datasets, *KCNIP1* displayed a more intermediate profile than the other candidates (Figure 31E), with expression in NB samples being broadly comparable to that detected in several healthy tissues. In line with this weaker contrast, restricting the survival analysis to stage 4 patients reduced statistical power and attenuated the separation between the high- and low-expression groups (Figure 31F).

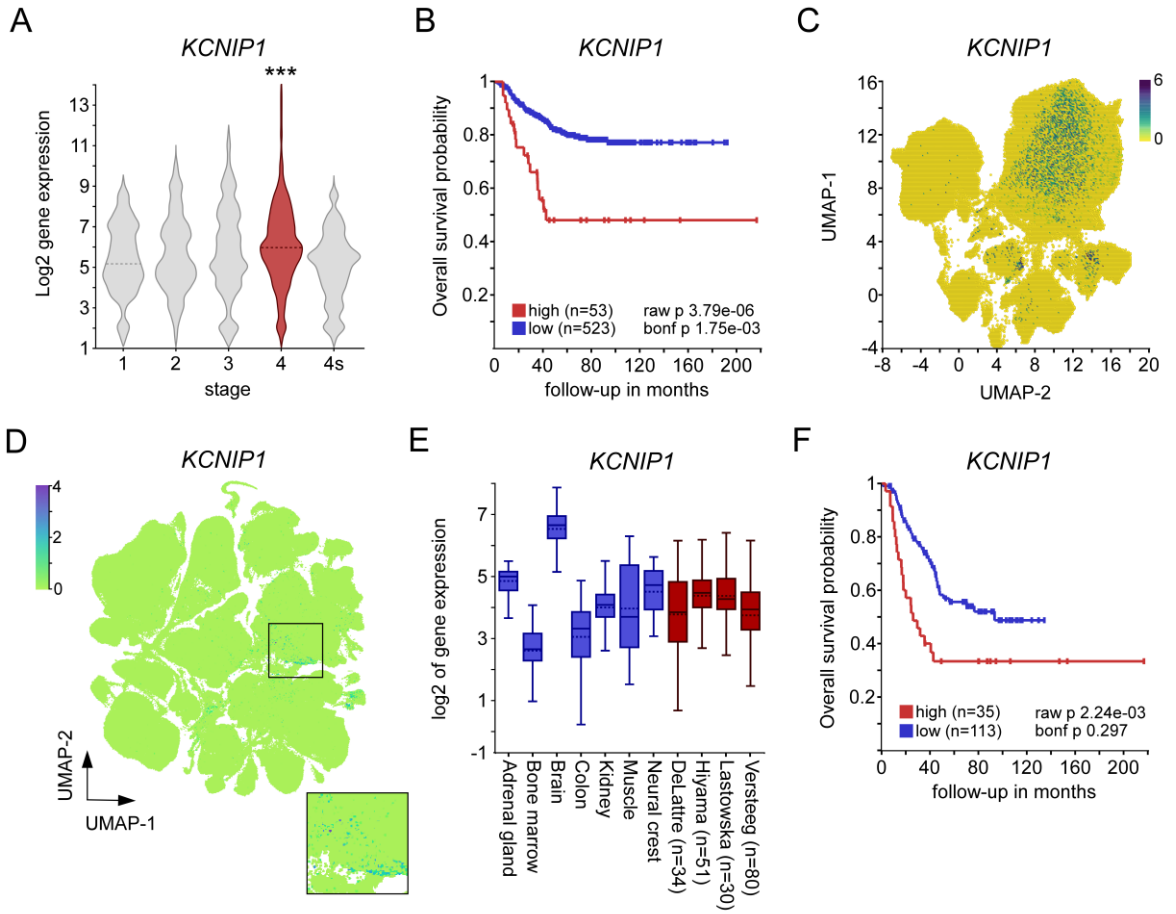

Figure 31. *KCNIP1* clinical relevance analysis. A. Log2 gene expression for *KCNIP1* in R2 platform (Kocak) across disease stages. Significance refers to the comparison between Stage 4 and Stage 1 patients. B. Kaplan-Meier curves showing prognosis in high and low *KCNIP1* expression patients (Kocak). C. scRNA-seq KCNIP1 gene expression data from NBAtlas NB patients (de Preter, n=68 patients) across cell types. D. Tabula sapiens UMAP of scRNA-seq gene expression in healthy tissues. E. Healthy tissues (purple) gene expression compared to four different NB datasets (Red; DeLattre

(n=34), Hiyama (n=51), Lastowska (n=30) and Versteeg (n=80). F. Kaplan-Meier curved showing prognosis in high and low *KCNIP1* expression stage 4 patients (Kocak).

Because *ASCL1* and *DLL3* were incorporated as additional candidates and are also functionally linked within the same biological pathway, they are presented together in the following section. Their joint evaluation was intended not only to maintain coherence in the analysis, but also to reflect the biological relationship between these two genes and facilitate interpretation of their shared and distinct features as potential NB targets.

At the expression level, both *ASCL1* and *DLL3* were significantly upregulated in metastatic patient group across the Kocak cohort (Figure 32A and 32G) and the SEQC cohort (data not shown). In survival analyses, higher expression of both genes was associated with poorer prognosis in the Kocak dataset (Figure 32B and 32H), with the separation between groups becoming increasingly evident over longer follow-up periods. In the NBAtlas single-cell data, *ASCL1* and *DLL3* showed the highest tumor-cell specificity among all candidates, with minimal expression in non-malignant populations (Figure 32C and 32I). This pattern was reinforced by Tabula Sapiens analysis, in which both genes showed near-residual expression across healthy tissues (Figure 32D and 32J). When healthy tissue expression was compared with NB datasets, DLL3 displayed a marked tumor-versus-normal contrast (Figure 32K). *ASCL1* also showed higher expression in NB datasets; however, the difference was less pronounced, as baseline expression in certain healthy tissues, including adrenal gland, brain, and skeletal muscle, reached levels comparable to those observed in tumor samples (Figure 32E). For both *ASCL1* and *DLL3*, the overall survival pattern was maintained after restricting the analysis to metastatic patients (Figure 32F and 32L).

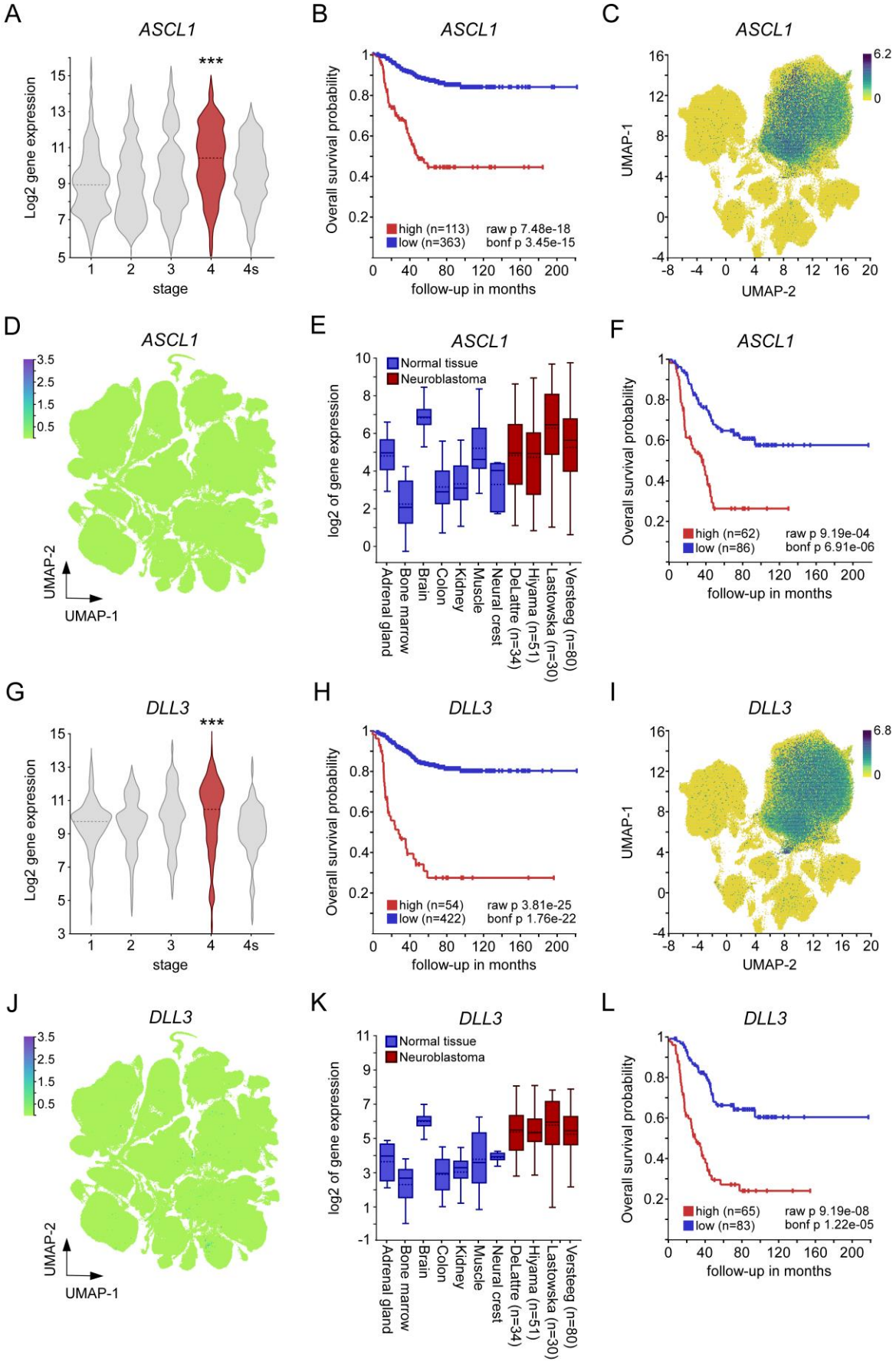
A
ASCL1
***
Log2 gene expression
stage
1
2
3
4
4s
B
ASCL1
Overall survival probability
high (n=113)
low (n=363)
raw p 7.48e-18
bonf p 3.45e-15
follow-up in months
C
ASCL1
UMAP-1
UMAP-2
6.2
0
D
ASCL1
UMAP-2
UMAP-1
E
ASCL1
Normal tissue
Neuroblastoma
log2 of gene expression
Adrenal gland
Bone marrow
Brain
Colon
Kidney
Muscle
Neural crest
DeLattre (n=34)
Hiyama (n=51)
Lastowska (n=30)
Versteeg (n=80)
F
ASCL1
Overall survival probability
high (n=62)
low (n=86)
raw p 9.19e-04
bonf p 6.91e-06
follow-up in months
G
DLL3
***
Log2 gene expression
stage
H
DLL3
Overall survival probability
high (n=54)
low (n=422)
raw p 3.81e-25
bonf p 1.76e-22
follow-up in months
I
DLL3
UMAP-1
UMAP-2
6.8
0
J
DLL3
UMAP-2
UMAP-1
K
DLL3
Normal tissue
Neuroblastoma
log2 of gene expression
Adrenal gland
Bone marrow
Brain
Colon
Kidney
Muscle
Neural crest
DeLattre (n=34)
Hiyama (n=51)
Lastowska (n=30)
Versteeg (n=80)
L
DLL3
Overall survival probability
high (n=65)
low (n=83)
raw p 9.19e-08
bonf p 1.22e-05
follow-up in months

Figure 32. *ASCL1* and *DLL3* clinical relevance analysis. A and G. Log2 gene expression for *ASCL1* and *DLL3* in R2 platform (Kocak) across disease stages. Significance refers to the comparison between Stage 4 and Stage 1 patients. B and H. Kaplan-Meier curves showing prognosis in high and low *ASCL1* and *DLL3* expression patients (Kocak). C and I. scRNA-seq *ASCL1* and *DLL3* gene expression data from NBAtlas NB patients (de Preter, n=68 patients) across cell types. D and J. Tabula sapiens UMAP of scRNA-seq gene expression in healthy tissues. E and K. Healthy tissues (purple) gene expression compared to four different NB datasets (Red; DeLattre (n=34), Hiyama (n=51), Lastowska (n=30) and Versteeg (n=80). F and L. Kaplan-Meier curved showing prognosis in high and low *ASCL1* and *DLL3* expression stage 4 patients (Kocak).

4.13 Prioritization of downregulated metastatic drivers

Then, to broaden the identification of potential drivers of metastatic colonization and proliferation, we also analyzed downregulated genes after the integrative ATAC/RNA-seq analysis (Table 13).

Table 13. Potential downregulated targets after ATAC-seq and RNA-seq gene integration. Fold change express mean across significant cell lines.

Gene	Protein function	Subcellular location	Fold change
HS6ST3	Enzyme (sulfotransferasa)	Golgi apparatus membrane	−2.45 ± 0.35
KCNMB4	Subunit K^+ Channel	Cell membrane	−1.16 ± 0.01
LMNB1	Component nuclear lamina	Nucleus lamina	−1.11 ± 0.02
OSBPL3	Lipid metabolism	Endoplasmic reticulum, Cell membrane, Cytosol	−1.42 ± 0.20
VSNL1	Neuron-specific Ca+ sensor	Cell membrane, cytosol	−3.98 ± 2.30

As performed for upregulated genes, the clinical relevance of downregulated genes was assessed using public patient datasets from the R2 platform.

In the Kocak NB cohort, *HS6ST3* was significantly downregulated in metastatic patient groups (stage 4) (Figure 33A). In line with this, lower expression of *HS6ST3* was associated with poorer overall survival (Figure 33B). When the analysis was restricted to metastatic patients, the same tendency was observed, although with reduced statistical significance (Figure 33C).

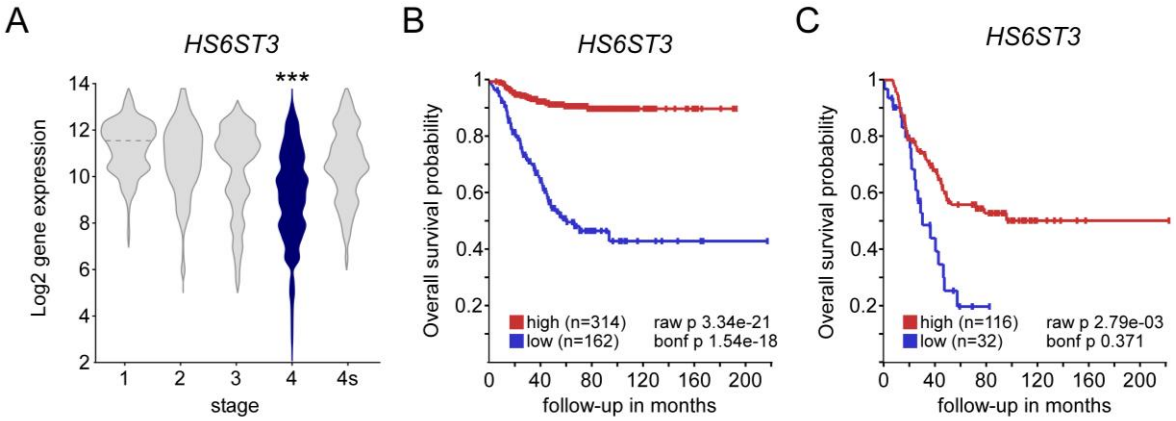

Figure 33. *HS6ST3* clinical relevance analysis. A. Log2 gene expression for *HS6ST3* in R2 platform (Kocak) across disease stages. Significance refers to the comparison between Stage 4 and Stage 1 patients. B. Kaplan-Meier curves showing prognosis in high and low *HS6ST3* expression patients (Kocak). C. Kaplan-Meier curve analysis for stage 4 patients.

KCNMB4 was likewise significantly downregulated in stage 4 patients (Figure 34A), and lower expression levels of *KCNMB4* were associated with worse overall survival (Figure 34B). However, after limiting the Kaplan-Meier analysis to stage 4 patients, this association was no longer evident, likely due to the very small number of patients classified as low KCNMB4 expression (Figure 34C).

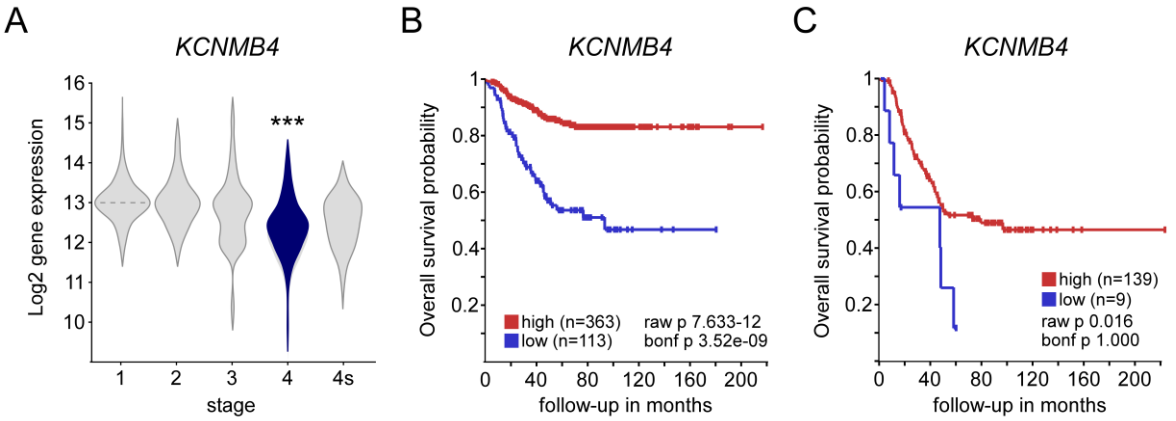

Figure 34. *KCNMB4* clinical relevance analysis. A. Log2 gene expression for *KCNMB4* in R2 platform (Kocak) across disease stages. Significance refers to the comparison between Stage 4 and Stage 1 patients. B. Kaplan-Meier curves showing prognosis in high and low *KCNMB4* expression patients (Kocak). C. Kaplan-Meier curve analysis for stage 4 patients.

Similarly, OSBPL3 was significantly downregulated in metastatic patient group (Figure 35A). Moreover, lower expression of *OSBPL3* was associated with poorer overall survival (Figure 35B). Notably, this pattern was preserved after restricting the analysis to stage 4 patients (Figure 35C).

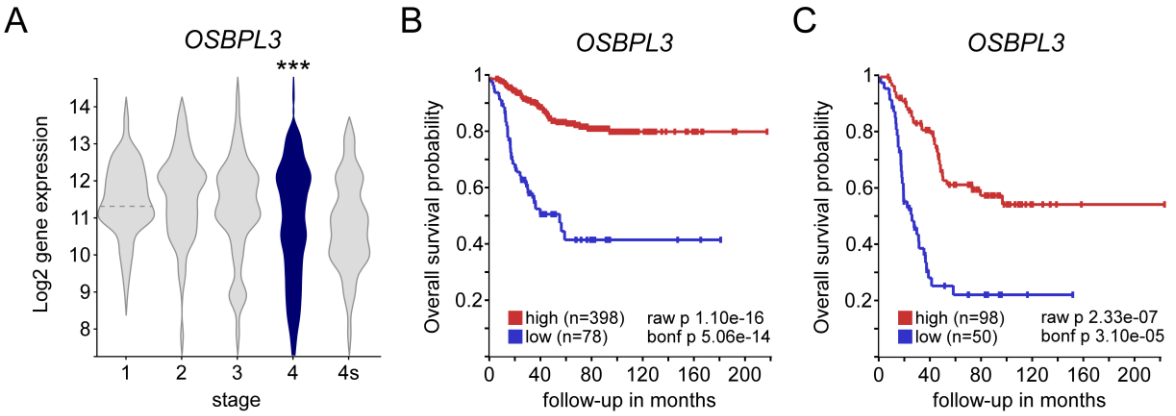

Figure 35. *OSBPL3* clinical relevance analysis. A. Log2 gene expression for *OSBPL3* in R2 platform (Kocak) across disease stages. Significance refers to the comparison between Stage 4 and Stage 1 patients. B. Kaplan-Meier curves showing prognosis in high and low *OSBPL3* expression patients (Kocak). C. Kaplan-Meier curve analysis for stage 4 patients.

VSNL1 was also significantly downregulated in metastatic patient groups (stage 4) (Figure 36A). Consistent with this pattern, lower expression of *VSNL1* was associated with poorer overall survival (Figure 36B). After restricting the Kaplan-Meier filtering to stage 4 patients, the same trend maintained, although Bonferroni-corrected significance was lost (Figure 36C).

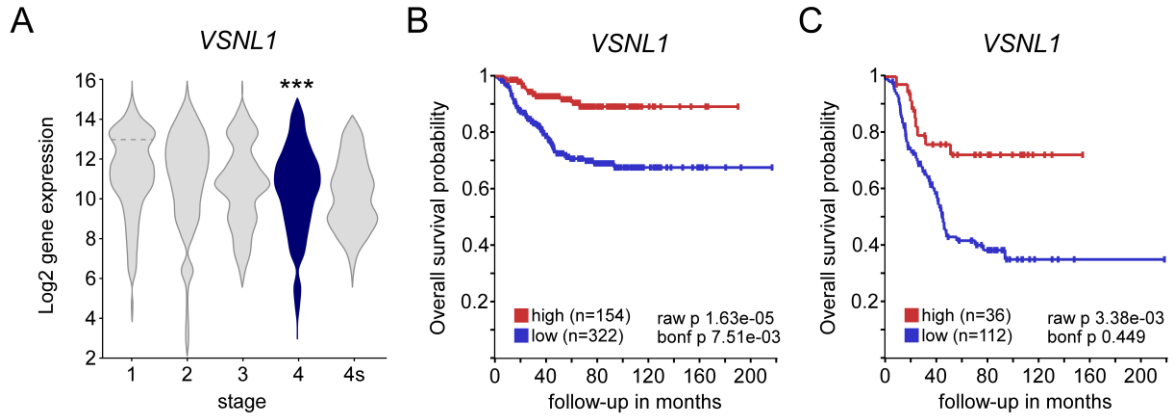

Figure 36. *VSNL1* clinical relevance analysis. A. Log2 gene expression for *VSNL1* in R2 platform (Kocak) across disease stages. Significance refers to the comparison between Stage 4 and Stage 1 patients. B. Kaplan-Meier curves showing prognosis in high and low *VSNL1* expression patients (Kocak). C. Kaplan-Meier curve analysis for stage 4 patients.

5. DISCUSSION

5.1 Overcoming limitations in *in vivo* modeling of metastatic neuroblastoma

Approximately 50% of patients with NB present metastatic disease at diagnosis, and metastasis, together with relapse, remains the principal causes of NB-related mortality[101]. Despite this clear clinical relevance, the mechanisms driving metastatic progression in NB remain insufficiently understood, highlighting a major gap in the field. Although this question can be addressed through both clinical and experimental approaches, progress in mechanistic and translational studies continues to be constrained by the limited availability of preclinical models that reliably reproduce metastatic NB[212]. This limitation is particularly relevant because most NB patients present with disseminated disease at diagnosis[101], whereas low-risk tumors belong to a biologically distinct subgroup with a low propensity for progression to overt metastatic disease[213]. Accordingly, experimental efforts may be more informative when focused on established metastatic tumors rather than on early dissemination steps, which are largely inaccessible to therapeutic intervention.

To overcome these limitations, different approaches have been used, including the use of patient-derived xenografts (PDXs) and human NB cell lines. Orthotopic PDX models have proven particularly valuable for recapitulating clinically relevant metastatic niches such as bone, bone marrow, and liver[201]. However, limited availability of NB patient samples in many research centers remains a significant constraint. Conversely, a wide variety of human NB cell lines have been established over the past decades, encompassing the main biological and genetic features of the disease and have become indispensable tools for preclinical research. Numerous studies have employed these cell lines for *in vivo* modelling in mice[195,214]. In particular, efforts to generate reliable metastatic models have focused on diverse cell delivery approaches, including intravenous tail-vein and intracardiac injections[214–217], intrafemoral injection[174,200,218,219], intrasplenic injection[174,200,218,219],

or the generation of primary tumors either subcutaneously[220–222] or orthotopically[223,224], which allows for spontaneous metastatic dissemination[199].

Despite this wide range of available approaches, metastatic NB modeling remains poorly characterized, both in technical implementation and in the metastatic sites reported. Here, we establish a robust and reproducible tail-vein metastasis model using human NB cell lines. While this strategy bypasses early steps of the metastatic cascade, it reliably generates lesions in organs where NB metastasis are frequently found in patients, enabling standardized preclinical drug testing and mechanistic studies of the interaction of tumoral cells with the metastatic TME[202].

5.2 Neuroblastoma cell lines generate clinically relevant metastatic lesions in mice

Our results demonstrate that the majority of NB cell lines colonize clinically relevant tissues, including liver and bone marrow, in agreement with previous metastatic models[195,214,215]. Additionally, metastatic engraftment was also observed in other organs such as ovaries, adrenal glands, kidneys, and lungs, consistent with other earlier reports[195,217,225] and providing alternative models for the study of less common metastatic sites. Conversely, certain cell lines failed to colonize any organ within selected time frames, likely undergoing elimination during the metastatic process due to the high energetic and adaptive demands required for survival, niche establishment, and outgrowth[226]. These findings support the notion that metastatic competence is not solely dictated by the host environment but also depends on intrinsic properties of malignant tumor cells[227,228]. Indeed, metastatic capacity is shaped not only by biological traits but also by physical constraints. In this setting, the tumor implantation site can significantly influence metastatic efficiency and organ tropism in experimental models, largely depending on the first capillary bed encountered[229]. It is well established that, in several cancer models, tail-vein injection predominantly results in pulmonary metastases due to capillary trapping in the lung vasculature (Figure 6)[230]. However, this outcome is not consistently observed in any

of our NB models, despite the expected physical tropism and the fact that lung metastases do occur in NB patients albeit at a lower frequency. In contrast, intracardiac and intracarotid injections have been shown to increase the incidence of brain metastases by bypassing the pulmonary circulation[229–231], while caudal artery injection facilitates direct tumor cell delivery to the bone marrow, thereby enhancing skeletal colonization[232]. Moreover, intra-organ injections, such as intrasplenic, intrahepatic, or intrafemoral administration, can efficiently generate tumor growth within the target organ[174,218,219]. However, these approaches bypass key steps of the metastatic cascade, including tumor cell dissemination, intravasation, circulation, and homing to distant sites, thereby failing to recapitulate the multifocal metastatic dissemination typically observed in patients. Notably, despite these route-dependent biases, tail-vein injection in our models did result in bone marrow and lung metastases for specific NB cell lines, indicating that beyond technical and physical determinants, the phenotypic and genetic background of tumor cells critically governs their ability to colonize distinct metastatic niches.

Comparative analyses assessing the metastatic behavior of the same tumor cell line injected through different routes remain scarce. For instance, Han et al.[233] described differences in metastatic burden following orthotopic versus subcutaneous injection, showing that orthotopic injection better resembles the clinical setting after dissemination. However, further studies will be essential to determine whether the apparent lack of metastatic capacity observed in certain NB cell lines following tail-vein injection reflects intrinsic biological limitations or, instead, route-dependent constraints of the experimental system. For example, MDA-MB-435 human breast cancer cells do not typically metastasize to bone in spontaneous metastasis models but readily do so following intracardiac injection, underscoring the strong influence of the injection route on metastatic organotropism[231]. Taken together, the appropriate selection of a metastatic model generation strategy should be guided primarily by three parameters: the specific stages of the metastatic cascade under

investigation, the target metastatic site, and the intrinsic metastatic competence of the cancer cells themselves[234].

5.3 Correlation between IVIS and histological analyses

In the LAN-6 model, tail vein injection of tumor cells led to a progressive increase in the *in vivo* bioluminescence signal over several weeks. However, at sacrifice, neither macro- nor micrometastases were detected through macroscopic examination or histological assessment. This lack of histological confirmation contrasted with the clear *in vivo* signal and was not observed to the same extent in the other models, in which longitudinal IVIS monitoring was broadly consistent with the metastatic lesions detected in the histological analyses. Therefore, rather than indicating a general limitation of bioluminescence-based follow-up, this finding may reflect model-specific limitation in tissue-level detection at the time of analysis.

A plausible explanation is that metastatic involvement in this model occurred as small, sparse, or anatomically restricted tumor cell deposits that were not captured by routine histological sampling. This possibility is supported by recent work showing that, particularly in bone marrow, histology may substantially underestimate metastatic burden when compared with more sensitive detection methods, despite extensive serial sectioning[235]. In that study, histology detected tumors cells in only a minority of samples that were positive by alternative approaches, highlighting the difficulty of identifying small and dispersed metastatic foci in bone.

Accordingly, the absence of detectable metastases in LAN-6 after necropsy should be interpreted with caution and does not necessarily indicate a true lack of metastatic engraftment, especially after the detected bioluminescence by IVIS. Additional analyses, including deeper sectioning or complementary methods such as *ex vivo* imaging or flow cytometry would be required to clarify the basis of this discordance.

5.4 Neuroblastoma cell lines genetic background and metastatic pattern

One of the objectives of this study was to determine whether shared genetic features across different NB cell lines correlate with similar metastatic capacity and organ distribution. Despite the inclusion of a diverse panel of cell lines with distinct genetic backgrounds, and the presence of overlapping molecular alterations among subsets of these lines, limited association was observed between genetic characteristics and metastatic dissemination pattern and frequency. Notably, stratification by 11q status was the only analysis that suggested a clear potential common pattern; however, this finding was based solely on the two cell lines harboring 11q loss and should therefore not be interpreted as evidence of a robust association. These two models nevertheless showed a very similar distribution and frequency of metastatic involvement including high engraftment in the liver, lung, ovary and kidney. Conversely, metastatic organ tropism did not segregate according to *MYCN* status, or the origin (primary tumor vs metastasis) of the cell lines[94]. These results suggest that metastatic behavior is more strongly influenced by cell line–specific properties than by consistent associations between individual genetic features and specific metastatic sites. They also highlight the value of integrating clinical, genetic, and phenotypic information to better contextualize NB cell line models and guide their rational selection for functional and translational studies. Moreover, deeper profiling of the molecular and chromosomal features of our NB cell lines by whole exome sequencing (WES) along with deeper statistical analyses of obtained data may uncover additional genetic background and metastatic pattern correlations that were not apparent with the data available to date.

In conclusion, we evaluated a panel of ten human NB cell lines widely used in preclinical research, both *in vitro* and *in vivo*, and demonstrated that several of these lines are capable of colonizing distant organs following tail-vein injection in immunocompromised mice, thereby closely mimicking the dissemination pattern of human NB at diagnosis. Collectively, these models encompass a wide range of

molecular alterations relevant to NB biology and establish a robust and reproducible experimental framework to generate a broad spectrum of metastatic sites, providing a valuable platform for future studies on drug development and metastatic tumor biology.

5.5 Characterization of the epigenetic landscape in metastatic neuroblastoma

Among metastatic sites, the bone marrow represents a particularly critical microenvironment, serving not only as a frequent destination for DTCs but also as a protective niche that promotes dormancy, therapeutic resistance, and subsequent relapse[152,154]. Moreover, hepatic metastases occur in approximately 30% of patients with metastatic NB and its presence along with concomitant bone or orbital involvement predicts poor survival[99,168]. Understanding the biological mechanisms that govern bone marrow and liver colonization and deciphering the epigenomic and transcriptomic adaptations that tumor cells undergo during metastatic progression is essential for clarifying disease biology and perhaps informing the selection of new therapeutic strategies.

In NB, the relative paucity of recurrent metastasis-specific driver mutations suggests that heritable non-genetic mechanisms including epigenetic reprogramming and transcriptional state changes contribute substantially to metastatic progression locking in metastatic phenotypes[236]. Consistent with this, even with minimal genetic differences from the original tumor cells, metastatic populations can express genes that are highly active, prone to metastasis, indicating that transcriptional programs promoting metastasis are present in human cancers[237–240]. Together, these observations motivate direct interrogation of chromatin accessibility and transcriptional output in metastatic lesions.

In this work, we profiled epigenomic and transcriptomic changes in liver and bone marrow lesions from metastatic NB models and compared them to matched subcutaneous primary tumors. Subcutaneous xenografts remain widely used in

cancer research due to their practical advantages, including ease of implantation, rapid and reproducible growth, and straightforward longitudinal monitoring[241–243]. However, subcutaneous tumors do not recapitulate key features of the native organ context and can differ in stromal interactions, vascularization and microenvironmental cues which can influence tumor biology and therapeutic response, particularly in drug testing settings[243–246]. Therefore, different mouse model systems are best viewed as complementary rather than interchangeable, with subcutaneous, orthotopic and metastatic settings each capturing distinct aspects of tumor growth, adaptation and treatment response[245]. Here, subcutaneous tumors served as a robust and tractable reference for cross-sample comparisons within our multi-omic framework and, importantly, were generated in independent cohorts of mice, ensuring that the metastatic phenotype was not constrained by paired sampling of the primary tumor within the same animal. This comparison was intentionally designed to filter out molecular differences associated only with generic proliferative capacity. Relative to *in vitro*–cultured cells, primary xenograft tumors provide a physiologically constrained context in which vascularization, hypoxia, and stromal interactions are already present. As a result, the analysis is less dominated by broad growth-related programs and better positioned to reveal mechanisms specifically required for metastatic adaptation and outgrowth in a hostile tissue environment. Furthermore, while some metastasis vs control differences may reflect site-dependent effects of primary tumor location, inclusion of two metastatic sites provides an internal check: changes shared across liver and bone marrow are less likely to reflect idiosyncrasies of the subcutaneous setting alone, whereas organ-restricted patterns are consistent with metastatic-site-associated regulation.

Several studies have leveraged mouse models to nominate therapeutic candidates by comparing transcriptomic profiles across disease compartments[197,223,247]. However, mRNA abundance alone does not necessarily reflect protein levels or functional dependency and can be influenced by sample management, tumor purity,

microenvironmental composition, and post-transcriptional regulation[248]. Importantly, permissive or 'plastic' chromatin may allow malignant cells to regulate alternative transcriptional states, gene pathways or developmental programs, a subset of which may be pro-oncogenic or adaptive to the metastatic niche[236,249]. Despite the potential centrality of these chromatin mechanisms to metastatic adaptation, few studies have incorporated a systematic view of the epigenetic landscape at metastatic sites[82] . Therefore, integrating ATAC-seq with RNA-seq adds an orthogonal regulatory layer that not only strengthens candidate prioritization by focusing on expression changes supported by concordant chromatin remodeling, but also supports characterization of metastasis-associated and organ-associated regulatory programs.

Our ATAC-seq data highlighted broad variability in chromatin accessibility. Notably, the extent of chromatin remodeling varied substantially across models. SK-N-BE(2) and NBL-S displayed far broader accessibility changes than SK-N-AS, suggesting differential epigenetic plasticity that may reflect distinct capacities chromatin regulation upon metastatic adaptation. Accessibility patterns were also partly organ-restricted. This was particularly evident in SK-N-AS, which showed marked organ-to-organ divergence, with substantially more accessibility changes in the liver than in the bone marrow. Conversely, CHLA-90 appeared more plastic in the bone marrow niche, where it showed a more open chromatin landscape, whereas in the liver, with less changes, it was predominantly closed. These results are consistent with the notion that the metastatic niche actively shapes—or selects for—specific epigenomic configurations in tumor cells[236,250]. Beyond these observations, chromatin accessibility information revealed by ATAC-seq in this thesis enabled the further interpretation of discordant accessibility–expression cases, the identification of organ-restricted accessibility biological programs and the prioritization of genes with regulatory support.

Complementing bulk multi-omics, single-cell approaches in other studies have refined the metastatic niche by resolving tumor and microenvironmental compartments and capturing heterogeneity that bulk profiles can mask. For example, Hochheuser et al., (2024)[251] reported that DTCs display copy number variations profiles distinct from those of the primary tumor, indicating spatial clonal evolution and higher cell-cycle activity in bone marrow. Mei et al., (2024)[252] identified shared NB states aligned with the sympathoadrenal (SA) differentiation axis and described metastatic bone marrow as a highly immunosuppressive niche enriched in exhausted T cells, Tregs, and reprogrammed macrophages. Despite these advances, linking the temporal dynamics of metastatic dissemination to transcriptomic state transitions remains challenging due to the scarcity of longitudinal paired material. Avian embryo NB models have partially addressed this gap, suggesting that metastases retain an early sympathetic neuroblast identity while phenotypically adapting to each tissue they colonize[253]. Crucially, while scRNA-seq resolves which states are present, it provides limited insight into the regulatory mechanisms that establish and maintain them. Integrating transcriptomics with epigenomic profiling is therefore a key next step to reconstruct networks linking chromatin architecture to transcriptional outputs and to identify core regulatory nodes driving metastatic NB[254]. These considerations provide a conceptual basis for the integrative analysis we implement here.

5.6 Epigenomic and transcriptomic integration reveals multilayered regulation

By combining ATAC- and RNA-seq across metastatic lesions at bulk resolution, we assessed how often accessibility changes are translated into transcriptional modulation in liver metastases. Figure 14 summarizes this analysis and shows that, despite extensive changes in chromatin accessibility, the overlap between differential expression and differential accessibility is generally low, with higher overlapping observed in SK-N-AS and NBL-S models. This modest concordance is

consistent with the broader observation that accessibility and expression are frequently discordant, and that many transcriptional changes can occur without measurable accessibility changes at nearby regulatory regions, and vice versa, depending on baseline chromatin permissiveness, cellular context and analytic thresholds[255].

Beyond technical factors (peak-to-gene assignment, distance cutoffs, and significance thresholds), several biological mechanisms can account for this unconcordant pattern.

A first set of mechanisms concerns loci that become more accessible without an increase in gene expression. In comparative studies, promoters and enhancers may already be accessible in both conditions, meaning that transcriptional changes are more commonly driven by shifts in TF availability and cofactor recruitment than by further opening of the chromatin [256]. Consistent with this view, multiple TFs have been linked to increased metastatic potential and the maintenance of metastatic transcriptional programs, suggesting that their activity can dominate transcriptional output independently of local accessibility changes[257–260]. A second, non-mutually exclusive, explanation involves distal regulatory architecture. Robust transcriptional induction may also require the coordinated activation of distal enhancers and histone mark remodeling, whose establishment and organization can drive gene expression even when promoter-proximal regions are already open[71,261]. Indeed, novel epigenomic techniques have been developed to investigate higher-order chromatin organization. For instance, Hi-C enables genome-wide mapping of chromatin interactions by measuring the frequency of contacts between distant genomic regions, thereby providing insights into long-range transcriptional regulation and enhancer-promoter interactions[262,263]. Finally, post-transcriptional regulation (e.g., RNA stability, miRNA control, translation efficiency) may further contribute to the observed discordance, decoupling mRNA abundance from upstream chromatin changes and underscoring that ATAC-seq and RNA-seq

integration provide valuable insights while it cannot capture all regulatory dependencies[255].

The complementary—and perhaps less intuitive—pattern concerns loci that become more compacted without a corresponding decrease in gene expression. One explanation is that ATAC-seq captures accessibility changes at specific regions, and the closed peaks are not necessarily the regulatory elements that are rate-limiting for transcription of the associated gene. In other words, key promoter-proximal elements and/or the relevant distal enhancers may remain accessible, allowing master TF to continue binding and sustaining transcriptional output despite localized compaction elsewhere[71]. This model is also consistent with the broader view that TF are primary specifiers of cellular identity, whereas chromatin regulators often act to reinforce or stabilize programs already defined by those factors[249,264,265]. Finally, a substantial fraction of chromatin alterations may represent "passenger" events. Analogous to passenger mutations, these epigenetic changes may have limited functional impact because they occur in genomic regions that are not essential for transcriptional control or cellular fitness. Thus, such regions can undergo further compaction to maintain genome organization and stability without necessarily driving downregulation of the associated gene[249].

In this context, to further assess the contribution of TF availability to metastatic gene regulation, we intersected our integrated ATAC-seq/RNA-seq upregulated gene sets from liver metastases models with the curated human TF census[266]. This approach enabled us to quantify the proportion of differentially regulated genes in liver metastases encoding bona fide DNA-binding TFs (Figure 37).

Across cell lines, the number of upregulated TFs varied markedly. Models such as SK-N-AS and NBL-S, which exhibit broader transcriptional reprogramming overall, also showed a proportionally higher enrichment of TF-encoding genes within their metastatic signature. Importantly, although these cell lines with larger numbers of differentially expressed genes are inherently more likely to have a greater absolute

number of TFs, the presented pattern may itself be biologically informative, suggesting that metastatic transcriptional landscape may involve active rewiring of gene expression regulatory elements. In contrast, SK-N-BE(2) and CHLA-90 displayed a more restricted transcriptional shift accompanied by limited TF modulation, potentially reflecting a more constrained or stable regulatory architecture.

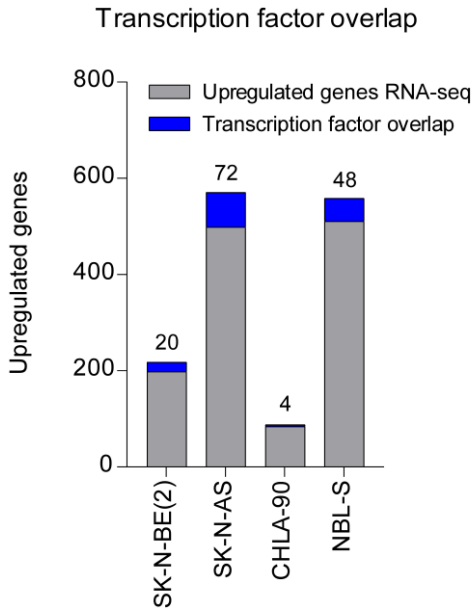

Figure 37. Overlap of human transcription factor census[266] with ATAC/RNA-seq upregulated genes across liver metastases models.

Taken together, these findings support the notion that TF regulatory reprogramming may represent a key layer of metastatic adaptation in our NB models. Rather than chromatin accessibility changes alone dictating transcriptional output, the presence and modulation of lineage-defining or metastasis-associated TFs may act as primary drivers of gene expression programs, thereby contributing to the variable degree of ATAC/RNA-seq concordance observed across models.

5.7 RNA-seq integration refines the biological processes identified by ATAC-seq

Our analysis approach allowed us to find biological processes that were consistently enriched or downregulated across several models. Among upregulated processes,

enrichment of cell projection organization, receptor signaling, regulation of transport, and vasculature development are consistent with metastatic adaptation to the liver microenvironment, where communication with niche cues and access to vascular programs can support metastatic outgrowth[250,267,268]. Consistent with this, transcriptomic analyses in NB patient cohorts have likewise shown enrichment of angiogenesis-related signatures in metastatic samples[269]. Conversely, the downregulated processes include cell adhesion, cell junction organization, and multiple neuronal/synaptic programs, suggesting a shift away from adhesion- and lineage-associated features that may accompany dissemination and metastatic state transitions[250]. A notable feature of this analysis is that several biological processes including neuronal programs appear among both upregulated and downregulated gene sets, which may initially seem contradictory but likely reflects coordinated, directionally coherent regulation within the same pathway. Signaling pathways are rarely regulated in a binary on/off manner; rather, their net output is shaped by the simultaneous transcriptional induction of activating components and repression of negative regulators[270]. In this framework, the co-occurrence of up- and downregulated genes annotated to the same process (e.g. Neurogenesis and Cell Projection Organization) is not paradoxical but instead consistent with a program of active pathway tuning, where metastatic cells reinforce specific signaling outputs by coordinately amplifying positive effectors and suppressing countervailing signals. Altogether, this interpretation aligns with the broader concept of transcriptional buffering and pathway canalization observed during developmental transitions and oncogenic reprogramming[249].

Notably, the analysis of biological process enrichment after ATAC-seq and RNA-seq integration revealed that many pathways previously identified by ATAC-seq alone were not retained, indicating that inferring the modulation of metastatic processes solely from chromatin accessibility does not deterministically predict functional programs. Indeed, differentially accessible genomic regions associated with genes involved in specific biological processes, yet lacking concordant transcriptional

changes, may reflect a "poised" or "primed" chromatin state. In other words, metastatic cells may carry the chromatin state of regulatory programs that were transiently engaged or repressed at earlier stages of the metastatic cascade but are no longer transcriptionally required at the time of sample collection[271,272].

For instance, GO terms such as cell migration and axon guidance were enriched among upregulated ATAC-seq regions but did not remain significant after RNA-seq integration. This pattern is consistent with the notion that migratory programs may have been epigenetically activated during circulation, or early colonization, when motility and guidance are critical [128,129], yet become transcriptionally attenuated once tumor cells establish themselves within a secondary niche.

In contrast, downregulated biological processes, particularly those related to cell-cell adhesion, were consistently detected across both ATAC-seq and RNA-seq analyses. This concordance suggests that certain regulatory adaptations remain stable throughout the metastatic cascade, and particularly that loss of cell-cell adhesion represents a hallmark of metastatic competence required for dissemination and invasion[273,274].

Although for bone marrow metastases RNA-seq data were not available, ATAC-seq profiling revealed substantial overlap in enriched biological processes compared with liver lesions. In this sense, genes associated with cell migration and axon guidance again displayed increased chromatin accessibility, whereas cell-cell adhesion related genes showed reduced accessibility. These findings suggest that core metastatic programs operate independently of the ultimate organ of colonization and support the existence of a conserved metastatic regulatory backbone in our models, consistent with the concept that dissemination-associated programs are broadly engaged prior to niche-specific adaptation[130].

Interestingly, bone marrow metastases uniquely exhibited increased accessibility of genes involved in chromatin remodeling. This observation raises the possibility that metastatic cells within the bone marrow niche retain heightened epigenetic

plasticity, potentially reflecting the strong selective and regulatory pressures imposed by the highly specialized and dynamic bone marrow microenvironment[137,156].

5.8 Potential therapeutic targets associated with neuroblastoma metastasis

Unlike many pediatric cancers, high-risk NB has a comparatively active drug-development ecosystem, with several therapies on the development pipeline[121]. Consistent with this, between 2011 and 2020, a total of 192 therapeutic trials evaluating 78 different targets were available to children with NB (among other diagnoses), with most trials targeting the relapsed/refractory setting[275]. Nevertheless, individual patients may still have few rational trial options with available slots at the time treatment is needed[121]. Approximately half of these trials evaluated single agents as part of the phase I protocol. The inclusion of these agents in phase II and phase III trials will go in line with the broader therapeutic goal in NB of developing combinations that can be rapidly integrated into frontline therapy and/or built upon established backbones such as irinotecan-, topotecan-, and temozolomide-based regimens[276–280].

Current NB-directed strategies that have reached—or are being prioritized for—clinical translation largely fall into three categories: (i) immunotherapy, including CAR-T approaches and anti-GD2 antibodies (dinutuximab, dinutuximab beta, and naxitamab)[281,282]; (ii) targeting specific genomic alterations that, despite being present at low frequency, enable treatment stratification (e.g., ALK activating mutations/amplifications, and RAS pathway alterations); and (iii) exploiting vulnerabilities linked to telomere maintenance mechanisms[53,283].

Notably, several recent developments have begun to reshape the therapeutic landscape more substantially. The FDA approval of difluoromethylornithine (DFMO) in December 2023 for relapse risk reduction in high-risk NB represents a potential valuable addition to the post-consolidation standard of care. DFMO irreversibly

inhibits ornithine decarboxylase (ODC), which is a rate-limiting enzyme in polyamine biosynthesis and a downstream effector of MYC, and since its inclusion, it has achieved a 4-year EFS of 84% in newly diagnosed patients in phase II trials [284]. In parallel, lorlatinib, a third generation ALK inhibitor with broad mutation coverage and high CNS penetration, has been evaluated in a phase I trial (NCT03107988) in combination with chemotherapy and will be evaluated as a frontline therapy in a phase III trial (NCT03126916), reflecting the maturation of ALK directed therapy beyond salvage settings [122].

Additionally, the most recent Neuroblastoma Drug Development (NDD) forum celebrated in 2023 highlighted an additional category with the potential to be transformative, including inhibitory antibodies and targeted protein degradation[121].

In this work, we align with this latter direction by prioritizing target discovery for metastatic disease, aiming to prioritize the identification of metastasis expressed genes that may be targeted in patients with disseminated tumors. Inhibiting such candidates could potentially impair tumor cell growth and/or adaptation to metastatic sites either by directly blocking their function or by perturbing the pathways that sustain their adaptation and growth in distant organs. Although increased mRNA abundance is not always a reliable proxy for protein levels[285], transcriptomic analyses of metastatic models and relapsed patient cohorts have repeatedly proven informative for nominating candidate dependencies[252,253,269,286]. Importantly, transcriptome-informed precision oncology frameworks are already being deployed clinically, as illustrated by MAPPYACTS, which combines WES with RNA-seq to generate patient-specific molecular profiles that extend beyond DNA alterations alone[287].

Thus, integrating epigenomic profiling in our models allowed us to prioritize transcriptional changes supported by concordant chromatin accessibility, adding an orthogonal layer of evidence that strengthens confidence in the shortlisted targets.

Based on our integrative analyses, the following subset of candidates have emerged as particularly promising therapeutic targets:

GFRA2

GFRA2 is a protein-coding gene located on chromosome 8 (chr8:21,690,398–21,812,370) and spanning 121,973 bases, which encodes a 52 kDa protein. GFRA2 is a glycosylphosphatidylinositol-anchored cell-surface protein that bind neurotrophic ligands and form signaling complexes with the RET tyrosine kinase, thereby enabling ligand-dependent signal transduction. Increasing evidence suggests that GFRA2 is not only involved in neurotrophic signaling, but also associated with aggressive disease states in cancer, where it may connect extracellular microenvironmental cues with tumor cell growth and adaptation. These features make GFRA2 of interest both as a biological mediator and as a potential translational target[288–290].

From a therapeutic point of view, the fact that GFRA2 is a surface-exposed receptor makes it attractive for targeted strategies. Orentas et al. (2017)[291] first applied a surfaceome-driven strategy to identify paired tumor antigens for CAR-based targeting, with the aim to reduce on-target/off-tumor toxicity through dual antigen recognition. Within this framework, *GFRA2* was identified as an overexpressed antigen in NB and proposed in combination with additional targets including *GFRA3* as part of a dual recognition strategy.

Posterior functional studies showed that *GFRA2* directly support tumor fitness by engaging growth and adaptation pathways. For instance, in NB it has been shown that, after overexpression, *GFRA2* promotes proliferation through PTEN inhibition and activation of PI3K/AKT signaling, while its silencing using shRNA decreases proliferation[289]. In other cancers, such as pancreatic cancer, it mediates nerve-derived NRTN signaling via RET to enhance HK2-dependent glycolysis and tumor growth[290].

Rather than functioning solely as a tumor-versus-normal discriminator, GFRA2 may also serve as a marker of biological heterogeneity within tumors. In gastric cancer, for instance, bioinformatic analyses of patient datasets have indicated that, despite lower overall *GFRA2* expression in tumor samples compared with normal tissue, higher *GFRA2* expression within the tumor cohort is associated with advanced disease stage, worse overall survival, and specific microenvironmental features, including mast cell infiltration[288]. This pattern supports the idea that GFRA2 may identify a more aggressive intratumoral state. Consistent with this, we observed *GFRA2* upregulation in liver metastases in three of our NB models, together with increased chromatin accessibility at the *GFRA2* locus in two of them, supporting metastasis-associated regulatory activation rather than a purely incidental expression change. Notably, several chromatin accessibility events mapped to intergenic regions near *GFRA2*, potentially consistent with the involvement of regulatory regions that may contribute to *GFRA2* transcriptional control in this metastatic context.

Additionally, Villalard et al., (2024)[253] used in vivo cell migration assays in chick embryos to define transcriptional patterns across distinct tumor populations, including primary tumors and bone marrow metastases. Within this analysis, members of the GFRA family, particularly *GFRA1* and *GFRA3*, were highly expressed in bone marrow metastatic cells, although *GFRA1* was also detected at high levels in other tumor populations. These findings suggest that GFRA family genes may serve as transcriptional markers of aggressive and metastatic tumor states. Together, these observations support a coherent model in which elevated *GFRA2*—such as in our liver metastatic lesions—may reflect selection for, or induction of, tumor cell states that better exploit trophic niche signals and engage downstream programs that promote growth, survival, and metabolic adaptation[288–290].

Overall, the available evidence positions *GFRA2* as a strong candidate target in metastatic NB, with potential relevance both as a mediator of aggressive disease biology and as a therapeutic entry point.

GRK5

GRK5 is a protein-coding gene located on chromosome 10 (chr10:119,207,543–119,459,745), spanning 252,203 bases, and encodes a 67-kDa protein. It belongs to the G protein-coupled receptor kinase (GRK) subfamily within the serine/threonine protein kinase family and functions by phosphorylating activated G protein-coupled receptors, thereby promoting their desensitization and deactivation. Beyond its canonical role in receptor signaling, *GRK5* has been implicated in human disease contexts, including heart disease and diabetes mellitus, supporting its broader biological relevance.

GRK5 is recognized as a pro-tumorigenic regulator whose elevated expression and activity align with key cancer hallmarks, most consistently invasion/metastasis, sustained proliferative signaling, and resistance to cell death, across multiple tumor types[292–295]. Accordingly, *GRK5* depletion or inhibition consistently suppresses migration and invasion while increasing focal adhesions across tumor models[292–294]. In our NB models, *GRK5* upregulation in liver metastases is accompanied by increased chromatin accessibility at the *GRK5* locus in two cell lines, indicating coordinated transcriptomic and epigenomic activation in the metastatic state. This pattern is consistent with cross-cancer evidence that GRK5 enhances cellular programs required for metastatic progression—particularly cytoskeletal plasticity, adhesion turnover, and invasive behavior—and reinforces proliferative and survival capacity that would favor metastatic colonization and outgrowth[292–295].

Mechanistically, GRK5 contributes to tumor-promoting programs linked to both motility and survival. Gain-of-function studies indicate that GRK5 promotes cytoskeletal remodeling through the GRPR/GRP-CDC42/ROCK1 axis in triple-negative breast cancer and through phosphorylation of moesin at T66 in prostate

cancer[292,293]. Complementing these observations, loss of function studies have shown that GRK5 is required for tumor cell fitness in several contexts. For instance, in non-squamous cell lung cancer, *GRK5* depletion through shRNA reduced proliferation and migration *in vitro* and xenograft tumor formation *in vivo*[294]. In pediatric rhabdomyosarcoma (RMS), *GRK5* silencing by CRISPR impaired sphere formation and increased programmed cell death in tumor cells *in vitro*. Notably, some of these effects may not depend exclusively on its kinase activity, as GRK5 has also been shown to function though interaction with NFAT1[295].

An additional NB-relevant layer is provided by a preclinical NB study of sunitinib, a multi-kinase inhibitor. In support of the therapeutic tractability of *GRK5*, sunitinib has been used in vitro in breast cancer models as a pharmacological approach complementary to *GRK5* silencing using siRNA and shRNA. In that setting, *GRK5* inhibition was associated with reduced migratory and invasive behavior, supporting a role for this kinase in tumor cell motility[292]. This pharmacological evidence is further reinforced by a preclinical study in NB, in which sunitinib showed antitumor and antimetastatic activity in vitro, including marked reduction in liver metastasis, together with inhibition of VEGFR/PDGFR signaling and downregulation of angiogenic programs[296]. These results highlight that multi-kinase inhibitors can produce anti-metastatic effects through a combination of tumor-intrinsic and microenvironmental mechanisms. However, it is important to note that sunitinib, like other multi-kinase inhibitors, has limited specificity an may also inhibit additional kinases.

ASCL1/DLL3 axis

ASCL1 and *DLL3* are discussed together since they are part of a biologically regulatory axis. *ASCL1* is a protein-coding gene located on chromosome 12 (chr12:102,957,674–102,960,513), spanning 2,840 bases and encoding a 25-kDa transcription factor that regulates neuronal differentiation, adrenergic lineage identity, and transcriptional plasticity[297–299]. Consistent with this role, *ASCL1* has been

described as a master regulator of neuroendocrine programs and as a pioneer factor capable of reshaping chromatin accessibility and reinforcing lineage-specific transcriptional networks in many cancers[297–299]. *DLL3*, one of its downstream-regulated genes, is a protein-coding gene located on chromosome 19 (chr19:39,498,895–39,508,481), spanning 9,587 bases and encoding a 65-kDa transmembrane member of the delta-like ligand family characterized by a DSL domain, EGF repeats, and a transmembrane region. In this context, *DLL3* is particularly relevant because it may act as a therapeutically accessible readout of *ASCL1*-driven oncogenic programs. Thus, while *ASCL1* is likely to function as an upstream biological driver but is difficult to target directly owing to its nuclear localization, *DLL3* represents a more tractable therapeutic vulnerability within the same regulatory axis.

DLL3 is an atypical Notch ligand that repeatedly emerges in neuroendocrine tumor biology as both a marker of aggressive disease and a therapeutically actionable surface antigen. In small cell lung cancer (SCLC), DLL3 positivity is linked to poor outcomes and acts as an independent prognostic risk factor when integrated into clinical models[300]. In parallel, *DLL3* expression is tightly linked to the neuroendocrine transcriptional program: *DLL3* correlates with *ASCL1* across large SCLC patient series, supporting the notion that DLL3 marks ASCL1-driven disease biology and may help identify patients with DLL3-high tumors, who are more likely to benefit from DLL3-directed strategies[301]. Beyond being a biomarker, DLL3 exerts direct oncogenic functions by promoting tumor growth, migration, and invasion through modulation of SNAI1/Snail in models of SCLC[302]. At a broader level, pan-cancer studies showed *DLL3* expression levels to be associated with other clinically-relevant features such as M2 macrophage infiltration and microsatellite instability[300]. Currently, the therapeutic strategies targeting DLL3 are varied, including antibody-drug conjugates (ADCs; e.g. Rova-T), bispecific T-cell engagers (BiTEs), and chimeric antigen receptor (CAR) T-cell therapies[303].

Krytska et al. (2022)[304] extended *DLL3* relevance beyond SCLC by showing that *DLL3* could be a potential candidate for NB treatment after demonstrating antitumoral effects and increased overall survival on *in vivo* PDX models using Rova-T. However, although transcripts can be elevated, surface DLL3 protein was shown to be heterogeneous across 35 human samples, indicating that transcriptional upregulation does not always translate into antigen presentation on tumor cells[304]. In this context, our data add a metastasis-focused layer: *DLL3* is upregulated in liver metastases in our models and we also observe higher *DLL3* mRNA levels in stage 4 patients.

DLL3-directed antibody-drug conjugates development (e.g., Rova-T) ultimately failed in late-stage SCLC trials due to severe toxicities. This includes severe edema, pleural and pericardial effusion, photosensitivity reactions and thrombocytopenia, potentially caused by the premature release of the drug into the circulation leading to systemic toxicity and motivating a shift toward alternative approaches[303]. This has resulted into a shift towards a DLL3-directed T-cell engager (bispecific T-cell engagers, BiTEs). A bispecific T cell engager (BiTE) is a type of tandem of two single chain variable framents (scFv) in which one scFv is capable of binding to a T cell (CD3 subunit of the T cell receptor) and the second scFv binds to an antigen on tumor cells[305]. Particularly, tarlatamab has demonstrated clinical activity in SCLC metastatic patients, with a median overall survival of 13 months in phase I clinical trials (NCT03319940). Subsequently, tarlatamab has been proposed as a first-line treatment in phase III clinical trials (NCT06117774 and NCT06211036), which has accelerated FDA approval in metastatic SCLC and validated DLL3 as a druggable antigen[303,306]. These developments reinforce DLL3 as an attractive target due to its high expression in tumors compared with normal tissue, while expanding the therapeutic toolbox toward CAR-T and radioimmunotherapy concepts[303].

Together, these findings are consistent with *DLL3* being part of a metastasis-associated, transcriptionally activated program. However, previously reported

heterogeneity in DLL3 protein expression adds an important translational nuance, indicating that RNA-level enrichment in advanced or metastatic settings should ideally be complemented by protein-level evaluation when considering DLL3-directed therapeutic strategies[289].

5.9 Inferring bone marrow transcriptional activity from chromatin accessibility

Having identified liver-enriched candidates through matched RNA-seq and ATAC-seq, we sought to evaluate whether these targets might also be relevant in other metastatic sites. Given the unavailability of matched transcriptomic data for bone marrow metastases in our models, we leveraged chromatin accessibility as a complementary readiness marker to infer potential cross-site relevance.

We intersected the potential candidates in liver target list with the bone marrow ATAC-seq dataset to assess whether these genes show evidence of regulatory activation in bone marrow lesions, reasoning that genes with open chromatin at their loci would be more likely to emerge as transcriptomic candidates if RNA-seq data were available. This analysis identified *GRK5* and *GFRA2* as the unique significantly accessible in the three models of bone marrow metastases, in addition to their prioritization in liver, suggesting that these genes may represent putative pan-metastatic targets in our experimental setting. Importantly, this inference is based on chromatin accessibility alone and does not demonstrate increased expression or functional dependency in bone marrow. Therefore, confirmation through matched RNA-seq and targeted functional validation will be required to substantiate pan-metastatic relevance.

5.10 Bidirectional analysis revealed downregulated metastatic drivers

In addition to activated (open/upregulated) candidates, our integrative ATAC/RNA-seq framework captured a complementary set of downregulated genes supported by chromatin closing, indicating that metastatic progression in NB involves not only

gain of pro-metastatic programs but also repression of specific transcriptional modules. After transcriptomic data mining analyses questioning the clinical relevance of downregulated drivers, *HS6ST3, KCNMB4, OSBPL3* and *VSNL1* showed significantly lower expression in stage 4 tumors, and this reduced expression was associated with poorer overall survival in the Kocak cohort. These four metastatic driver genes exhibit context-dependent deregulation across tumor types in the literature.

VSNL1

VSNL1 is a protein-coding gene located on chromosome 2 (chr2:17,539,020–17,657,018), spanning 117,999 bases and encoding a 22-kDa neuronal calcium sensor protein. As a member of the visinin/recoverin subfamily, VSNL1 is strongly expressed in cerebellar granule cells, where it associates with membranes in a calcium-dependent manner and contributes to the regulation of intracellular signaling, including pathways linked to adenylyl cyclase activity. Given its neuronal expression profile and signaling-related functions, VSNL1 may be of particular interest in the context of NB-associated regulatory programs.

In gastrointestinal cancers—including colorectal and gastric tumors—*VSNL1* overexpression correlates with lymph node metastasis, advanced TNM stage, and reduced survival, as showed in a study using a total of 168 patient samples, with and without lymph node invasion[307]. Moreover, mechanistic evidence linked *VSNL1* overexpression to increased proliferation and migration[308,309]. Particularly, shRNA silencing of *VSNL1 in vitro* reduced colony formation capabilities and also caused a subsequent downregulation of different migratory-related proteins such as vimentin and N-cadherin[308,309]. Conversely, in neural tumors such as medulloblastoma, *VSNL1* expression is associated with a favorable prognostic marker[310]. Furthermore, in glioblastoma, *in vitro* overexpression of the oncogenic miR-671-5p axis was associated with reduced *VSNL1* expression and increased migration in wound-

healing assays, consistent with a potential tumor-suppressive role for VSNL1 in this context[310].

OSBPL3

OSBPL3 gene encodes a 101-kDa member of the oxysterol-binding protein (OSBP) family, a group of intracellular lipid receptors. Located on chromosome 7 (chr7:24,796,537–24,981,845) and spanning 185,309 bases, this protein has been implicated in the regulation of cell adhesion and actin cytoskeleton organization[311,312].

OSBPL3 displayed a reversed clinical association in NB compared to epithelial cancers. In colorectal and pancreatic cancers, higher *OSBPL3* expression correlates with aggressiveness, pro-invasive signaling, and immunosuppressive microenvironment features[313]. In contrast, NB data showed that lower expression—accompanied by chromatin closing—associated with metastatic disease and worse survival.

HS6ST3

HS6ST3 is a protein-coding gene located on chromosome 13 (chr13:96,090,107–96,839,562) and spanning 749,456 bases, which encodes a 55-kDa member of the heparan sulfate sulfotransferase family. By modifying heparan sulfate chains, HS6ST3 contributes to protein–glycan interactions involved in proliferation, differentiation, adhesion, migration, inflammation, and coagulation[314].

Similar to *OSBPL3*, *HS6ST3* also displayed reversed clinical associations in NB compared to adult cancers. For instance, in breast cancer, *HS6ST3* silencing reduced growth, migration, and invasion through modulation of IGF1R and pro-apoptotic pathways[315] while in NB metastatic patients showed lower expression and associated with worse overall survival, in line with our liver mouse models.

KCNMB4

KCNMB4 is a protein-coding gene located on chromosome 12 (chr12:70,366,290–70,434,292), spanning 68,003 bases and encoding a 24-kDa protein. It encodes an auxiliary β subunit of the large-conductance, voltage- and calcium-activated potassium (BK/maxiK) channel, where it modulates the calcium sensitivity and gating kinetics of the pore-forming KCNMA1 α subunit. Through this regulatory role, KCNMB4 contributes to the control of membrane excitability, a process that is particularly relevant in neuronal tissues and other electrically responsive cell types.

KCNMB4 has been implicated in NB biology through its role in modulating the activation the action potential of neurons, and has also been associated with resistance to chemotherapy through gene overexpression in nasopharyngeal carcinoma[316,317]. In osteosarcoma, *KCNMB4* has been reported to form a fusion with cyclin D3 (KCNMB4–CCND3) in nearly 10% of cases, where it has been linked to increased migratory capacity in transwell assays[318]. However, in our NB models, *KCNMB4* showed to be downregulated in liver metastases together with chromatin closing events, a pattern that is more consistent with the loss of a tumor suppressor function and may suggest a context-dependent role.

Overall, by integrating RNA-seq and ATAC-seq across metastatic NB models, our analyses provide a bidirectional view of metastasis-associated regulatory remodeling. On the one hand, we select three high-priority candidates (*GFRA2, GRK5, DLL3)* with translational potential for targeting metastatic disease, supported by coherent multi-omic evidence in our models and by sufficient external biological context to justify further investigation.

Conversely, rather than representing actionable vulnerabilities, the genes downregulated in metastases and associated with chromatin closing (*HS6ST3, KCNMB4, OSBPL3,* and *VSNL1*) may define a clinically relevant loss-associated signature. However, because tumor-suppressive functions for these genes have only

been reported in selected tumor types, this interpretation should be considered context dependent.

Table 14. Summary of potential drivers of metastatic neuroblastoma after RNA- and ATAC-seq integration.

Gene	Subcellular location	Related biological processes
GFRA2	Cell membrane	Enzyme link receptor signaling
GRK5	Cell membrane, nucleus, cytoplasm	Regulation of cell proliferation
DLL3	Cell membrane	Regulation of cell differentiation, epithelium development and anatomical structure morphogenesis
VSNL1	Cytosol	Regulation of signal transduction
OSBLP3	Cell membrane, ER membrane	Bile acid biosynthetic process
HS6ST3	Membrane	Heparan sulfate proteoglycan biosynthetic process
KCNMB4	Membrane	Action potential, chemical synaptic transmission, potassium ion transport

ER: Endoplasmic reticulum

5.11 Target identification beyond multi-omics integration

Although our prioritization strategy focused on candidates supported by the integrative analysis of ATAC- and RNA-seq data, the RNA-seq results alone also identified additional genes that may be relevant to metastatic NB. These candidates were not retained in the multi-omic selection because their transcriptional upregulation was not accompanied by detectable changes in chromatin accessibility. However, as discussed above, this lack of concordance does not necessarily preclude biological relevance, since gene expression changes can occur independently of local accessibility changes detected by ATAC-seq.

Within this group (see Annex III), genes such as *MRPS30, NPPC*, and *RSL1D1* emerged as potentially interesting candidates, as they were upregulated in at least three of our metastatic liver models and, in the transcriptomic Kocak data cohort, were also associated with higher expression in stage 4 patients and poor prognosis. Although these genes were not prioritized by the integrative ATAC-

and RNA-seq workflow, their transcriptomic behavior suggests that they may still contribute to metastatic progression through mechanisms not reflected by differential chromatin accessibility in our models.

Among these candidates, *RSL1D1* is especially noteworthy. It has been reported to be overexpressed in colorectal cancer relative to normal tissue, and functional studies have shown that its overexpression enhances cell proliferation of colorectal cancer cells *in vitro* and promotes liver metastasis formation *in vivo*[319]. In addition, integrative epigenomic and transcriptomic analyses in lung adenocarcinoma have identified *RSL1D1* as a potential candidate, showing hypomethylation together with increased expression in tumor patient tissue compared with normal tissue[320]. These observations support the possibility that *RSL1D1* may contribute to aggressive tumor behavior across different tumor types and justify its consideration as a candidate relevant to neuroblastoma metastasis.

MRPS30 and *NPPC* also warrant consideration, as they have been linked to breast and small cell lung cancer, respectively, where they have been reported to be upregulated in tumor patient samples relative to normal tissue[321,322]. Therefore, although these genes were not selected as primary targets in our multi-omic framework, their recurrent association with aggressive disease supports the idea that RNA-seq-only candidates may still represent biologically and therapeutically relevant vulnerabilities deserving further validation in NB metastasis.

6. CONCLUSIONS

First: Tail vein injection of neuroblastoma cell lines results in metastatic disease in mice that recapitulates patterns observed in patients.

Second: Chromatin accessibility changes vary across neuroblastoma cell lines and metastatic organs, indicating distinct adaptive capacities. Despite this variability, shared regulatory elements were identified across models, suggesting the presence of conserved regulatory programs associated with metastasis.

Third: Chromatin accessibility changes do not always translate into transcriptomic changes in liver metastases, indicating the involvement of additional regulatory layers.

Fourth: Multi-omic integration identified a set of candidate targets, among which *GFRA2, GRK5* and *DLL3* emerged as particularly promising in metastatic NB.

7. BIBLIOGRAPHY

1. National Cancer Institute. NCI Dictionary of Cancer Terms. *https://www.cancer.gov/publications/dictionaries/cancer-terms/def/pediatric-cancer?utm*. (2026).

2. Rodriguez-Galindo, C. *et al.* Toward the Cure of All Children With Cancer Through Collaborative Efforts: Pediatric Oncology As a Global Challenge. *Journal of Clinical Oncology* **33**, 3065 (2015).

3. Pui, C. H., Gajjar, A. J., Kane, J. R., Qaddoumi, I. A. & Pappo, A. S. Challenging issues in pediatric oncology. *Nat. Rev. Clin. Oncol.* **8**, 540–549 (2011).

4. Meadows, A. T. Pediatric cancer survivorship: research and clinical care. *J. Clin. Oncol.* **24**, 5160–5165 (2006).

5. Siegel, R. L., Miller, K. D., Fuchs, H. E. & Jemal, A. Cancer Statistics, 2021. *CA Cancer J. Clin.* **71**, 7–33 (2021).

6. Oeffinger, K. C. *et al.* Chronic health conditions in adult survivors of childhood cancer. *N. Engl. J. Med.* **355**, 1572–1582 (2006).

7. Kopp, L. M., Gupta, P., Pelayo-Katsanis, L., Wittman, B. & Katsanis, E. Late effects in adult survivors of pediatric cancer: A guide for the primary care physician. *American Journal of Medicine* **125**, 636–641 (2012).

8. Varni, J. W., Limbers, C. A. & Burwinkle, T. M. Parent proxy-report of their children's health-related quality of life: an analysis of 13,878 parents' reliability and validity across age subgroups using the PedsQL 4.0 Generic Core Scales. *Health Qual. Life Outcomes* **5**, (2007).

9. Kattner, P. *et al.* Compare and contrast: pediatric cancer versus adult malignancies. *Cancer and Metastasis Reviews* **38**, 673–682 Preprint at https://doi.org/10.1007/s10555-019-09836-y (2019).

10. B, V. *et al.* Genetic alterations during colorectal-tumor development. *N. Engl. J. Med.* **319**, 525–532 (1988).

11. Brown, K. F. *et al.* The fraction of cancer attributable to modifiable risk factors in England, Wales, Scotland, Northern Ireland, and the United Kingdom in 2015. *British Journal of Cancer 2018 118:8* **118**, 1130–1141 (2018).

12. Gröbner, S. N. *et al.* The landscape of genomic alterations across childhood cancers. *Nature* **555**, 321–327 (2018).

13. Huether, R. *et al.* The landscape of somatic mutations in epigenetic regulators across 1,000 paediatric cancer genomes. *Nature Communications 2014 5:1* **5**, 3630- (2014).

14. Downing, J. R. *et al.* The Pediatric Cancer Genome Project. *Nat. Genet.* **44**, 619–622 (2012).

15. Westhoff, M. A. *et al.* Cell death-based treatment of childhood cancer. *Cell Death Dis.* **9**, (2018).

16. World Health Organization (WHO). *https://www.who.int/* (2019).

17. Ahmed, A. A., Zhang, L., Reddivalla, N. & Hetherington, M. Neuroblastoma in children: Update on clinicopathologic and genetic prognostic factors. *Pediatr. Hematol. Oncol.* **34**, 165–185 (2017).

18. Yanik, F., Karamustafaoglu, Y. A. & Yoruk, Y. A rare mediastinal occurrence of neuroblastoma in an adult: case report. *Sao Paulo Med. J.* **137**, 104–106 (2019).

19. Vargo, M. M. Brain Tumors and Metastases. *Phys. Med. Rehabil. Clin. N. Am.* **28**, 115–141 (2017).

20. Molenaar, J. J. *et al.* Sequencing of neuroblastoma identifies chromothripsis and defects in neuritogenesis genes. *Nature* **483**, 589–593 (2012).

21. Monje, M. Open questions: why are babies rarely born with cancer? *BMC biology,* **16**, 129 (2018).

22. Zhang, J. *et al.* Germline Mutations in Predisposition Genes in Pediatric Cancer. *N. Engl. J. Med.* **373**, 2336–2346 (2015).

23. Wolpert, L. Do we understand development? *Science (1979).* **266**, 571–572 (1994).

24. Gulati, G. S. *et al.* Single-cell transcriptional diversity is a hallmark of developmental potential. *Science* **367**, 405–411 (2020).

25. Davidson, E. H. & Erwin, D. H. Gene regulatory networks and the evolution of animal body plans. *Science* **311**, 796–797 (2006).

26. Weinreb, C., Rodriguez-Fraticelli, A., Camargo, F. D. & Klein, A. M. Lineage tracing on transcriptional landscapes links state to fate during differentiation. *Science* **367**, (2020).

27. Messerschmidt, D. M., Knowles, B. B. & Solter, D. DNA methylation dynamics during epigenetic reprogramming in the germline and preimplantation embryos. *Genes Dev.* **28**, 812–828 (2014).

28. Berger, S. L., Kouzarides, T., Shiekhattar, R. & Shilatifard, A. An operational definition of epigenetics. *Genes Dev.* **23**, 781–783 (2009).

29. Schneider, R. & Grosschedl, R. Dynamics and interplay of nuclear architecture, genome organization, and gene expression. *Genes Dev.* **21**, 3027–3043 (2007).

30. Dillon, N. Heterochromatin structure and function. *Biol. Cell* **96**, 631–637 (2004).

31. Ahuja, N., Sharma, A. R. & Baylin, S. B. Epigenetic Therapeutics: A New Weapon in the War Against Cancer. *Annual review of medicine* **67**, 73–89.

32. Dawson, M. A. & Kouzarides, T. Cancer epigenetics: From mechanism to therapy. *Cell* **150**, 12–27 (2012).

33. Silber, R. *et al.* Methylation of nucleic acids in normal and leukemic leukocytes. *Biochim. Biophys. Acta* **123**, 638–40 (1966).

34. Craddock, V. M. & Magee, P. N. Analysis of bases of rat-liver nucleic acids after administration of the carcinogen dimethylnitrosamine. *Biochem. J.* **100**, 724–32 (1966).

35. Feinberg, A. P. & Tycko, B. The history of cancer epigenetics. *Nat. Rev. Cancer* **4**, 143–53 (2004).

36. Berman, B. P. *et al.* Regions of focal DNA hypermethylation and long-range hypomethylation in colorectal cancer coincide with nuclear lamina-associated domains. *Nat. Genet.* **44**, 40–6 (2011).

37. Chi, P., Allis, C. D. & Wang, G. G. Covalent histone modifications--miswritten, misinterpreted and mis-erased in human cancers. *Nat. Rev. Cancer* **10**, 457–69 (2010).

38. Zhao, S., Allis, C. D. & Wang, G. G. The language of chromatin modification in human cancers. *Nat. Rev. Cancer* **21**, 413–430 (2021).

39. Ward, E., DeSantis, C., Robbins, A., Kohler, B. & Jemal, A. Childhood and adolescent cancer statistics, 2014. *CA Cancer J. Clin.* **64**, 83–103 (2014).

40. Irwin, M. S. & Park, J. R. Neuroblastoma: Paradigm for precision medicine. *Pediatr. Clin. North Am.* **62**, 225–256 (2015).

41. G. M. Brodeur, M. D. Hogarty, Y. P. Mosse and J. M. Maris, "Neuroblastoma," In P. A. Pizzo, P. C. Adamson and D. G. Poplack, Eds., Principles and Practice of Pediatric Oncology. 6th Edition, Lippincott Williams and Wilkins, Philadelphia, 2011, pp. 886-92.... https://www.scirp.org/reference/referencespapers?referenceid=1010379.

42. Hoehner, J. C. *et al.* A developmental model of neuroblastoma: differentiating stroma-poor tumors' progress along an extra-adrenal chromaffin lineage. *Lab. Invest.* **75**, 659–75 (1996).

43. Tomolonis, J. A., Agarwal, S. & Shohet, J. M. Neuroblastoma pathogenesis: deregulation of embryonic neural crest development. *Cell and Tissue Research* **372,** 245–262 Preprint at https://doi.org/10.1007/s00441-017-2747-0 (2018).

44. Sauka-Spengler, T. & Bronner-Fraser, M. A gene regulatory network orchestrates neural crest formation. *Nat. Rev. Mol. Cell Biol.* **9**, 557–568 (2008).

45. Zimmerman, K. A. *et al.* Differential expression of myc family genes during murine development. *Nature 1986 319:6056* **319**, 780–783 (1986).

46. Marshall, G. M. *et al.* The prenatal origins of cancer. *Nature Reviews Cancer* **14**, 277–289 Preprint at https://doi.org/10.1038/nrc3679 (2014).

47. Reiff, T. *et al.* Neuroblastoma phox2b variants stimulate proliferation and dedifferentiation of immature sympathetic neurons. *J. Neurosci.* **30**, 905–915 (2010).

48. Krona, C. *et al.* Analysis of neuroblastoma tumour progression; loss of PHOX2B on 4p13 and 17q gain are early events in neuroblastoma tumourigenesis. *Int. J. Oncol.* **32**, 575–83 (2008).

49. Bourdeaut, F. *et al.* Germline mutations of the paired-like homeobox 2B (PHOX2B) gene in neuroblastoma. *Cancer Lett.* **228**, 51–58 (2005).

50. Schwab, M. *et al.* Amplified DNA with limited homology to myc cellular oncogene is shared by human neuroblastoma cell lines and a neuroblastoma tumour. *Nature* **305**, 245–248 (1983).

51. Adhikary, S. & Eilers, M. Transcriptional regulation and transformation by Myc proteins. *Nat. Rev. Mol. Cell Biol.* **6**, 635–645 (2005).

52. Look, A. T. *et al.* Clinical relevance of tumor cell ploidy and N-myc gene amplification in childhood neuroblastoma: a Pediatric Oncology Group study. *J. Clin. Oncol.* **9**, 581–591 (1991).

53. Matthay, K. K. *et al.* Neuroblastoma. *Nat. Rev. Dis. Primers* **2**, (2016).

54. Weiss, W. A., Aldape, K., Mohapatra, G., Feuerstein, B. G. & Bishop, J. M. Targeted expression of MYCN causes neuroblastoma in transgenic mice. *EMBO J.* **16**, 2985–2995 (1997).

55. Huang, M. & Weiss, W. A. Neuroblastoma and MYCN. *Cold Spring Harb. Perspect. Med.* **3**, (2013).

56. Sausen, M. *et al.* Integrated genomic analyses identify ARID1A and ARID1B alterations in the childhood cancer neuroblastoma. *Nat. Genet.* **45**, 12–17 (2013).

57. Chen, Y. *et al.* Oncogenic mutations of ALK kinase in neuroblastoma. *Nature 2008 455:7215* **455**, 971–974 (2008).

58. Janoueix-Lerosey, I. *et al.* Somatic and germline activating mutations of the ALK kinase receptor in neuroblastoma. *Nature 2008 455:7215* **455**, 967–970 (2008).

59. Heukamp, L. C. *et al.* Targeted expression of mutated ALK induces neuroblastoma in transgenic mice. *Sci. Transl. Med.* **4**, (2012).

60. Berry, T. *et al.* The ALKF1174L Mutation Potentiates the Oncogenic Activity of MYCN in Neuroblastoma. *Cancer Cell* **22**, 117–130 (2012).

61. Mossé, Y. P. *et al.* Identification of ALK as a major familial neuroblastoma predisposition gene. *Nature* **455**, 930–935 (2008).

62. De La Fuente, R., Baumann, C. & Viveiros, M. M. Role of ATRX in chromatin structure and function: implications for chromosome instability and human disease. *Reproduction* **142**, 221–234 (2011).

63. Cheung, N. K. V. *et al.* Association of age at diagnosis and genetic mutations in patients with neuroblastoma. *JAMA* **307**, 1062–1071 (2012).

64. Peifer, M. *et al.* Telomerase activation by genomic rearrangements in high-risk neuroblastoma. *Nature 2015 526:7575* **526**, 700–704 (2015).

65. Attiyeh, E. F. *et al.* Chromosome 1p and 11q deletions and outcome in neuroblastoma. *N. Engl. J. Med.* **353**, 2243–2253 (2005).

66. Bown, N. *et al.* 17q gain in neuroblastoma predicts adverse clinical outcome. U.K. Cancer Cytogenetics Group and the U.K. Children's Cancer Study Group. *Med. Pediatr. Oncol.* **36**, 14–9 (2001).

67. Henrich, K. O., Schwab, M. & Westermann, F. 1p36 tumor suppression--a matter of dosage? *Cancer Res.* **72**, 6079–6088 (2012).

68. Mandriota, S. J. *et al.* Ataxia-telangiectasia mutated (ATM) silencing promotes neuroblastoma progression through a MYCN independent mechanism. *Oncotarget* **6**, 18558–18576 (2015).

69. Mlakar, V. *et al.* 1q deletion in neuroblastoma: a review of biological and clinical implications. https://doi.org/10.1186/s12943-017-0686-8 doi:10.1186/s12943-017-0686-8.

70. Whyte, W. A. *et al.* Master transcription factors and mediator establish super-enhancers at key cell identity genes. *Cell* **153**, 307–319 (2013).

71. Hnisz, D. *et al.* XSuper-enhancers in the control of cell identity and disease. *Cell* **155**, 934 (2013).

72. van Groningen, T. *et al.* A NOTCH feed-forward loop drives reprogramming from adrenergic to mesenchymal state in neuroblastoma. *Nature Communications 2019 10:1* **10**, 1530- (2019).

73. Van Groningen, T. *et al.* Neuroblastoma is composed of two super-enhancer-associated differentiation states. *Nat. Genet.* **49**, 1261–1266 (2017).

74. Boeva, V. *et al.* Heterogeneity of neuroblastoma cell identity defined by transcriptional circuitries. *Nat. Genet.* **49**, 1408–1413 (2017).

75. Soldatov, R. *et al.* Spatiotemporal structure of cell fate decisions in murine neural crest. *Science* **364**, (2019).

76. Whyte, W. A. *et al.* Master transcription factors and mediator establish super-enhancers at key cell identity genes. *Cell* **153**, 307–319 (2013).

77. Wang, C. *et al.* Alternative approaches to target Myc for cancer treatment. *Signal Transduction and Targeted Therapy 2021 6:1* **6**, 117- (2021).

78. Decaesteker, B. *et al.* TBX2 is a neuroblastoma core regulatory circuitry component enhancing MYCN/FOXM1 reactivation of DREAM targets. *Nature Communications 2018 9:1* **9**, 4866- (2018).

79. Durbin, A. D. *et al.* Selective gene dependencies in MYCN-amplified neuroblastoma include the core transcriptional regulatory circuitry. *Nat. Genet.* **50**, 1240–1246 (2018).

80. Thirant, C. *et al.* Reversible transitions between noradrenergic and mesenchymal tumor identities define cell plasticity in neuroblastoma. *Nat. Commun.* **14**, (2023).

81. Gautier, B. *et al.* AAV2/9-mediated silencing of PMP22 prevents the development of pathological features in a rat model of Charcot-Marie-Tooth disease 1 A. *Nat. Commun.* **12**, (2021).

82. Yu, W. *et al.* Longitudinal single-cell multiomic atlas of high-risk neuroblastoma reveals chemotherapy-induced tumor microenvironment rewiring. *Nat. Genet.* **57**, 1142–1154 (2025).

83. Yuan, X. *et al.* Single-cell profiling of peripheral neuroblastic tumors identifies an aggressive transitional state that bridges an adrenergic-mesenchymal trajectory. *Cell Rep.* **41**, 111455 (2022).

84. Rajbhandari, P. *et al.* IL-10 Signaling Remodels Adipose Chromatin Architecture to Limit Thermogenesis and Energy Expenditure. *Cell* **172**, 218-233.e17 (2018).

85. Gartlgruber, M. *et al.* Super enhancers define regulatory subtypes and cell identity in neuroblastoma. *Nat. Cancer* **2**, 114–128 (2021).

86. Teitz, T. *et al.* Caspase 8 is deleted or silenced preferentially in childhood neuroblastomas with amplification of MYCN. *Nat. Med.* **6**, 529–535 (2000).

87. Fulda, S. *et al.* Sensitization for death receptor- or drug-induced apoptosis by re-expression of caspase-8 through demethylation or gene transfer. *Oncogene* **20**, 5865–5877 (2001).

88. Hopkins-Donaldson, S. *et al.* Loss of caspase-8 expression in neuroblastoma is related to malignancy and resistance to TRAIL-induced apoptosis. *Med. Pediatr. Oncol.* **35**, 608–11 (2000).

89. Fulda, S. & Debatin, K. M. Apoptosis pathways in neuroblastoma therapy. *Cancer Lett.* **197**, 131–135 (2003).

90. Gonzalez-Gomez, P. *et al.* Aberrant methylation of multiple genes in neuroblastic tumours: Relationship with MYCN amplification and allelic status at 1p. *Eur. J. Cancer* **39**, 1478–1485 (2003).

91. Harada, K. *et al.* Deregulation of caspase 8 and 10 expression in pediatric tumors and cell lines. *Cancer Res.* **62**, 5897–901 (2002).

92. Fulda, S. *et al.* Loss of caspase-8 expression does not correlate with MYCN amplification, aggressive disease, or prognosis in neuroblastoma. *Cancer Res.* **66**, 10016–10023 (2006).

93. Yue, C., Zhang, Q., Sun, F. & Pan, Q. Global, regional and national burden of neuroblastoma and other peripheral nervous system tumors, 1990 to 2021 and predictions to 2035: visualizing epidemiological characteristics based on GBD 2021. *Neoplasia (United States)* **60**, (2025).

94. London, W. B. *et al.* Clinical and biologic features predictive of survival after relapse of neuroblastoma: A report from the International Neuroblastoma Risk Group Project. *Journal of Clinical Oncology* **29**, 3286–3292 (2011).

95. Vo, K. T. *et al.* Clinical, biologic, and prognostic differences on the basis of primary tumor site in neuroblastoma: A report from the International Neuroblastoma Risk Group project. *Journal of Clinical Oncology* **32**, 3169–3176 (2014).

96. Musarella, M. A., Chan, H. S. L., DeBoer, G. & Gallie, B. L. Ocular Involvement in Neuroblastoma: Prognostic Implications. *Ophthalmology* **91**, 936–940 (1984).

97. Kaatsch, P. Epidemiology of childhood cancer. *Cancer Treat. Rev.* **36**, 277–285 (2010).

98. Pudela, C., Balyasny, S. & Applebaum, M. A. Nervous system: Embryonal tumors: Neuroblastoma. *Atlas Genet. Cytogenet. Oncol. Haematol.* **24**, 284–290 (2020).

99. DuBois, S. G. et al. Metastatic sites in stage IV and IVS neuroblastoma correlate with age, tumor biology, and survival. J. Pediatr. Hematol. Oncol. **21**, 181–189 (1999).

100. Morgenstern, D. A. *et al.* Prognostic significance of pattern and burden of metastatic disease in patients with stage 4 neuroblastoma: A study from the International Neuroblastoma Risk Group database. *Eur. J. Cancer* **65**, 1–10 (2016).

101. Maris, J. M., Hogarty, M. D., Bagatell, R. & Cohn, S. L. Neuroblastoma. *Lancet* **369**, 2106–2120 (2007).

102. Brodeur, G. M. & Bagatell, R. Mechanisms of neuroblastoma regression. *Nat. Rev. Clin. Oncol.* **11**, 704–713 (2014).

103. BECKWITH, J. B. & PERRIN, E. V. IN SITU NEUROBLASTOMAS: A CONTRIBUTION TO THE NATURAL HISTORY OF NEURAL CREST TUMORS. *Am. J. Pathol.* **43**, 1089–104 (1963).

104. Ambros, I. M. & Ambros, P. F. Schwann cells in neuroblastoma. *Eur. J. Cancer* **31**, 429–434 (1995).

105. Ambros, I. M. *et al.* Role of ploidy, chromosome 1p, and Schwann cells in the maturation of neuroblastoma. *N. Engl. J. Med.* **334**, 1505–1511 (1996).

106. Shimada, H. *et al.* The International Neuroblastoma Pathology Classification (the Shimada system). *Cancer* **86**, 364–72 (1999).

107. Ambros, I. M. *et al.* Morphologic features of neuroblastoma (Schwannian stroma-poor tumors) in clinically favorable and unfavorable groups. *Cancer* **94**, 1574–1583 (2002).

108. Ikeda, H. *et al.* Experience with International Neuroblastoma Staging System and Pathology Classification. *Br. J. Cancer* **86**, 1110–1116 (2002).

109. Monclair, T. *et al.* The International Neuroblastoma Risk Group (INRG) staging system: An INRG Task Force report. *Journal of Clinical Oncology* **27**, 298–303 (2009).

110. De Bernardi, B. *et al.* Treatment of localised resectable neuroblastoma. Results of the LNESG1 study by the SIOP Europe Neuroblastoma Group. *Br. J. Cancer* **99**, 1027 (2008).

111. Nuchtern, J. G. *et al.* A prospective study of expectant observation as primary therapy for neuroblastoma in young infants: a Children's Oncology Group study. *Ann. Surg.* **256**, 573–580 (2012).

112. Hero, B. *et al.* Localized infant neuroblastomas often show spontaneous regression: results of the prospective trials NB95-S and NB97. *J. Clin. Oncol.* **26**, 1504–1510 (2008).

113. Twist, C. J. *et al.* Defining Risk Factors for Chemotherapeutic Intervention in Infants With Stage 4S Neuroblastoma: A Report From Children's Oncology Group Study ANBL0531. *J. Clin. Oncol.* **37**, 115–124 (2019).

114. Pinto, N. R. *et al.* Advances in risk classification and treatment strategies for neuroblastoma. *Journal of Clinical Oncology* **33**, 3008–3017 Preprint at https://doi.org/10.1200/JCO.2014.59.4648 (2015).

115. Park, J. R. *et al.* Effect of Tandem Autologous Stem Cell Transplant vs Single Transplant on Event-Free Survival in Patients With High-Risk Neuroblastoma: A Randomized Clinical Trial. *JAMA* **322**, 746 (2019).

116. Kohler, J. A. *et al.* Treatment of children over the age of one year with unresectable localised neuroblastoma without MYCN amplification: results of the SIOPEN study. *Eur. J. Cancer* **49**, 3671–3679 (2013).

117. Matthay, K. K. *et al.* Treatment of high-risk neuroblastoma with intensive chemotherapy, radiotherapy, autologous bone marrow transplantation, and 13-cis-retinoic acid. Children's Cancer Group. *N. Engl. J. Med.* **341**, 1165–1173 (1999).

118. Basta, N. O. *et al.* Factors associated with recurrence and survival length following relapse in patients with neuroblastoma. *Br. J. Cancer* **115**, 1048–1057 (2016).

119. Moreno, L. *et al.* Accelerating drug development for neuroblastoma - New Drug Development Strategy: an Innovative Therapies for Children with Cancer, European Network for Cancer Research in Children and Adolescents and International Society of Paediatric Oncology Europe Ne…. *Expert Opin. Drug Discov.* **12**, 801–811 (2017).

120. June, C. H. & Sadelain, M. Chimeric Antigen Receptor Therapy. *N. Engl. J. Med.* **379**, 64–73 (2018).

121. DuBois, S. G. *et al.* Accelerating Drug Development for Neuroblastoma: Consensus Statement From the Third Neuroblastoma Drug Development Strategy Forum. *Pediatr. Blood Cancer* **72**, (2025).

122. Goldsmith, K. C. *et al.* Lorlatinib with or without chemotherapy in ALK-driven refractory/relapsed neuroblastoma: phase 1 trial results. *Nat. Med.* **29**, 1092–1102 (2023).

123. Fischer, M. *et al.* Ceritinib in paediatric patients with anaplastic lymphoma kinase-positive malignancies: an open-label, multicentre, phase 1, dose-escalation and dose-expansion study. *Lancet Oncol.* **22**, 1764–1776 (2021).

124. Moreno, L. *et al.* Bevacizumab, Irinotecan, or Topotecan Added to Temozolomide for Children With Relapsed and Refractory Neuroblastoma: Results of the ITCC-SIOPEN BEACON-Neuroblastoma Trial. *Journal of clinical oncology: official journal of the American Society of Clinical Oncology*, **42**, 1135–1145 (2024).

125. Gray, J. C. *et al.* JCO-25-01868_Dinutuximab Beta Added to Temozolomide-Based Chemotherapy for Children With Relapsed and Refractory Neuroblastoma: Results of the ITCC-SIOPEN BEACON Immuno Phase II Trial. *Journal of clinical oncology: official journal of the American Society of Clinical Oncology* **44**, 176–187 (2025).

126. Fidler, I. J. Selection of successive tumour lines for metastasis. *Nat. New Biol.* **242**, 148–149 (1973).

127. Ara, T. & DeClerck, Y. A. Mechanisms of invasion and metastasis in human neuroblastoma. *Cancer Metastasis Rev.* **25**, 645–657 (2006).

128. Nguyen, D. X., Bos, P. D. & Massagué, J. Metastasis: from dissemination to organ-specific colonization. *Nat. Rev. Cancer* **9**, 274–284 (2009).

129. Chaffer, C. L. & Weinberg, R. A. A perspective on cancer cell metastasis. *Science* **331**, 1559–1564 (2011).

130. Massagué, J. & Obenauf, A. C. Metastatic colonization by circulating tumour cells. *Nature* **529**, 298–306 (2016).

131. Nagrath, S. *et al.* Isolation of rare circulating tumour cells in cancer patients by microchip technology. *Nature* **450**, 1235–1239 (2007).

132. Labelle, M., Begum, S. & Hynes, R. O. Direct Signaling between Platelets and Cancer Cells Induces an Epithelial-Mesenchymal-Like Transition and Promotes Metastasis. *Cancer Cell* **20**, 576–590 (2011).

133. Al-Mehdi, A. B. *et al.* Intravascular origin of metastasis from the proliferation of endothelium-attached tumor cells: a new model for metastasis. *Nat. Med.* **6**, 100–102 (2000).

134. Aird, W. C. Phenotypic heterogeneity of the endothelium: I. Structure, function, and mechanisms. *Circ. Res.* **100**, 158–173 (2007).

135. Budczies, J. *et al.* The landscape of metastatic progression patterns across major human cancers. *Oncotarget* **6**, 570–583 (2015).

136. Obenauf, A. C. & Massagué, J. Surviving at a distance: organ specific metastasis. *Trends Cancer* **1**, 76 (2015).

137. Oskarsson, T., Batlle, E. & Massagué, J. Metastatic stem cells: Sources, niches, and vital pathways. *Cell Stem Cell* **14**, 306–321 (2014).

138. Sosa, M. S., Bragado, P. & Aguirre-Ghiso, J. A. Mechanisms of disseminated cancer cell dormancy: an awakening field. *Nat. Rev. Cancer* **14**, 611–622 (2014).

139. Maris, J. M. Recent advances in neuroblastoma. *N. Engl. J. Med.* **362**, 2202–11 (2010).

140. Castleberry, R. P. Biology and treatment of neuroblastoma. *Pediatr. Clin. North Am.* **44**, 919–937 (1997).

141. Anner, R. M. & Drewinko, B. Frequency and significance of bone marrow involvement by metastatic solid tumors. *Cancer* **39**, 1337–44 (1977).

142. Singh, G., Krause, J. R. & Breitfeld, V. Bone marrow examination for metastatic tumor Aspirate and Biopsy. *Cancer*, **40**, 2317–2321.

143. Finklestein, J. Z., Ekert, H., Isaacs, H. & Higgins, G. Bone marrow metastases in children with solid tumors. *Am. J. Dis. Child.* **119**, 49–52 (1970).

144. Delta, B. G. & Pinkel, D. Bone marrow aspiration in children with malignant tumors. *J. Pediatr.* **64**, 542–546 (1964).

145. Bain, B. J., Clark, D. M., Wilkins, B. S. & Sovani, V. Bone Marrow Pathology. *Bone Marrow Pathology* https://doi.org/10.1002/9781394244843 (2025) doi:10.1002/9781394244843.

146. Hays, K. *Physiology of Normal Bone Marrow*. *Seminars in oncology nursing* **6**, 3–8. (1990).

147. Vall d'Hebron University Hospital. Bone Marrow Aspiration. *https://hospital.vallhebron.com/en/healthcare/diagnostic-tests/bone-marrow-aspiration#1* (2021).

148. Smith, S. R. & Reid, M. M. Neuroblastoma rosettes in aspirated bone marrow. *Br. J. Haematol.* **88**, 445–447 (1994).

149. Franklin, I. M. & Pritchard, J. Detection of bone marrow invasion by neuroblastoma is improved by sampling at two sites with both aspirates and trephine biopsies. *J. Clin. Pathol.* **36**, 1215–1218 (1983).

150. Reid, M. M. & Roald, B. Central review of bone marrow biopsy specimens from patients with neuroblastoma. *J. Clin. Pathol.* **49**, 691–692 (1996).

151. Reid, M. M. & Roald, B. Deterioration in performance in obtaining bone marrow trephine biopsy cores from children. European Neuroblastoma Study Group. *J. Clin. Pathol.* **52**, 851–852 (1999).

152. Paget, S. The distribution of secondary growths in cancer of the breast. 1889. *Cancer Metastasis Rev.* **8**, 98–101 (1989).

153. Chen, F., Han, Y. & Kang, Y. Bone marrow niches in the regulation of bone metastasis. *Br. J. Cancer* **124**, 1912–1920 (2021).

154. Price, T. T. *et al.* Dormant breast cancer micrometastases reside in specific bone marrow niches that regulate their transit to and from bone. *Sci. Transl. Med.* **8**, (2016).

155. Stadtfeld, M. & Graf, T. Assessing the role of hematopoietic plasticity for endothelial and hepatocyte development by non-invasive lineage tracing. *Development* **132**, 203–213 (2005).

156. Kaplan, R. N. *et al.* VEGFR1-positive haematopoietic bone marrow progenitors initiate the pre-metastatic niche. *Nature* **438**, 820–827 (2005).

157. Kim, B., Van Golen, C. M. & Feldman, E. L. Insulin-like growth factor-I signaling in human neuroblastoma cells. *Oncogene* **23**, 130–141 (2004).

158. Van Golen, C. M. *et al.* Insulin-like growth factor-I receptor expression regulates neuroblastoma metastasis to bone. *Cancer Res.* **66**, 6570–6578 (2006).

159. Van Golen, C. M., Castle, V. P. & Feldman, E. L. IGF-I receptor activation and BCL-2 overexpression prevent early apoptotic events in human neuroblastoma. *Cell Death Differ.* **7**, 654–665 (2000).

160. Stockhausen, M. T., Sjölund, J. & Axelson, H. Regulation of the Notch target gene Hes-1 by TGFalpha induced Ras/MAPK signaling in human neuroblastoma cells. *Exp. Cell Res.* **310**, 218–228 (2005).

161. Middlemas, D. S., Kihl, B. K., Zhou, J. & Zhu, X. Brain-derived neurotrophic factor promotes survival and chemoprotection of human neuroblastoma cells. *Journal of Biological Chemistry* **274**, 16451–16460 (1999).

162. Jaboin, J., Kim, C. J., Kaplan, D. R. & Thiele, C. J. Brain-derived neurotrophic factor activation of TrkB protects neuroblastoma cells from chemotherapy-induced apoptosis via phosphatidylinositol 3'-kinase pathway. *Cancer Res.* **62**, 6756–63 (2002).

163. Lahn, M. M., Sundell, K. L. & Paterson, B. M. The role of protein kinase C-alpha in malignancies of the nervous system and implications for the clinical development of the specific PKC-alpha inhibitor aprinocarsen (Review). *Oncol. Rep.* **11**, 515–22 (2004).

164. D'Angio, G. J., Evans, A. E. & Koop, C. E. SPECIAL PATTERN OF WIDESPREAD NEUROBLASTOMA WITH A FAVOURABLE PROGNOSIS. *The Lancet* **297**, 1046–1049 (1971).

165. Schleiermacher, G. *et al.* Treatment of stage 4s neuroblastoma--report of 10 years' experience of the French Society of Paediatric Oncology (SFOP). *Br. J. Cancer* **89**, 470–476 (2003).

166. Nickerson, H. J. *et al.* Favorable biology and outcome of stage IV-S neuroblastoma with supportive care or minimal therapy: a Children's Cancer Group study. *J. Clin. Oncol.* **18**, 477–486 (2000).

167. Katzenstein, H. M. *et al.* Prognostic significance of age, MYCN oncogene amplification, tumor cell ploidy, and histology in 110 infants with stage D(S) neuroblastoma: the pediatric oncology group experience--a pediatric oncology group study. *J. Clin. Oncol.* **16**, 2007–2017 (1998).

168. Zhao, X., Xu, Z. & Feng, X. Clinical characteristics and prognoses in pediatric neuroblastoma with bone or liver metastasis: data from the SEER 2010-2019. *BMC Pediatr.* **24**, (2024).

169. Brodt, P. Selection of a highly metastatic liver-colonizing subpopulation of Lewis lung carcinoma variant H-59 using murine hepatocyte monolayers. *Clin. Exp. Metastasis* **7**, 525–539 (1989).

170. Nicolson, G. L. Organ specificity of tumor metastasis: role of preferential adhesion, invasion and growth of malignant cells at specific secondary sites. *Cancer Metastasis Rev.* **7**, 143–188 (1988).

171. Stoolman, L. M. Adhesion molecules controlling lymphocyte migration. *Cell* **56**, 907–910 (1989).

172. Netland, P. A. & Zetter, B. R. Organ-specific adhesion of metastatic tumor cells in vitro. *Science* **224**, 1113–1115 (1984).

173. Tsuchida, Y., Yokomori, K., Saito, S., Kaku, H. & Bessho, F. Stage IV-S neuroblastoma involving the liver and ectopic liver. Report of an unusual case. *Cancer* **53**, 1609–11 (1984).

174. Kuwashima, N. Organ-specific adhesion of neuroblastoma cells in vitro: Correlation with their hepatic metastasis potential. *J. Pediatr. Surg.* **32**, 546–551 (1997).

175. Kushner, B. H., Kramer, K., LaQuaglia, M. P., Modak, S. & Cheung, N. K. V. Liver involvement in neuroblastoma: The memorial sloan-kettering experience supports treatment reduction in young patients. *Pediatric Blood and Cancer* **46** 278–284 (2006).

176. Bond, J. V. *Neuroblastoma Metastatic to the Liver in Infants*. *Archives of disease in childhood,* **51**, 879–882 (1976).

177. O'Malley, B., D'Angio, G. J. & Vawter, G. F. Late effects of roentgen therapy given in infancy. *Am. J. Roentgenol., Radium Therapy Nucl. Med.* **89**, (1963).

178. Neuhauser, E. B. D., Wittenborg, M. H., Berman, C. Z. & Cohen, J. Irradiation effects of roentgen therapy on the growing spine. *Radiology* **59**, 637–650 (1952).

179. Morgenstern, D. A. *et al.* Metastatic neuroblastoma confined to distant lymph nodes (stage 4N) predicts outcome in patients with stage 4 disease: A study from the

International Neuroblastoma Risk Group database. *Journal of Clinical Oncology* **32**, 1228–1235 (2014).

180. Rosen, E. M. *et al.* Stage IV-N: A favorable subset of children with metastatic neuroblastoma. *Med. Pediatr. Oncol.* **13**, 194–198 (1985).

181. Yamada, S. *et al.* Features and outcome of advanced neuroblastoma with distant lymph node metastasis. *Pediatr. Hematol. Oncol.* **9**, 49–56 (1992).

182. DuBois, S. G. *et al.* Lung metastases in neuroblastoma at initial diagnosis: A report from the International Neuroblastoma Risk Group (INRG) project. *Pediatr. Blood Cancer* **51**, 589–592 (2008).

183. Kammen, B. F. *et al.* Pulmonary metastases at diagnosis of neuroblastoma in pediatric patients: CT findings and prognosis. *AJR Am. J. Roentgenol.* **176**, 755–759 (2001).

184. Cowie, F., Corbett, R. & Pinkerton, R. *Lung Involvement in Neuroblastoma: Incidence and Characteristics*. *Med. Pediatr. Oncol* **28** (1997).

185. de la Monte, S. M., Moore, G. W. & Hutchins, G. M. Nonrandom distribution of metastases in neuroblastic tumors. *Cancer* **52**, 915–25 (1983).

186. Maman, S. *et al.* The metastatic microenvironment: Lung-derived factors control the viability of neuroblastoma lung metastasis. *Int. J. Cancer* **133**, 2296–2306 (2013).

187. Pantel, K. & Alix-Panabières, C. The clinical significance of circulating tumor cells. *Nat. Clin. Pract. Oncol.* **4**, 62–63 (2007).

188. Wikman, H., Vessella, R. & Pantel, K. Cancer micrometastasis and tumour dormancy. *APMIS* **116**, 754–770 (2008).

189. Páez, D. *et al.* Cancer dormancy: a model of early dissemination and late cancer recurrence. *Clin. Cancer Res.* **18**, 645–653 (2012).

190. Massagué, J. New concepts in tissue-specific metastases. *Clin. Adv. Hematol. Oncol.* **1**, 576–7 (2003).

191. Aguirre-Ghiso, J. A. Models, mechanisms and clinical evidence for cancer dormancy. *Nat. Rev. Cancer* **7**, 834–846 (2007).

192. Morris, J. A. *et al.* Biological variables in thoracic neuroblastoma: A Pediatric Oncology Group study. *J. Pediatr. Surg.* **30**, 296–303 (1995).

193. Witz, I. P. & Levy-Nissenbaum, O. The tumor microenvironment in the post-PAGET era. *Cancer Lett.* **242**, 1–10 (2006).

194. Johnsen, J. I., Krawczyk, E. & Kitlí Nska, J. Preclinical Models of Neuroblastoma-Current Status and Perspectives. *Cancers* **15**, 3314. (2023).

195. Bogenmann, E. A metastatic neuroblastoma model in SCID mice. *Int. J. Cancer* **67**, 379–385 (1996).

196. Chen, D. *et al.* LIN28B promotes neuroblastoma metastasis and regulates PDZ binding kinase. *Neoplasia (United States)* **22**, 231–241 (2020).

197. Seong, B. K. A. *et al.* A metastatic mouse model identifies genes that regulate neuroblastoma metastasis. *Cancer Res.* **77**, 696–706 (2017).

198. Yogev, O. *et al.* In vivo modeling of chemoresistant neuroblastoma provides new insights into chemorefractory disease and metastasis. *Cancer Res.* **79**, 5382–5393 (2019).

199. Bibby, M. C. Orthotopic models of cancer for preclinical drug evaluation: Advantages and disadvantages. *Eur. J. Cancer* **40**, 852–857 (2004).

200. Zhao, H. *et al.* Characterization of neuroblastoma bone invasion/metastasis in established bone metastatic model of SY5Y and KCNR cell lines. *Child's Nervous System* **29**, 1097–1105 (2013).

201. Braekeveldt, N. *et al.* Neuroblastoma patient-derived orthotopic xenografts retain metastatic patterns and geno- and phenotypes of patient tumours. *Int. J. Cancer* **136**, E252–E261 (2015).

202. Townsend, E. C. *et al.* The Public Repository of Xenografts Enables Discovery and Randomized Phase II-like Trials in Mice. *Cancer Cell* **29**, 574–586 (2016).

203. Murphy, B. *et al.* Evaluation of Alternative In Vivo Drug Screening Methodology: A Single Mouse Analysis. *Cancer Res.* **76**, 5798–5809 (2016).

204. Galluzzi, L., Senovilla, L., Zitvogel, L. & Kroemer, G. The secret ally: immunostimulation by anticancer drugs. *Nat. Rev. Drug Discov.* **11**, 215–233 (2012).

205. Maguire, C. A. *et al.* Triple Bioluminescence Imaging for In Vivo Monitoring of Cellular Processes. *Molecular therapy. Nucleic acids*, **2**, e99. (2013).

206. Sherman, B. T. *et al.* DAVID: a web server for functional enrichment analysis and functional annotation of gene lists (2021 update). *Nucleic Acids Res.* **50**, W216–W221 (2022).

207. Huang, D. W., Sherman, B. T. & Lempicki, R. A. Systematic and integrative analysis of large gene lists using DAVID bioinformatics resources. *Nat. Protoc.* **4**, 44–57 (2009).

208. Casper, J. *et al.* The UCSC Genome Browser database: 2026 update. *Nucleic Acids Res.* **54**, D1331–D1335 (2026).

209. R2: Genomics Analysis and Visualization Platform. *(https://r2platform.com)*.

210. Abdulla, S. *et al.* CZ CELL×GENE Discover: A single-cell data platform for scalable exploration, analysis and modeling of aggregated data. *bioRxiv* 2023.10.30.563174 (2023) doi:10.1101/2023.10.30.563174.

211. DepMap: The Cancer Dependency Map Project at Broad Institute. *https://depmap.org/portal/*.

212. Krawczyk, E. & Kitlińska, J. Preclinical Models of Neuroblastoma-Current Status and Perspectives. *Cancers (Basel).* **15**, (2023).

213. Berthold, F., Spix, C., Kaatsch, P. & Lampert, F. Incidence, Survival, and Treatment of Localized and Metastatic Neuroblastoma in Germany 1979–2015. *Pediatric Drugs* **19**, 577–593 (2017).

214. Ren, Y. *et al.* Inhibition of tumor growth and metastasis in vitro and in vivo by targeting macrophage migration inhibitory factor in human neuroblastoma. *Oncogene* **25**, 3501–3508 (2006).

215. Laut, A. K. *et al.* CHD5 inhibits metastasis of neuroblastoma. *Oncogene* **41**, 622–633 (2022).

216. Hua, Y. *et al.* Isatin inhibits the invasion and metastasis of SH-SY5Y neuroblastoma cells in vitro and in vivo. *Int. J. Oncol.* **58**, 122–132 (2021).

217. Bhoopathi, P. *et al.* Regulation of neuroblastoma migration, invasion, and in vivo metastasis by genetic and pharmacological manipulation of MDA-9/Syntenin. *Oncogene* **38**, 6781–6793 (2019).

218. Lee, S. *et al.* FAK is a critical regulator of neuroblastoma liver metastasis. *Oncotarget* **3**, 1576–1587 (2012).

219. Megison, M. L., Stewart, J. E., Nabers, H. C., Gillory, L. A. & Beierle, E. A. FAK inhibition decreases cell invasion, migration and metastasis in MYCN amplified neuroblastoma. *Clin. Exp. Metastasis* **30**, 555–568 (2013).

220. Kashima, K. *et al.* Inhibition of lymphatic metastasis in neuroblastoma by a novel neutralizing antibody to vascular endothelial growth factor-D. *Cancer Sci.* **103**, 2144–2152 (2012).

221. Wu, P. Y. *et al.* Activation of Aryl Hydrocarbon Receptor by Kynurenine Impairs Progression and Metastasis of Neuroblastoma. *Cancer Res.* **79**, 5550–5562 (2019).

222. Shmakova, A. A. *et al.* Urokinase Receptor uPAR Downregulation in Neuroblastoma Leads to Dormancy, Chemoresistance and Metastasis. *Cancers (Basel).* **14**, (2022).

223. Lee, W. G., Asuelime, G. E., Asuelime-Smith, M. B. T., Chen, S. Y. & Kim, E. S. Differential RNA Expression Between Metastatic and Primary Neuroblastoma Cells. *Journal of Surgical Research* **298**, 240–250 (2024).

224. Patterson, D. M. *et al.* Effect of MDM2 and vascular endothelial growth factor inhibition on tumor angiogenesis and metastasis in neuroblastoma. *Angiogenesis* **14**, 255–266 (2011).

225. Zhang, L., Yeger, H., Das, B., Irwinz, M. S. & Baruchel, S. Tissue microenvironment modulates CXCR4 expression and tumor metastasis in neuroblastoma. *Neoplasia* **9**, 36–46 (2007).

226. Fidler, I. J. & Zeidman, I. Enhancement of experimental metastasis by x-ray: a possible mechanism. *J. Med.* **3**, 172–7 (1972).

227. Fidler, I. J. Metastasis: Quantitative Analysis of Distribution and Fate of Tumor Emboli Labeled With 125I-5-Iodo-2′ -deoxyuridine. *JNCI: Journal of the National Cancer Institute* **45**, 773–782 (1970).

228. Greene, H. S. & Harvey, E. K. the relationship between the dissemination of tumor cells and the distribution of metastases. *Cancer Res.* **24**, 799–811 (1964).

229. Ottewell, P. D., Coleman, R. E. & Holen, I. From genetic abnormality to metastases: murine models of breast cancer and their use in the development of anticancer therapies. *Breast Cancer Res. Treat.* **96**, 101–113 (2006).

230. Arguello, F., Baggs, R. B. & Frantz, C. N. A murine model of experimental metastasis to bone and bone marrow. *Cancer Res.* **48**, 6876–81 (1988).

231. Harms, J. F. & Welch, D. R. MDA-MB-435 human breast carcinoma metastasis to bone. *Clin. Exp. Metastasis* **20**, 327–334 (2003).

232. Kuchimaru, T. *et al.* A reliable murine model of bone metastasis by injecting cancer cells through caudal arteries. *Nat. Commun.* **9**, (2018).

233. Han, R. *et al.* Different tumorigenicity and distinct metastasis and gene signature between orthotopic and subcutaneous neuroblastoma xenografted mice. *Aging* **14**, 1932–1940 (2022).

234. Pouliot, N. P. H. B. B. A. *Investigating Metastasis Using In Vitro Platforms*. (Landes Bioscience, Austin (TX), (2013).

235. Haider, M. T. *et al.* Comparison of ex vivo bioluminescence imaging, Alu-qPCR and histology for the quantification of spontaneous lung and bone metastases in subcutaneous xenograft mouse models. *Clin. Exp. Metastasis* **41**, 103–115 (2024).

236. Patel, S. A. & Vanharanta, S. Epigenetic determinants of metastasis. *Molecular oncology,* **11**, 79–96 (2017).

237. Minn, A. J. *et al.* Genes that mediate breast cancer metastasis to lung. *Nature* **436**, 518–524 (2005).

238. Bos, P. D. *et al.* Genes that mediate breast cancer metastasis to the brain. *Nature* **459**, 1005–1009 (2009).

239. Vanharanta, S. *et al.* Epigenetic expansion of VHL-HIF signal output drives multiorgan metastasis in renal cancer. *Nat. Med.* **19**, 50–56 (2013).

240. Jacob, L. S. *et al.* Metastatic Competence Can Emerge with Selection of Preexisting Oncogenic Alleles without a Need of New Mutations. *Cancer Res.* **75**, 3713–3719 (2015).

241. Morton, C. L. & Houghton, P. J. Establishment of human tumor xenografts in immunodeficient mice. *Nat. Protoc.* **2**, 247–250 (2007).

242. Stribbling, S. M. & Ryan, A. J. The cell-line-derived subcutaneous tumor model in preclinical cancer research. *Nat. Protoc.* **17**, 2108–2128 (2022).

243. Fernandez, J. L. *et al.* A Comparative Analysis of Orthotopic and Subcutaneous Pancreatic Tumour Models: Tumour Microenvironment and Drug Delivery. *Cancers 2023, Vol. 15,* **15**, (2023).

244. Gengenbacher, N., Singhal, M. & Augustin, H. G. Preclinical mouse solid tumour models: status quo, challenges and perspectives. *Nat. Rev. Cancer* **17**, 751–765 (2017).

245. Stribbling, S. M., Beach, C. & Ryan, A. J. Orthotopic and metastatic tumour models in preclinical cancer research. *Pharmacol. Ther.* **257**, 108631 (2024).

246. Sheng, Y. *et al.* Impact of Subcutaneous Versus Orthotopic Implantations on Patient-Derived Xenograft Transcriptomic Profiles. *Cancer research communications* **5**, 871–880 (2025).

247. Morandi, F. *et al.* Bone Marrow-Infiltrating Human Neuroblastoma Cells Express High Levels of Calprotectin and HLA-G Proteins. *PLoS One* **7**, e29922 (2012).

248. Liu, Y., Beyer, A. & Aebersold, R. On the Dependency of Cellular Protein Levels on mRNA Abundance. *Cell* **165**, 535–550 (2016).

249. Flavahan, W. A., Gaskell, E. & Bernstein, B. E. Epigenetic plasticity and the hallmarks of cancer. *Science* **357**, (2017).

250. Fares, J., Fares, M. Y., Khachfe, H. H., Salhab, H. A. & Fares, Y. Molecular principles of metastasis: a hallmark of cancer revisited. *Signal Transduct. Target. Ther.* **5**, (2020).

251. Caroline Hochheuser, A. *et al.* Metastatic tumor cells in bone marrow differ from paired neuroblastoma tumor and contain subsets with therapy-resistant characteristics. *bioRxiv* 2024.09.13.612231 (2024) doi:10.1101/2024.09.13.612231.

252. Mei, S. *et al.* Single-cell analyses of metastatic bone marrow in human neuroblastoma reveals microenvironmental remodeling and metastatic signature. *JCI Insight* **9**, (2024).

253. Villalard, B. *et al.* Neuroblastoma plasticity during metastatic progression stems from the dynamics of an early sympathetic transcriptomic trajectory. *Nat. Commun.* **15**, (2024).

254. He, G. Q. *et al.* Dissecting neuroblastoma heterogeneity through single-cell multi-omics: insights into development, immunity, and therapeutic resistance. *Oncogene 2025 45:2* **45**, 123–139 (2025).

255. Kiani, K., Sanford, E. M., Goyal, Y. & Raj, A. Changes in chromatin accessibility are not concordant with transcriptional changes for single-factor perturbations. *Mol. Syst. Biol.* **18**, (2022).

256. Klemm, S. L., Shipony, Z. & Greenleaf, W. J. Chromatin accessibility and the regulatory epigenome. *Nat. Rev. Genet.* **20**, 207–220 (2019).

257. Brady, J. J. *et al.* An Arntl2-Driven Secretome Enables Lung Adenocarcinoma Metastatic Self-Sufficiency. *Cancer Cell* **29**, 697–710 (2016).

258. Denny, S. K. *et al.* Nfib Promotes Metastasis through a Widespread Increase in Chromatin Accessibility. *Cell* **166**, 328–342 (2016).

259. Cheung, W. K. C. *et al.* Control of alveolar differentiation by the lineage transcription factors GATA6 and HOPX inhibits lung adenocarcinoma metastasis. *Cancer Cell* **23**, 725–738 (2013).

260. Winslow, M. M. *et al.* Suppression of lung adenocarcinoma progression by Nkx2-1. *Nature* **473**, 101–104 (2011).

261. Bacabac, M. & Xu, W. Oncogenic super-enhancers in cancer: mechanisms and therapeutic targets. *Cancer Metastasis Rev.* **42**, 471–480 (2023).

262. Dekker, J., Marti-Renom, M. A. & Mirny, L. A. Exploring the three-dimensional organization of genomes: interpreting chromatin interaction data. *Nat. Rev. Genet.* **14**, 390–403 (2013).

263. Bonev, B. & Cavalli, G. Organization and function of the 3D genome. *Nat. Rev. Genet.* **17**, 661–678 (2016).

264. Zaret, K. S. & Mango, S. E. Pioneer transcription factors, chromatin dynamics, and cell fate control. *Curr. Opin. Genet. Dev.* **37**, 76–81 (2016).

265. Lee, T. I. & Young, R. A. Transcriptional regulation and its misregulation in disease. *Cell* **152**, 1237–1251 (2013).

266. Lambert, S. A. *et al.* The Human Transcription Factors. *Cell* **172**, 650–665 (2018).

267. Hayakawa, Y. *et al.* IFN-gamma-mediated inhibition of tumor angiogenesis by natural killer T-cell ligand, alpha-galactosylceramide. *Blood* **100**, 1728–33 (2002).

268. Harris, A. L., Kerr, D. J., Pezzella, F. & Ribatti, D. Accessing the vasculature in cancer: revising an old hallmark. *Trends Cancer* **10**, 1038–1051 (2024).

269. Rifatbegovic, F. *et al.* Neuroblastoma cells undergo transcriptomic alterations upon dissemination into the bone marrow and subsequent tumor progression. *Int. J. Cancer* **142**, 297–307 (2018).

270. Housden, B. E. & Perrimon, N. Spatial and temporal organization of signaling pathways. *Trends Biochem. Sci.* **39**, 457–464 (2014).

271. Bernstein, B. E. *et al.* A Bivalent Chromatin Structure Marks Key Developmental Genes in Embryonic Stem Cells. *Cell* **125**, 315–326 (2006).

272. Rada-Iglesias, A. *et al.* A unique chromatin signature uncovers early developmental enhancers in humans. *Nature* **470**, 279–285 (2011).

273. Hanahan, D. & Weinberg, R. A. Hallmarks of cancer: The next generation. *Cell* **144**, 646–674 (2011).

274. Lamouille, S., Xu, J. & Derynck, R. Molecular mechanisms of epithelial-mesenchymal transition. *Nat. Rev. Mol. Cell Biol.* **15**, 178–196 (2014).

275. Nader, J. H. *et al.* Systematic review of clinical drug development activities for neuroblastoma from 2011 to 2020. *Pediatr. Blood Cancer* **70**, (2023).

276. Kushner, B. H., Kramer, K., Modak, S. & Cheung, N. K. V. Irinotecan plus temozolomide for relapsed or refractory neuroblastoma. *J. Clin. Oncol.* **24**, 5271–5276 (2006).

277. London, W. B. *et al.* Phase II randomized comparison of topotecan plus cyclophosphamide versus topotecan alone in children with recurrent or refractory neuroblastoma: a Children's Oncology Group study. *J. Clin. Oncol.* **28**, 3808–3815 (2010).

278. Bagatell, R. *et al.* Phase II study of irinotecan and temozolomide in children with relapsed or refractory neuroblastoma: a Children's Oncology Group study. *J. Clin. Oncol.* **29**, 208–213 (2011).

279. Di Giannatale, A. *et al.* Phase II study of temozolomide in combination with topotecan (TOTEM) in relapsed or refractory neuroblastoma: a European Innovative Therapies for Children with Cancer-SIOP-European Neuroblastoma study. *Eur. J. Cancer* **50**, 170–177 (2014).

280. Moreno, L. *et al.* Combination Early-Phase Trials of Anticancer Agents in Children and Adolescents. *Journal of Clinical Oncology* **41**, 3408–3422 (2023).

281. Mody, R. *et al.* Irinotecan, temozolomide, and dinutuximab with GM-CSF in children with refractory or relapsed neuroblastoma: A report from the children's Oncology group. *Journal of Clinical Oncology* **38**, 2160–2169 (2020).

282. Del Bufalo, F. *et al.* GD2-CART01 for Relapsed or Refractory High-Risk Neuroblastoma. *N. Engl. J. Med.* **388**, 1284–1295 (2023).

283. Ackermann, S. *et al.* A mechanistic classification of clinical phenotypes in neuroblastoma. *Science* **362**, 1165–1170 (2018).

284. Oesterheld, J. *et al.* Eflornithine as Postimmunotherapy Maintenance in High-Risk Neuroblastoma: Externally Controlled, Propensity Score-Matched Survival Outcome Comparisons. *Journal of Clinical Oncology* **42**, 90–102 (2024).

285. Chakraborty, S., Hosen, M. I., Ahmed, M. & Shekhar, H. U. Onco-Multi-OMICS Approach: A New Frontier in Cancer Research. *Biomed Res. Int.* **2018**, (2018).

286. Lazic, D. *et al.* Landscape of Bone Marrow Metastasis in Human Neuroblastoma Unraveled by Transcriptomics and Deep Multiplex Imaging. *Cancers (Basel).* **13**, (2021).

287. Berlanga, P. *et al.* The European MAPPYACTS Trial: Precision Medicine Program in Pediatric and Adolescent Patients with Recurrent Malignancies. *Cancer Discov.* **12**, 1266–1281 (2022).

288. Yang, S., Li, J. & Cai, X. The high expression of glial cell line-derived neurotrophic factor receptor alpha Ⅱ (GFRA2) as a predictor of poor prognosis in gastric cancer patients: A survival and regression analysis approach. *Heliyon* **9**, (2023).

289. Li, Z. *et al.* GDNF family receptor alpha 2 promotes neuroblastoma cell proliferation by interacting with PTEN. *Biochem. Biophys. Res. Commun.* **510**, 339–344 (2019).

290. Cui, R. *et al.* Neurturin-induced activation of GFRA2-RET axis potentiates pancreatic cancer glycolysis via phosphorylated hexokinase 2. *Cancer Lett.* **621**, (2025).

291. Orentas, R. J. *et al.* Paired expression analysis of tumor cell surface antigens. *Front. Oncol.* **7**, (2017).

292. Sommer, A. K. *et al.* Downregulation of GRK5 hampers the migration of breast cancer cells. *Sci. Rep.* **9**, (2019).

293. Chakraborty, P. K. *et al.* G protein-coupled receptor kinase GRK5 phosphorylates moesin and regulates metastasis in prostate cancer. *Cancer Res.* **74**, 3489–3500 (2014).

294. Jiang, L. P. *et al.* GRK5 functions as an oncogenic factor in non-small-cell lung cancer. *Cell Death Dis.* **9**, (2018).

295. Pham, T., Robinson, K., Vleeshouwer-Neumann, T., Annis, J. E. & Chen, E. Y. *Characterization of GRK5 as a Novel Regulator of Rhabdomyosarcoma Tumor Cell Growth and Self-Renewal*. *Oncotarget* vol. 11 www.oncotarget.com (2020).

296. Zhang, L. *et al.* In vivo antitumor and antimetastatic activity of Sunitinib in preclinical Neuroblastoma mouse model. *Neoplasia* **11**, 426–435 (2009).

297. Wang, C. *et al.* Prognostic and biological function value of OSBPL3 in colorectal cancer analyzed by multi-omic data analysis. *BMC Gastroenterol.* **23**, (2023).

298. Nouruzi, S. *et al.* ASCL1 activates neuronal stem cell-like lineage programming through remodeling of the chromatin landscape in prostate cancer. *Nat. Commun.* **13**, (2022).

299. Takumida, H. *et al.* Integrative epigenome and transcriptome analyses reveal transcriptional programs differentially regulated by ASCL1 and NEUROD1 in small cell lung cancer. *Oncogene* **44**, 3113–3125 (2025).

300. Zhang, X. *et al.* A novel nomogram based on DLL3 and PD-L1 for predicting the prognosis of patients with small cell lung cancer. *BMC Cancer* **25**, (2025).

301. Hu, C. *et al.* ASCL1 and DLL3 expressions and their clinicopathological implications in surgically resected pure small cell lung cancer: A study of 247 cases from the National Cancer Center of China. *Thorac. Cancer* **13**, 338–345 (2022).

302. Furuta, M. *et al.* DLL3 regulates the migration and invasion of small cell lung cancer by modulating Snail. *Cancer Sci.* **110**, 1599–1608 (2019).

303. Su, P. L. *et al.* DLL3-guided therapies in small-cell lung cancer: from antibody-drug conjugate to precision immunotherapy and radioimmunotherapy. *Molecular Cancer* vol. 23 Preprint at https://doi.org/10.1186/s12943-024-02012-z (2024).

304. Krytska, K. *et al.* Evaluation of the DLL3-targeting Antibody–Drug Conjugate Rovalpituzumab Tesirine in Preclinical Models of Neuroblastoma. *Cancer Research Communications* **2**, 616–623 (2022).

305. Huehls, A. M., Coupet, T. A. & Sentman, C. L. Bispecific T cell engagers for cancer immunotherapy. *Immunol. Cell Biol.* **93**, 290 (2014).

306. Mullard, A. FDA approves first DLL3 × CD3 bispecific T-cell engager for lung cancer. *Nat. Rev. Drug Discov.* **23**, 487 (2024).

307. Akagi, T. *et al.* Visinin-like protein-1 overexpression is an indicator of lymph node metastasis and poor prognosis in colorectal cancer patients. *Int. J. Cancer* **131**, 1307–1317 (2012).

308. Dai, Q. Q., Wang, Y. Y., Jiang, Y. P., Li, L. & Wang, H. J. VSNL1 Promotes Gastric Cancer Cell Proliferation and Migration by Regulating P2X3/P2Y2 Receptors and Is a Clinical Indicator of Poor Prognosis in Gastric Cancer Patients. *Gastroenterol. Res. Pract.* **2020**, (2020).

309. He, C. *et al.* VSNL1 Promotes Cell Proliferation, Migration, and Invasion in Colorectal Cancer by Binding with COL10A1. *Ann Clin Lab Sci.* **52**, 60-72 (2022).

310. Korshunov, A. *et al.* Transcriptional profiling of medulloblastoma with extensive nodularity (MBEN) reveals two clinically relevant tumor subsets with VSNL1 as potent prognostic marker. *Acta Neuropathol.* **139**, 583–596 (2020).

311. Weber-Boyvat, M. *et al.* OSBP-related protein 3 (ORP3) coupling with VAMP-associated protein A regulates R-Ras activity. *Exp. Cell Res.* **331**, 278–291 (2015).

312. Lehto, M. *et al.* The R-Ras interaction partner ORP3 regulates cell adhesion. *J. Cell Sci.* **121**, 695–705 (2008).

313. Jiao, H. li *et al.* Retraction Note: Upregulation of OSBPL3 by HIF1A promotes colorectal cancer progression through activation of RAS signaling pathway(Cell Death and Disease, 10.1038/s41419-020-02793-3). *Cell Death and Disease* **13** Preprint at https://doi.org/10.1038/s41419-022-05367-7 (2022).

314. Habuchi, H. *et al.* The occurrence of three isoforms of heparan sulfate 6-O-sulfotransferase having different specificities for hexuronic acid adjacent to the targeted N- sulfoglucosamine. *Journal of Biological Chemistry* **275**, 2859–2868 (2000).

315. Iravani, O., Bay, B. H. & Yip, G. W. C. Silencing HS6ST3 inhibits growth and progression of breast cancer cells through suppressing IGF1R and inducing XAF1. *Exp. Cell Res.* **350**, 380–389 (2017).

316. Liu, L. *et al.* PRMT5 upregulates KCNMB4 expression via histone methylation to promote paclitaxel resistance in advanced nasopharyngeal carcinoma. *Cell Death Dis.* **17**, (2026).

317. Bao, J. *et al.* Microarray data analysis of neuroblastoma: Expression of SOX2 downregulates the expression of MYCN. *Mol. Med. Rep.* **12**, 6867–6872 (2015).

318. Yang, J. *et al.* Recurrent LRP1-SNRNP25 and KCNMB4-CCND3 fusion genes promote tumor cell motility in human osteosarcoma. *J. Hematol. Oncol.* **7**, (2014).

319. Liu, X. *et al.* RSL1D1 promotes the progression of colorectal cancer through RAN-mediated autophagy suppression. *Cell Death Dis.* **13**, (2022).

320. Mukherjee, A., Boonbangyang, M. & K. S, M. Unraveling the intricate molecular landscape and potential biomarkers in lung adenocarcinoma through integrative epigenomic and transcriptomic profiling. Scientific reports **15**(1), 9154 (2025).

321. Shirani, N., Mahdi-Esferizi, R., Eshraghi Samani, R., Tahmasebian, S. & Yaghoobi, H. In silico identification and in vitro evaluation of MRPS30-DT lncRNA and MRPS30 gene expression in breast cancer. *Cancer Rep. (Hoboken)* **7**, (2024).

322. Zhou, W. *et al.* A public data-based molecular classification of small cell lung cancer by neuroactive signaling networks unveils distinct microenvironment landscapes and immunotherapy-related prognostic biomarkers. *Transl. Lung Cancer Res.* **14**, 4983–4999 (2025).

Annex I: List of publications

During these years doing my PhD I had the chance to participate in other research projects of the Neural Tumors laboratory, as well as in collaborations with other research groups, including the publication of my MSc work as a first author:

(1) Jiménez, C., Antonelli, R., Nadal-Ribelles, M., Devis-Jauregui, L., Latorre, P., Solé, C., Masanas, M., Molero-Valenzuela, A., Soriano, A., Sánchez de Toledo, J., Llobet-Navas, D., Roma, J., Posas, F., de Nadal, E., Gallego, S., Moreno, L., & Segura, M. F. (2022). Structural disruption of BAF chromatin remodeller impairs neuroblastoma metastasis by reverting an invasiveness epigenomic program. *Molecular cancer*, *21*(1), 175. https://doi.org/10.1186/s12943-022-01643-4

(2) Molero-Valenzuela, A., Fontova, P., Alonso-Carrillo, D., Carreira-Barral, I., Torres, A. A., García-Valverde, M., Benítez-García, C., Pérez-Tomás, R., Quesada, R., & Soto-Cerrato, V. (2022). A Novel Late-Stage Autophagy Inhibitor That Efficiently Targets Lysosomes Inducing Potent Cytotoxic and Sensitizing Effects in Lung Cancer. *Cancers*, *14*(14), 3387. https://doi.org/10.3390/cancers14143387

Annex II: Research article published as first author (under review)

''Loss of BAX in a Neuroblastoma Patient Reveals Delayed Apoptosis but Sustained Chemotherapy Sensitivity''

Adrià Molero-Valenzuela; Isabel de Rojas-P; Guillem Pons; María José Pérez-García; Gabriela Guillén; Andrea Vilaplana; Sergio Manresa-Vera; Paula Pérez-Albert; Marta Garrido; Lorena Valero-Arrese; Raquel Hladun, Marta Miera-Maluenda; Ariadna Boloix; Josep Roma; Aroa Soriano; Lucas Moreno; Miguel F. Segura

NPJ Precision Oncology. 2026

Annex III: RNA-seq upregulated genes in three or more cell lines

Item	Occurences	Present In
BNC2	4	SK-N-BE(2), SK-N-AS, CHLA-90, NBL-S
AATK	3	SK-N-AS, CHLA-90, NBL-S
ADAMTS1	3	SK-N-BE(2), SK-N-AS, NBL-S
ADRA1A	3	SK-N-BE(2), SK-N-AS, CHLA-90
AFAP1	3	SK-N-BE(2), SK-N-AS, NBL-S
ANGPTL4	3	SK-N-BE(2), SK-N-AS, NBL-S
APBA1	3	SK-N-BE(2), SK-N-AS, NBL-S
ASCL1	3	SK-N-BE(2), SK-N-AS, NBL-S
BEND4	3	SK-N-BE(2), SK-N-AS, NBL-S
CALCRL	3	SK-N-BE(2), SK-N-AS, CHLA-90
CEBPD	3	SK-N-AS, CHLA-90, NBL-S
CNTNAP3C	3	SK-N-BE(2), SK-N-AS, NBL-S
DLL3	3	SK-N-AS, CHLA-90, NBL-S
DUSP10	3	SK-N-BE(2), SK-N-AS, NBL-S
FAM225A	3	SK-N-BE(2), SK-N-AS, NBL-S
FAM225B	3	SK-N-BE(2), SK-N-AS, NBL-S
GABARAPL1	3	SK-N-BE(2), SK-N-AS, NBL-S
GFRA2	3	SK-N-BE(2), SK-N-AS, NBL-S
GRK5	3	SK-N-BE(2), SK-N-AS, NBL-S
ID3	3	SK-N-AS, CHLA-90, NBL-S
IQCJ-SCHIP1	3	SK-N-BE(2), SK-N-AS, NBL-S
ITSN2	3	SK-N-BE(2), SK-N-AS, NBL-S
KCNIP1	3	SK-N-BE(2), SK-N-AS, NBL-S
KCNJ6	3	SK-N-BE(2), SK-N-AS, NBL-S
KLF2	3	SK-N-AS, CHLA-90, NBL-S
LINC01695	3	SK-N-BE(2), SK-N-AS, NBL-S
LRRC70	3	SK-N-BE(2), SK-N-AS, NBL-S
MEF2D	3	SK-N-BE(2), SK-N-AS, NBL-S
MEST	3	SK-N-BE(2), SK-N-AS, NBL-S
MIR548V	3	SK-N-BE(2), SK-N-AS, CHLA-90
MRPS30	3	SK-N-BE(2), SK-N-AS, CHLA-90
MSX2	3	SK-N-BE(2), CHLA-90, NBL-S
NOL4	3	SK-N-BE(2), SK-N-AS, NBL-S
NPPC	3	SK-N-AS, CHLA-90, NBL-S
NYAP2	3	SK-N-BE(2), SK-N-AS, NBL-S
PCAT14	3	SK-N-BE(2), SK-N-AS, NBL-S
PIK3IP1	3	SK-N-BE(2), SK-N-AS, NBL-S
PKIB	3	SK-N-AS, CHLA-90, NBL-S
PPM1J	3	SK-N-AS, CHLA-90, NBL-S
PRAG1	3	SK-N-AS, CHLA-90, NBL-S
RASD1	3	SK-N-AS, CHLA-90, NBL-S
RFTN1	3	SK-N-BE(2), SK-N-AS, NBL-S
RSL1D1	3	SK-N-BE(2), SK-N-AS, NBL-S
SCHIP1	3	SK-N-BE(2), SK-N-AS, NBL-S

SEZ6L	3	SK-N-BE(2), SK-N-AS, NBL-S
SLC25A27	3	SK-N-BE(2), SK-N-AS, NBL-S
SLC25A37	3	SK-N-BE(2), SK-N-AS, NBL-S
SLC35F2	3	SK-N-BE(2), SK-N-AS, CHLA-90
STK3	3	SK-N-BE(2), CHLA-90, NBL-S
TBX3	3	SK-N-BE(2), SK-N-AS, NBL-S
TMCC3	3	SK-N-BE(2), SK-N-AS, NBL-S
TMEM235	3	SK-N-BE(2), SK-N-AS, NBL-S
TRIB2	3	SK-N-AS, CHLA-90, NBL-S
TTC17	3	SK-N-BE(2), SK-N-AS, NBL-S
TTYH2	3	SK-N-BE(2), SK-N-AS, NBL-S

The work presented in this thesis was funded by competitive grants from Instituto Salud Carlos III (PI23/01144) and Generalitat de Catalunya AGAUR/European Social Fund; as well as by the non-profit organizations Fira dels Somnis de Balaguer and Neuroblastoma por Leire.